JSTR
ASEAN Journal of Scientific and Technological Reports
Vol. 25 No. 1
January-March 2022
ISSN 2773-8752 (online)

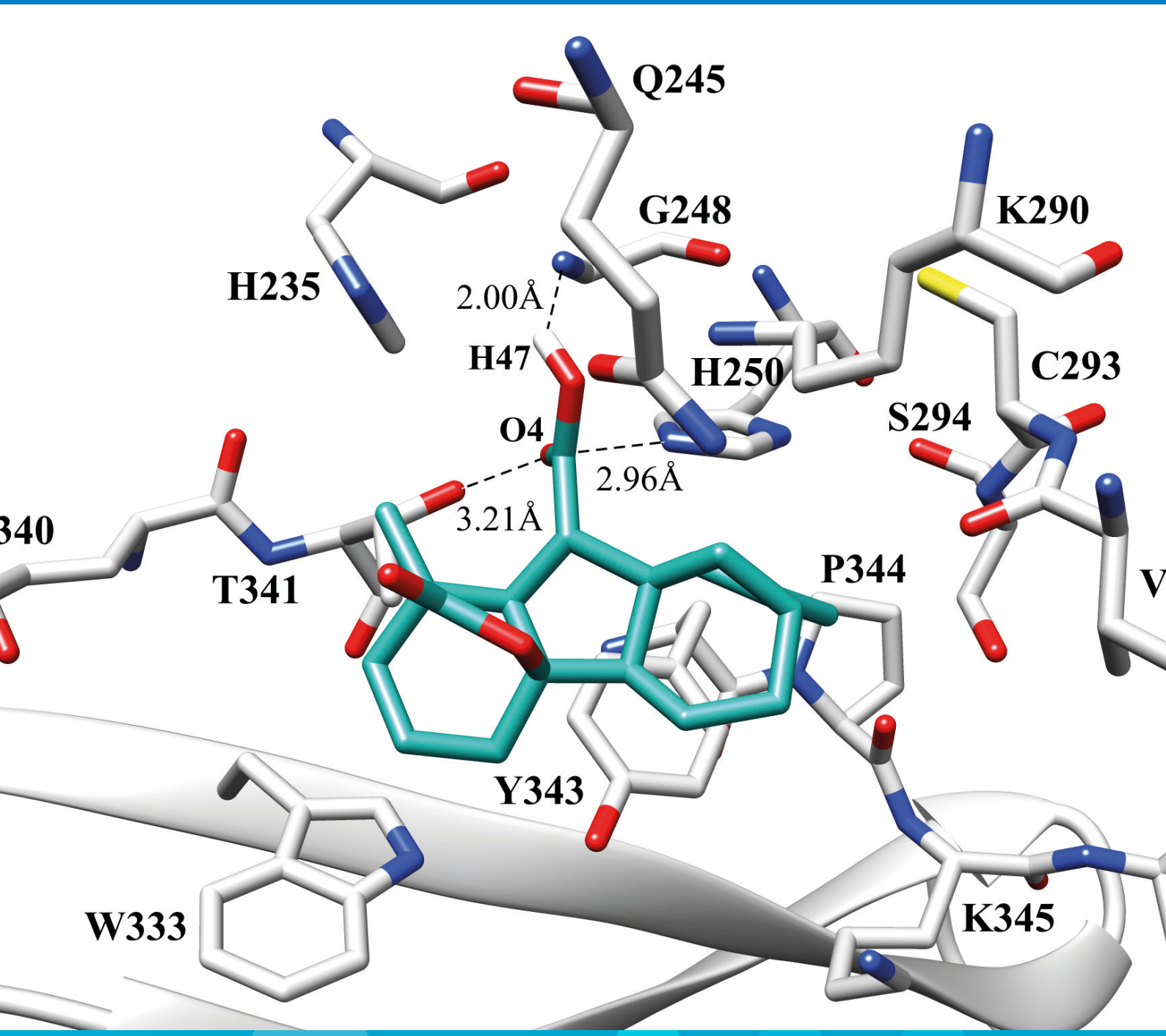

ASEAN Journal of Scientific and Technological Reports (AJSTR)

Name	ASEAN Journal of Scientific and Technological Reports (AJSTR)
Owner	Thaksin University
Advisory Board	Assoc. Prof. Dr. Wichai Chumni (President of Thaksin University, Thailand) Assoc. Prof. Kasem Asawatreratanakul (Vice President for Academic Affairs and International Affairs, Thaksin University, Thailand) Assoc. Prof. Dr. Nathapong Chitniratna (Vice President for Research and Academic Services, Thaksin University, Thailand) Assoc. Prof. Dr. Samak Kaewsuksaeng (Acting of the Research and Development Institute, Thaksin University, Thailand) Asst. Prof. Dr. Prasong Kessaratikoon (Dean of the Graduate School, Thaksin University, Thailand)
Editor-in-Chief	Assoc. Prof. Dr. Sompong O-Thong, Thaksin University, Thailand

Session Editors

1. Assoc. Prof. Dr. Jatuporn Kaew-On, Thaksin University, Thailand
2. Assoc. Prof. Dr. Samak Kaewsuksaeng, Thaksin University, Thailand
3. Asst. Prof. Dr. Komkrich Chokprasombat, Thaksin University, Thailand
4. Asst. Prof. Dr. Noppamas Pukkhem, Thaksin University, Thailand
5. Asst. Prof. Dr. Rattana Jariyaboon, Prince of Songkla University, Thailand

Editorial Board Members

1. Prof. Dr. Hidenari Yasui, University of Kitakyushu, Japan
2. Prof. Dr. Jose Antonio Alvarez Bermejo, University of Almeria, Spain
3. Prof. Dr. Tjokorda Gde Tirta Nindhia, Udayana University in Bali, Indonesia
4. Prof. Dr. Tsuyoshi Imai, Yamaguchi University, Japan
5. Prof. Dr. Ullah Mazhar, The University of Agriculture, Peshawar, Pakistan
6. Prof. Dr. Win Win Myo, University of Information Technology, Myanmar
7. Prof. Dr. Yves Gagnon, University of Moncton, Canada
8. Assoc. Prof. Dr. Chen-Yeon Chu, Feng Chia University, Taiwan
9. Assoc. Prof. Dr. Gulam Murtaza, Government College University Lahore, Lahore, Pakistan
10. Assoc. Prof. Dr. Jompob Waewsak, Thaksin University, Thailand
11. Assoc. Prof. Dr. Khan Amir Sada, American University of Sharjah, Sarjah, United Arab Emirates.
12. Assoc. Prof. Dr. Sappasith Klomklao, Thaksin Univerrsity, Thailand
13. Asst. Prof. Dr. Dariusz Jakobczak, National University, Pakistan
14. Asst. Prof. Dr. Prawit Kongjan, Prince of Songkla University, Thailand
15. Asst. Prof. Dr. Shahrul Isamail, Universiti Malaysia Terengganu, Malaysia
16. Asst. Prof. Dr. Sureewan Sittijunda, Mahidol University, Thailand
17. Dr. Nasser Ahmed, Kyushu University, Fukuoka, Japan
18. Dr. Peer Mohamed Abdul, Universiti Kebangsaan Malaysia, Malaysia
19. Dr. Sriv Tharith, Royal University of Phnom Penh, Cambodia
20. Dr. Khwanchit Suwannoppharat, Thaksin University, Thailand

Staff: Journal Management Division

1. Miss Kanyanat Liadrak, Thaksin University, Thailand
2. Miss Ornkamon Kraiwong, Thaksin University, Thailand
3. Miss Phimnada Maneewong, Thaksin University, Thailand
4. Miss Ranee Sunsang, Thaksin University, Thailand

Contact Us Research and Development Institute Thaksin University 222 M. 2 Ban-Prao sub-district, Pa-Pra-Yom district, Phatthalung province, Thailand
Tel. 0 7460 9600 # 7242 , E-mail: aseanjstr@tsu.ac.th

Editorial

The ASEAN Journal of Scientific and Technological Reports (AJSTR) Vol. 25 No. 1 (January - March 2022) ISSN 2773-8752 (Online) is the second issue under the name of AJSTR. This issue is published 8 worth reading research articles. These exciting research articles were reviewed and answered by experts from various universities and institutions. We sincerely hope that some of the research papers will help guide and motivate our active researchers to produce and create their research more valuable shortly. The AJSTR has served our energetic readers and customers on the international level. For this reason, all selected and accepted research articles will be written and organized in English. Furthermore, the new international editorial board of AJSTR has also been set up and started to administrate and manage all the journal's business simultaneously. From now on, the AJSTR and a new editorial team are ready to organize, manage, publish, and deliver all good quality articles written in well organized English to the world of academic society. I would like to introduce AJSTR editorial board members as below.

Editor-in-Chief Assoc. Prof. Dr. Sompong O-Thong, Thaksin University, Thailand

Session Editors
Assoc. Prof. Dr. Jatuporn Kaew-On, Thaksin University, Thailand
Asst. Prof. Dr. Komkrich Chokprasombat, Thaksin University, Thailand
Asst. Prof. Dr. Noppamas Pukkhem, Thaksin University, Thailand
Assoc. Prof. Dr. Samak Kaewsuksaeng, Thaksin University, Thailand
Asst. Prof. Dr. Rattana Jariyaboon, Prince of Songkla University, Thailand

Editorial Board Members
Asst. Prof. Dr. Prawit Kongjan, Prince of Songkla University, Thailand
Prof. Dr. Tsuyoshi Imai, Yamaguchi University, Japan
Prof. Dr. Hidenari Yasui, University of Kitakyushu, Japan
Assoc. Prof. Dr. Chen-Yeon Chu, Feng Chia University, Taiwan
Dr. Peer Mohamed Abdul, Universiti Kebangsaan Malaysia, Malaysia
Assoc. Prof. Dr. Jompob Waewsak, Thaksin University, Thailand
Prof. Dr. Tjokorda Gde Tirta Nindhia, Udayana University in Bali, Indonesia
Assoc. Prof. Dr. Gulam Murtaza, Government College University Lahore, Lahore, Pakistan
Prof. Dr. Yves Gagnon, University of Moncton, Canada
Dr. Nasser Ahmed, Kyushu University, Fukuoka, Japan
Asst. Prof. Dr. Sureewan Sittijunda, Mahidol University, Thailand
Asst. Prof. Dr. Shahrul Isamail, Universiti Malaysia Terengganu, Malaysia
Assoc. Prof. Dr. Sappasith Klomklao, Thaksin Univerrsity, Thailand
Assoc. Prof. Dr. Khan Amir Sada, American University of Sharjah, Sarjah, United Arab Emirates.
Prof. Dr. Ullah Mazhar, The University of Agriculture, Peshawar, Pakistan
Dr. Sriv Tharith, Royal University of Phnom Penh, Cambodia
Prof. Dr. Jose Antonio Alvarez Bermejo, University of Almeria, Spain
Asst. Prof. Dr. Dariusz Jakobczak, National University, Pakistan
Prof. Dr. Win Win Myo, University of Information Technology, Myanmar
Dr. Khwanchit Suwannoppharat, Thaksin University, Thailand

Assoc. Prof. Dr. Sompong O-Thong
Journal Editor-in-Chief

List of Contents


มหาวิทยาลัยทักษิณ THAKSIN UNIVERSITY


JSTR
ASEAN Journal of Scientific
and Technological Reports


มหาวิทยาลัยทักษิณ THAKSIN UNIVERSITY

JSTR
ASEAN Journal of Scientific and Technological Reports

Research article

N,N-Dimethylbenzimidazolium Iodide as an Efficient Catalyst for a Green Reaction of Intermolecular Stetter Reaction in Water

Baramee Phungpis[1*] and Kanokkan Worawut[2]

[1] Faculty of Natural Resources, Rajamangala University of Technology Isan Sakon Nakhon Campus,Sakonnakhon 47160, Thailand; e-mail: Barameephungpis@yahoo.com
[2] Faculty of Natural Resources, Rajamangala University of Technology Isan Sakon Nakhon Campus,Sakonnakhon 47160, Thailand; e-mail: Kanokkan_pom@hotmail.co.th
* Correspondence: Barameephungpis@yahoo.com

Abstract: The development of greener methodologies is an important field in the framework of green chemistry. In this research study, *N,N*-dimethylbenzimidazolium iodide in NaOH was developed as an efficient catalyst for intermolecular stetter reaction in the greenest solvent (water) to afford the desired 1,4-addition products in good yields of 58-77%. Moreover, the benzimidazolium salt catalyst and NaOH mixture can be reused for at least 4 additional reactions with a consistent yield of 65%.

Keywords: 1,4-Addition; *N,N*-Dimethylbenzimidazolium iodide; Stetter reaction; Water

Graphical Abstract:

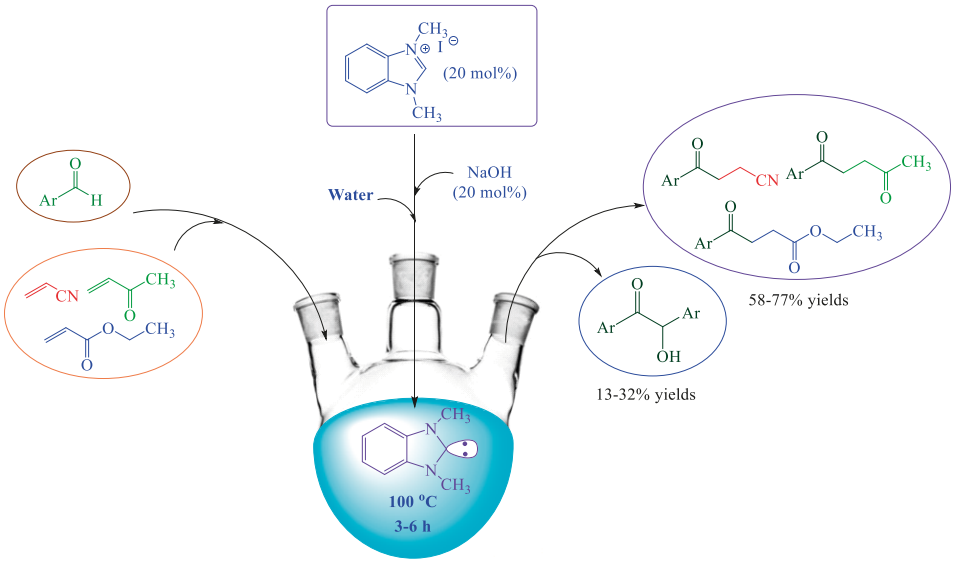

Citation:
Phungpis, B.; Worawut, K. *N,N*-Dimethylbenzimidazolium iodide as an efficient catalyst for a green reaction of intermolecular stetter reaction in water. *ASEAN J. Sci. Tech. Report.* **2022**, *25(1)*, 1-10. https://doi.org/10.55164/ajstr.v25i1.245292

Article history:
Received: October 5, 2021
Revised: January 4, 2022
Accepted: January 14, 2022
Available online: February 11, 2022

Publisher's Note:
This article is published and distributed under the terms of the Thaksin University.

1. Introduction

The use of water as a reaction has been intensively investigated in recent years owing to water reputation as the greenest solvent with nontoxicity, safety, and nature's solvent, mild conditions and possesses distinguished physical and chemical properties [1-2]. Besides, it exhibits powerful hydrogen bonding and a wide temperature range to remain in the liquid state. Many organic compound transformations have been carried out in water [3-4]. Many organic solvents like methylene chloride, dimethylformamide, acetone, benzene, methanol, toluene are carcinogenic and toxic to human health, which causes an environmental issue by polluting the atmosphere. For this reason, the organic reaction in an aqueous medium has become a new way of thinking about chemistry, as is the case for green chemistry.

Over the past decade, various organic reactions have been found to perform successfully synthesis in water of 2-amino-1,3,4-thiadiazoles [5], pyrimido[4,5-d]pyrimidine [6], pyrano[2,3-c]pyrazoles [7], substituted 3,4-dihydropyrimidin-2(1H)-ones [8], 2-amino-4-(5-hydroxy-3-methyl-1H-pyra¬zol-4-yl)-4H chromene-3-carbonitrile derivatives [9], spiroindoline-pyranopyrazoles [10] 2-aminothiazoles [11] and benzoin condensation [12].Type of *N*-heterocyclic carbenes (NHCs) (Figure 1) has attracted considerable interest in recent years due to their ability to reverse aldehydes' normal mode of reactivity, rendering them nucleophilic at the carbonyl carbon. Especially stetter reaction has received significant interest in organocatalyzed reactions due to their special electronic characteristics [13-16]. The utilization of organocatalytic activation of NHC for new bond-formation between aldehyde and electrophilic double bond opens up a new avenue for the synthesis of 1,4-dicarbonyl compounds, which are useful building blocks for the synthesis of a wide range of heterocyclic and carbocyclic compounds, including furans, thiophene, pyridazines, and pyrrole derivatives [17]. For example, the use of thiamine as a catalyst in Stetter reaction [18] and the catalytic reaction of NHC of enals [19] have been well-documented.

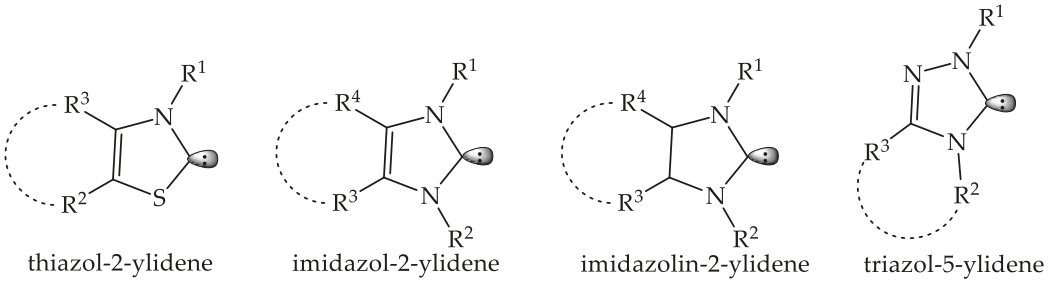

Figure 1. General types of N-heterocyclic carbenes

In the past, stetter reactions had to be carried out in aprotic solvents and conventional organic solvents such as dimethylformamide [20-21], ethanol [22] and dioxane [23]. Therefore, this reaction has also been carried out in ionic liquid catalyzed by thiazolium [24] and benzimidazolium salts [24], respectively. In our previous work, *N*,*N*-dimethylbenzimidazolium iodide was used as an effective and recyclable catalyst for stetter reaction in ionic liquid [Bmim]OH [25]. Herein, we report our extended investigation of greener aspects of stetter reaction in an aqueous medium catalyzed by *N*,*N*-dimethylbenzimidazolium iodide and NaOH.

2. Materials and Methods

All chemicals in the experiment were analytical grade and used directly without further purification. Melting points were determined in capillary tubes in a Buchi B 545 apparatus. The products were identified by comparing their melting points and spectral data (FTIR, ^{1}H & ^{13}C NMR) with those in the authentic samples. FT-IR spectra were obtained as KBr disks on a Shimadzu spectrometer which scans from 400 to 4000 wavenumber. The ^{1}H and ^{13}C NMR data were recorded on a Varian Mercury plus spectrometer (400 MHz). $CDCl_3$ was used as a solvent and internal standard. Coupling constant (*J*) are reported in Hertz (Hz) and the multiplicity abbreviations used are singlet (s), doublet (d), triplet (t), quartet (q), and multiplet (m).

2.1 General procedure for intermolecular stetter reaction between either acrylonitrile (2), ethyl acrylate (6) or methyl vinyl ketone (7) and aromatic aldehydes 1 catalysed by *N,N*-dimethylbenzimidazolium iodide (3) in water

N,N-dimethylbenzimidazolium iodide (**3**) (0.20 mmol) and NaOH (0.20 mmol) in water (5 mL) was added to either acrylonitrile (**2**), ethyl acrylate (**6**) or methyl vinyl ketone (**7**) (2.00 mmol) and aromatic aldehyde **1** (1.00 mmol) at a temperature range of room temperature to 100 °C under magnetic stirring for 3-6 h. After the completion of the reaction indicated by TLC (100% dichloromethane), the reaction mixture was extracted with ethyl acetate (3×30 mL). The combined organic extract was dried (anh. Na_2SO_4), and the solvent was removed under reduced pressure. The residue was purified using preparative thin-layer chromatography (silica gel, elution with dichloromethane). The purified corresponding 1,4-addition products **4a**-**l**, acyloin products **5a**-**d** with their physical data were listed below. The aqueous phase consists of catalyst, NaOH, and water was used as a recycling condition for the new reaction without purification.

4-Phenyl-4-oxobutanenitrile (4a): White crystals; Yield 75%; R_f = 0.51 (100% dichloromethane); m.p. 74-76 °C (lit. 74-76 °C) [26]; IR (KBr) ν_{max}: 3069, 2925, 2889, 2251, 1678, 1607, 1522 and 1413 cm^{-1}; ^1H NMR ($CDCl_3$): δ 7.97 (2H, d, *J* = 7.2 Hz, 2-*H* and 6-*H*), 7.63 (1H, t, *J* = 7.6 Hz, 4-*H*), 7.51 (2H, t, *J* = 7.6 Hz, 3-*H* and 5-*H*), 3.39 (2H, t, *J* = 7.2 Hz, CH_2CH_2CN) and 2.79 (2H, t, *J* = 7.2 Hz, CH_2CH_2CN); ^{13}C NMR ($CDCl_3$): δ 11.9, 34.3, 119.2, 128.0, 128.7, 133.9, 135.7 and 195.4

4-(4′-Chlorophenyl-4-oxobutanenitrile (4b): White crystals; Yield 77%; R_f = 0.45 (100% dichloromethane); m.p. 72-73 °C (lit. 72-73 °C) [27]; IR (KBr) ν_{max}: 3090, 3061, 2928, 2253, 1677, 1588, 1489, 1401 and 775 cm^{-1}; ^1H NMR ($CDCl_3$): δ 7.88 (2H, d, *J* = 8.4 Hz, 2-*H* and 6-*H*), 7.46 (2H, d, *J* = 8.4 Hz, 3-*H* and 5-*H*), 3.36 (2H, t, *J* = 7.2 Hz, CH_2CH_2CN) and 2.78 (2H, t, *J* = 7.2 Hz, CH_2CH_2CN); ^{13}C NMR ($CDCl_3$):δ 11.7, 34.3, 119.2, 129.3, 129.3, 133.9, 140.5 and 194.2

4-(4′-Tolyl)-4-oxobutanenitrile (4c): White crystals; Yield 71%; R_f = 0..52 (100% dichloromethane); m.p. 75-77 °C (lit. 75-77 °C) [28]; IR (KBr) ν_{max}: 3044, 2927, 2855, 2250, 1681, 1673, 1609 and 1425 cm^{-1}; ^1H NMR ($CDCl_3$): δ 7.87 (2H, d, *J* = 8.0 Hz, 2-*H* and 6-*H*), 7.29 (2H, d, *J* = 8.0 Hz, 3-*H* and 5-*H*), 3.38 (2H, t, *J* = 7.2 Hz, CH_2CH_2CN), 2.78 (2H, t, *J* = 7.2 Hz, CH_2CH_2CN) and 2.42 (3H, s, Ar-CH_3); ^{13}C NMR ($CDCl_3$): δ 11.8, 29.8, 34.1, 119.4, 128.1, 129.6, 133.2, 144.9 and 201.3

4-(Pyridin-4-yl)-4-oxobutanenitrile (4d): Yellow crystals; Yield 73%; R_f = 0.53 (100% dichloromethane); m.p. 135-137 °C (lit. 135-137 °C) [29]; IR (KBr) ν_{max}: 3070, 2954, 2925, 2257, 2681, 1690, 1581, 1450, 1332, 1216 and 1000 cm^{-1}; ^1H NMR δ 8.76 (2H, d, *J* = 8.4 Hz, 2′-*H* and 6′-*H*), 7.89 (2H, d, *J* = 8.4 Hz, 3′-*H* and 5′-*H*), 3.01 (2H, t, *J* = 7.2 Hz, CH_2CH_2CN) and 2.75 (2H, t, *J* = 7.2 Hz, CH_2CH_2CN); ^{13}C NMR δ 14.9, 38.9, 119.6, 122.6, 135.0, 135.3, 150.5 and 198.9

1-Phenyl-1,4-pentanedione (4e): Yellow crystals; Yield 73%; R_f = 0.56 (100% dichloromethane); m.p. 70-72 °C; IR (KBr) ν_{max}: 3417, 3050, 2900, 1718, 1676, 1596, 1446, 1353, 1211, 1162 and 1068 cm^{-1}; ^1H NMR δ 7.84 (2H, d, *J* = 7.2 Hz, 2-*H* and 6-*H*), 7.71 (1H, t, *J* = 7.6 Hz, 4-*H*), 7.44 (2H, t, *J* = 7.6 Hz, 3-*H* and 5-*H*), 3.23 (2H, t, *J* = 13.1 Hz, $CH_2CH_2COCH_3$), 2.84 (2H, t, *J* = 13.1 Hz, $CH_2CH_2COCH_3$) and 2.17 (3H, s, $CH_2CH_2COCH_3$); ^{13}C NMR δ 29.8, 32.3, 36.9, 127.8, 128.4, 132.9, 136.6, 198.3 and 206.9

1-(4′-Chlorophenyl)-1,4-pentanedione (4f): Yellow crystals; Yield 75%; R_f = 0.50 (100% dichloromethane); m.p. 71-73 °C; IR (KBr) ν_{max}: 3100, 2902, 1718, 1673, 1590, 1355, 1317, 1214 and 1089 cm^{-1}; ^1H NMR δ 7.90 (2H, d, *J* = 8.8 Hz, 2′-*H* and 6′-*H*), 7.41 (2H, d, *J* = 8.8 Hz, 3′-*H* and 5′-*H*), 3.21 (2H, t, *J* = 13.2 Hz, $CH_2CH_2COCH_3$), 2.75 (2H, t, *J* = 13.2 Hz, $CH_2CH_2COCH_3$) and 2.18 (3H, s, $CH_2CH_2COCH_3$); ^{13}C NMR δ 29.7, 32.1, 36.8, 128.1, 128.8, 134.9, 139.3, 197.1 and 206.8

1-(4′-Tolyl)-1,4-pentanedione (4g): Yellow crystals; Yield 70%; R_f = 0.48 (100% dichloromethane); m.p. 83-85 °C; IR (KBr) ν_{max}: 3091, 2914, 1708, 1679, 1584, 1390, 1321, 1217 and 1109 cm^{-1}; ^1H NMR δ 7.88 (2H, d, *J* = 8.4 Hz, 2′-*H* and 6′-*H*), 7.31 (2H, d, *J* = 8.4 Hz, 3′-*H* and 5′-*H*), 3.22 (2H, t, *J* = 13.2 Hz, $CH_2CH_2COCH_3$), 2.78 (2H, t, *J* = 13.2 Hz, $CH_2CH_2COCH_3$) and 2.16 (3H, s, $CH_2CH_2COCH_3$); ^{13}C NMR δ 11.9, 29.6, 32.2, 36.7, 128.9, 130.1, 134.5, 138.7, 198.1 and 206.7

1-(Pyridin-4-yl)-1,4-pentanedione (4h): Yellow crystals; Yield 72%; R_f = 0.42 (100% dichloromethane); m.p. 99-101 °C; IR (KBr) ν_{max}: 3111, 2969, 1711, 1679, 1593, 1375, 1319, 1214, 1111 and 1089 cm^{-1}; ^1H NMR δ 8.72 (2H, d, *J* = 8.8 Hz, 2′-*H* and 6′-*H*), 7.85 (2H, d, *J* = 8.8 Hz, 3′-*H* and 5′-*H*), 3.25 (2H, t, *J* = 13.2 Hz, $CH_2CH_2COCH_3$),

2.81 (2H, t, *J* = 13.2 Hz, C*H*$_2$CH$_2$COCH$_3$) and 2.17 (3H, s, CH$_2$CH$_2$COC*H*$_3$); ^{13}C NMR δ 29.9, 32.5, 36.9, 120.4, 134.6, 140.6, 198.3 and 206.8

Ethyl 4-phenyl-4-oxobutanoate (4i): Yellow liquid; Yield 62%; R$_f$ = 0.54 (100% dichloromethane); IR (neat) ν$_{max}$: 3030, 2949, 1723, 1640, 1569, 1448, 1389, 1260 and 1183 cm^{-1}; ^{1}H NMR δ 7.97 (2H, d, *J* = 7.6 Hz, 2′-*H* and 6′-*H*), 7.55 (1H, t, *J* = 7.6 Hz, 4′-*H*), 7.46 (2H, t, *J* = 7.6 Hz, 3′-*H* and 5′-*H*), 4.17 (2H, q, *J* = 7.6 Hz, OC*H*$_2$CH$_3$), 3.32 (2H, t, *J* = 6.8 Hz, CH$_2$C*H*$_2$CO$_2$CH$_2$CH$_3$), 2.73 (2H, t, *J* = 6.8 Hz, C*H*$_2$CH$_2$CO$_2$CH$_2$CH$_3$) and 1.26 (3H, t, *J* = 7.6 Hz, CO$_2$CH$_2$C*H*$_3$); ^{13}C NMR δ 14.3, 28.5, 33.5, 60.6, 128.2, 128.6, 133.4, 136.6, 172.9 and 198.2.

Ethyl 4-(4′-dichlorophenyl)-4-oxobutanoate (4j): White crystals; Yield 66%; R$_f$ = 0.55 (100% dichloromethane); mp 55-57 °C (lit. 56-58 °C) [30]; IR (KBr) ν$_{max}$: 3013, 2961, 1745, 1687, 1600, 1446, 1330 and 1273 cm^{-1}; ^{1}H NMR δ 7.86 (2H, d, *J* = 8.8 Hz, 2′-*H* and 6′-*H*), 7.36 (2H, d, *J* = 8.8 Hz, 3′-*H* and 5′-H), 4.09 (2H, q, *J* = 7.8 Hz, CO$_2$C*H*$_2$CH$_3$), 3.21 (2H, t, *J* = 6.8 Hz, CH$_2$C*H*$_2$CO$_2$CH$_2$CH$_3$), 2.68 (2H, t, *J* = 6.8 Hz, C*H*$_2$CH$_2$CO$_2$CH$_2$CH$_3$) and 1.22 (3H, t, *J* = 7.8 Hz, CO$_2$CH$_2$C*H*$_3$); ^{13}C NMR δ 14.2, 28.3, 33.3, 60.8, 128.9, 129.5, 134.7, 139.6, 172.7 and 197.1.

Ethyl 4-(4′-tolyl)-4-oxobutanoate (4k): White crystals; Yield 58%; R$_f$ = 0.49 (100% dichloromethane); mp 64-65 °C; IR (KBr) ν$_{max}$: 3059, 2971, 1748, 1690, 1596, 1451, 1323, 1179, 1005 and 763 cm^{-1}; ^{1}H NMR δ 7.87 (2H, d, *J* = 8.4 Hz, 2′-*H* and 6′-*H*), 7.38 (2H, d, *J* = 8.4 Hz, 3′-*H* and 5′-*H*), 4.09 (2H, q, *J* = 7.6 Hz, CO$_2$C*H*$_2$CH$_3$), 3.21 (2H, t, *J* = 6.8 Hz, CH$_2$C*H*$_2$CO$_2$CH$_2$CH$_3$), 2.68 (2H, t, *J* = 6.8 Hz, C*H*$_2$CH$_2$CO$_2$CH$_2$CH$_3$), 2.13 (3H , s, C*H*$_3$Ar) and 1.23 (3H, t, *J* = 7.6 Hz, CO$_2$CH$_2$C*H*$_3$); ^{13}C NMR δ 14.1, 28.4, 30.9, 33.2, 60.7, 128.9, 129.6, 134.8, 139.7, 172.9 and 196.9.

Ethyl 4-(pyridin-4-yl)-4-oxobutanoate (4l): Yellow liquid; Yield 64%; R$_f$ = 0.47 (100% dichloromethane); IR (neat) ν$_{max}$: 3100, 2983, 2911, 1735, 1680, 1590, 1453, 1361, 1223, 1165 and 1042 cm^{-1}; ^{1}H NMR δ 8.76 (2H, d, *J* = 8.8 Hz, 2′-*H* and 6′-*H*), 7.88 (2H, d, *J* = 8.8 Hz, 3′-*H* and 5′-*H*), 4.13 (2H, q, *J* = 7.6 Hz, CO$_2$C*H*$_2$CH$_3$), 3.01 (2H, t, *J* = 6.8 Hz, CH$_2$C*H*$_2$CO$_2$CH$_2$CH$_3$), 2.72 (2H, t, *J* = 6.8 Hz, C*H*$_2$CH$_2$CO$_2$CH$_2$CH$_3$) and 1.15 (3H, t, *J* = 7.6 Hz, CO$_2$CH$_2$C*H*$_3$); ^{13}C NMR δ 14.2, 27.8, 33.4, 60.7, 122.9, 135.0, 150.3, 173.0 and 196.7.

Benzoin (5a): White crystals; Yields 14-23%; R$_f$ = 0.25 (100% dichloromethane); m.p. 133-135 °C (lit. 134-136 °C) [31]; IR (KBr) ν$_{max}$: 3412, 3050, 3025, 2929, 1676, 1595, 1450, 1260, 1209 and 752 cm^{-1}; ^{1}H NMR (CDCl$_3$) δ 7.91(2H, d, *J* = 7.6 Hz, 2-*H* and 6-*H*), 7.52 (1H, t, *J* = 7.6 Hz, 4-*H*), 7.39 (2H, t, *J* = 7.6 Hz, 3-*H* and 5-*H*), 7.24-7.34 (5H, m, Ar-*H*), 5.97 (1H, s, C*H*) and 4.52 (1H, br s, O*H*); ^{13}C NMR (CDCl$_3$) δ 76.4, 127.9, 128.7, 128.7, 129.1, 133.7, 133.9, 139.2 and 198.8

4,4′-Dichlorobenzoin (5b): White crystals; Yields 15-26%; R$_f$ = 0.23 (100% dichloromethane); m.p. 87-88 °C (lit. 87-88 °C) [29]; IR (KBr) ν$_{max}$: 3421, 3063, 2927, 1679, 1595, 1479, 1408, 1262, 1207 and 1090 cm^{-1}; ^{1}H NMR (CDCl$_3$): δ 7.76 (2H, d, *J* = 8.8 Hz, 2-*H* and 6-*H*), 7.34 (2H, d, *J* = 8.8 Hz, 3-*H* and 5-*H*), 7.24 (2H, d, *J* = 8.8 Hz, 3′-*H* and 5′-*H*), 7.18 (2H, d, *J* = 8.8 Hz, 2′-*H* and 6′-*H*) and 5.81 (1H, s, C*H*); ^{13}C NMR (CDCl$_3$): δ 75.5, 129.1, 129.2, 129.5, 130.5, 131.6, 134.9, 137.3, 140.8 and 197.4

4,4′-Dimethylbenzoin (5c): White crystals; Yields 21-32%; R$_f$ = 0.22 (100% dichloromethane); m.p.: 75-77 °C (lit. 75 °C) [32]; IR (KBr) ν$_{max}$: 3442, 3044, 2929, 1678, 1607, 1520, 1449, 1374 and 1191 cm^{-1}; ^{1}H NMR (CDCl$_3$): δ 7.81 (2H, d, *J* = 8.8 Hz, 2-*H* and 6-*H*), 7.22 (2H, d, *J* = 8.8 Hz, 3-*H* and 5-*H*), 7.19 (2H, d, *J* = 8.4 Hz, 2′-*H* and 6′-*H*), 7.10 (2H, d, *J* = 8.4 Hz, 3′-*H* and 5′-*H*), 5.89 (1H, s, C*H*), 2.34 (3H, s, Ar-C*H*$_3$) and 2.30 (3H, s, Ar-C*H*$_3$); ^{13}C NMR (CDCl$_3$): δ 21.3, 21.8, 75.8, 127.8, 129.3, 129.4, 129.9, 131.1, 136.4, 138.5, 144.9 and 198.7

4,4′-Pyridoin (5d): Yellow crystals; Yields 13-25%; R$_f$ = 0.20 (100% dichloromethane); m.p. 153-155 °C; IR (KBr) ν$_{max}$: 3464, 3068, 2981, 2850, 1668, 1591, 1513, 1472, 1319, 1275, 1170, 1081, 819 cm^{-1}; ^{1}H NMR δ 8.77 (2H, d, *J* = 8.8 Hz, 2-*H* and 6-*H*), 8.55 (2H, d, *J* = 8.8 Hz, 3-*H* and 5-*H*), 7.94 (2H, d, *J* = 8.4 Hz, 2′-*H* and 6′-*H*), 7.20 (2H, d, *J* = 8.4 Hz, 3′-*H* and 5′-*H*), 6.09 (1H, s, C*H*); ^{13}C NMR (CDCl$_3$) δ: 75.6, 122.2, 122.6, 135.1, 137.5, 145.2, 150.5, 197.8

3. Results and Discussion

To investigate this intermolecular stetter reaction, the simple substrate benzaldehyde (**1a**) and acrylonitrile (**2**) were firstly surveyed, which was carried out under similar conditions as reported in the literature [24] by using 20 mol% of catalyst **3** and in the presence of 20 mol% of different bases and temperature

with water as the solvent. The screening of the optimized base, including temperature control, was carried out, and the results are summarized in Table 1.

Table 1. Optimization condition of intermolecular stetter reaction between benzaldehyde (**1a**) and acrylonitrile (**2**) catalyzed by *N*,*N*-dimethylbenzimidazolium iodide (**3**) in the presence of various bases in water

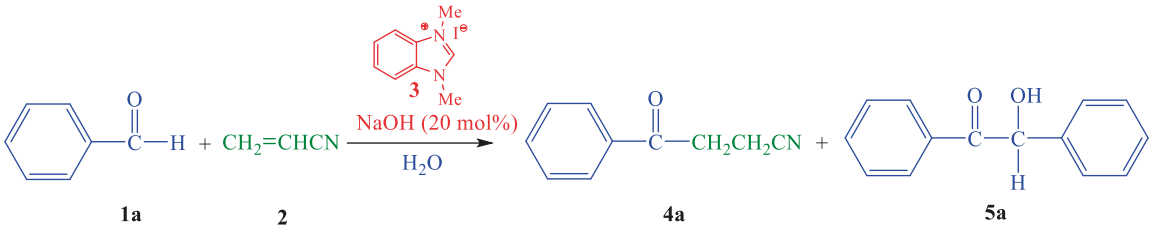

Entry	Base	Temp.	Time (h)	Yield **4a** (%)	Yield **5a** (%)
1	TEA	r.t.	12	n.d.	12
2	DBU	r.t.	12	n.d.	14
3	NaOH	r.t.	6	25	21
4	TEA	100	10	15	14
5	DBU	100	10	46	17
6	NaOH	100	4.5	75	18

Under this situation, when benzimidazolium salt **3** under the conditions of organic bases of triethylamine (TEA) and 1,8-diazabicyclo[5.4.0]undec-7-ene (DBU) at room temperature in the water was used, the reaction proceeded not smoothly and afforded only product of α-hydroxy ketone **5a** in 12 and 14%, respectively (Table 1, entries 1, 2). Unfortunately, desired 4-phenyl-4-oxobutanenitrile (**4a**) was low yield when the reaction was run with an ionic base of NaOH at room temperature in water (Table 1, entries 3).

The reaction between benzaldehyde (**1a**) and acrylonitrile (**2**) by using 20 mol% of *N*,*N*-dimethylbenzimidazolium iodide (**3**) and different base in water at 100 °C was carried out, and the resulting was listed in Table 1. In the case of this stetter reaction catalyzed by benzimidazolium salt **3** with NaOH in water provided 1,4-addition product **4a** in 75% yield that was higher than organic bases of TEA and DBU due to it being a strong base for better deprotonation of the catalyst. Moreover, NaOH provided more advantages than the organic base (TEA and DBU) because it is the inorganic base dissolved in an aqueous phase and easily separated from the products and reused. The increasing temperature from room temerature to 100 oC can increase the reaction rate, as shown in Table 1 that the reaction was faster at high temerature and increased the product. This result is consistent with previously reported studies [33]. The side product **5a** was still obtained in 14, 17, and 18% yields, respectively (Table 1, entries 4 to 6).

With the optimal reaction conditions established (Table 1), the extension of these reaction conditions between either acrylonitrile (**2**) or methyl vinyl ketone (**6**) and aldehydes **1a**-**d** was conducted with good yields (70-77%) of corresponding 1,4-addition products **4b**-**h** (Table 2, entries 1-7). In each case, small amounts of acyloins **5a**-**d** (13 to 23%) were also formed in these reactions.

In contrast, acyloins became the competitive side reaction when a less electrophilic double bond of ethyl acrylate (**7**) was used due to the Breslow intermediate reacted with more reactive aldehydes than less reactive ethyl acrylate, the desired product was provided with a lower yield of 1,4-additions **4i**-**l** in 62, 66, 58 and 64% yields, respectively. The less electrophilic double bond of ethyl acrylate (**7**) slightly decreased the yields of 1,4-additions **4i**-**l** and slightly increased reaction times (Table 2, entries 8-11).

Table 2. Intermolecular stetter reaction of aromatic aldehydes **1a-d** with acrylonitrile (**2**), ethyl acrylate (**6**) and methyl vinyl ketone (**7**) catalysed by *N,N*-dimethylbenzimidazolium iodide (**3**) (20 mol%) and NaOH (20 mol%) in water at 100 °C

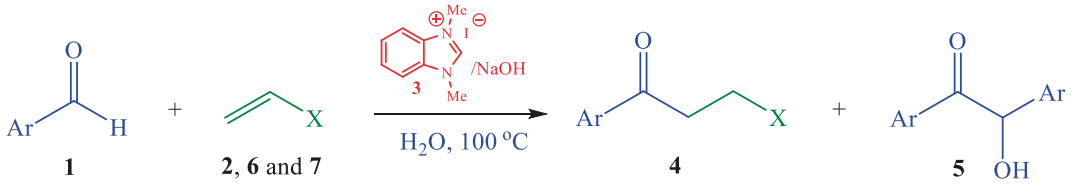

Entry	Aldehyde	X	Time (h)	Yield (%)	Yield (%)
1	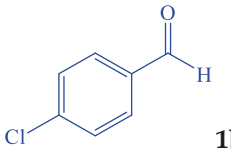 **1b**	CN (**2**)	3	77 (**4b**)	15 (**5b**)
2	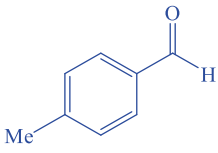 **1c**	CN (**2**)	5	71 (**4c**)	21 (**5c**)
3	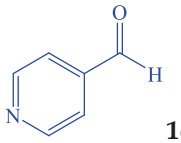 **1d**	CN (**2**)	3.5	73 (**4d**)	13 (**5d**)
4	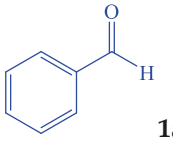 **1a**	$COCH_3$ (**6**)	4.5	73 (**4e**)	14 (**5a**)
5	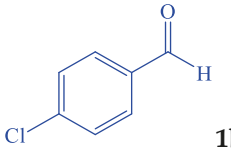 **1b**	$COCH_3$ (**6**)	3.5	75 (**4f**)	16 (**5b**)
6	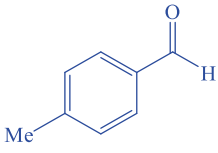 **1c**	$COCH_3$ (**6**)	5	70 (**4g**)	23 (**5c**)
7	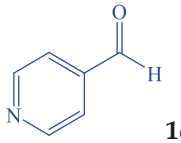 **1d**	$COCH_3$ (**6**)	4	72 (**4h**)	15 (**5d**)
8	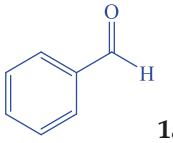 **1a**	$CO_2CH_2CH_3$ (**7**)	5	62 (**4i**)	23 (**5a**)
9	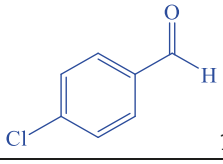 **1b**	$CO_2CH_2CH_3$ (**7**)	4	66 (**4j**)	26 (**5b**)

Table 2. Intermolecular stetter reaction of aromatic aldehydes **1a-d** with acrylonitrile (**2**), ethyl acrylate (**6**) and methyl vinyl ketone (**7**) catalysed by *N,N*-dimethylbenzimidazolium iodide (**3**) (20 mol%) and NaOH (20 mol%) in water at 100 °C (Continued)

Entry	Aldehyde	X	Time (h)	Yield (%)	Yield (%)
10	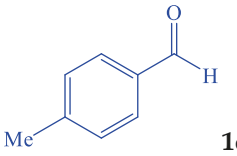 **1c**	$CO_2CH_2CH_3$ (**7**)	6	58 (**4k**)	32 (**5c**)
11	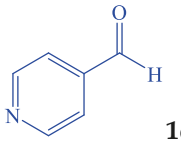 **1d**	$CO_2CH_2CH_3$ (**7**)	4.5	64 (**4l**)	22 (**5d**)

The catalytic cycle of the stetter reaction (green pathway) proposed similarly with a previous report [33], the *N,N*-dimethylbenzimidazolium iodide (**3**) is deprotonated by NaOH to form carbene **8,** which reacts with the aldehyde **1** to give the Breslow intermediate **10**. Then, subsequent nucleophilic attack of the Breslow intermediate **10** to the Michael acceptors **2**, **6** or **7** provides tetrahedral intermediate **11**. 1,4-Proton transfer by water and collapse of the tetrahedral intermediate **11** affords the 1,4-addition products **4a-i** and regenerates the carbene catalyst **8** (Scheme 1).

The side product **5a-d** is shown in the red pathway. The Breslow intermediate **10** is an acylation reagent, which reacts with another aldehyde **1** to provide an intermediate **13**. Water is deemed a proton shuttle in a 1,4-H shift process by simultaneously providing one proton to the oxygen and obtaining another from the hydroxyl group to give an intermediate **14** followed by the regeneration of the NHC catalyst and elimination of the acyloins **5a-d**.

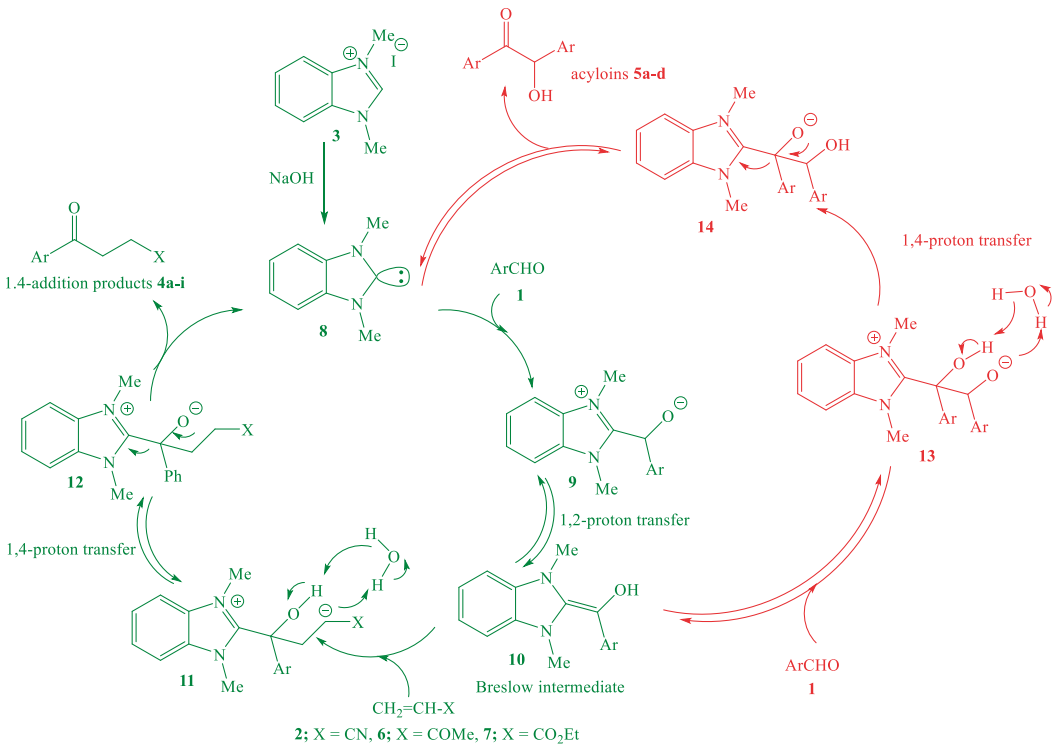

Scheme 1. Catalytic cycles of intermolecular stetter reaction (blue pathway) and acyloin condensation (red pathway) catalysed by *N,N*-dimethylbenzimidazolium iodide (**3**) and NaOH in water

Recycling of *N*,*N*-dimethylbenzimidazolium iodide (**3**) were examined for the intermolecular stetter reaction between benzaldehyde (**1a**) and acrylonitrile (**2**) in water. After the first run, which gave 1,4-addition product **4a** in 75% yields, the benzimidazolium salt **3** and NaOH in water after the reaction and extraction separation was reused in the same type of reaction for at least 5 cycles.

The recovered benzimidazolium salt **3** and NaOH in water was subjected to a second cycle with 1 equiv. of benzaldehyde (**1a**) and 2 equiv. of acrylonitrile (**2**) gave 4-phenyl-4-oxobutanenitrile (**4a**) in a 73% yield. Similarly, in the third, fourth, and fifth cycles, the yield of 1,4-addition products was 70%, 68%, and 65%, respectively (Table 3). The slight decrease in the yield may be due to the reduction of NaOH and the increase of water or the decomposition of some amount of catalyst in the reaction because the recycle condition came from the aqueous phase after extraction of the product and used without purification.

Table 3. Intermolecular stetter reaction between benzaldehyde (**1a**) and acrylonitrile (**2**) in recycled catalysed of *N*,*N*-dimethylbenzimidazolium iodide (**3**) and NaOH with water as the solvent

Run	Yield 4a (%)	Yield 5a (%)
1	75	18
2	73	17
3	70	14
4	68	13
5	65	11

4. Conclusions

Intermolecular stetter reaction between either acrylonitrile or methyl vinyl ketone and aromatic aldehydes in the presence of 20 mol% of *N*,*N*-dimethylbenzimidazolium iodide (**3**) and NaOH performed well in water and as an efficient green method, giving a good yield of products with corresponding acyloins as side products. NaOH plays an important role in this stetter reaction due to its strong basicity and recycling ability. The increasing reaction temperature can increase the reaction rate and product yields. Moderate yields of 1,4-addition products were observed upon treating aromatic aldehydes with a less reactive acceptor (ethyl acrylate). The recycle reaction system containing benzimidazolium salt **3** and NaOH after the extraction can be reused five times without significant loss of efficiency.

5. Acknowledgements

Financial support from the Thailand Science Research and Innovation and Faculty of Natural Resources, Rajamangala University of Technology Isan Sakonnakhon Campus are gratefully acknowledged.

Author Contributions:

Funding: The author(s) disclosed receipt of the following financial support for the research, authorship, and publication of this article: This work was supported by the Thailand Science Research and Innovation (Project ID: 4128) and Faculty of Natural Resources, Rajamangala University of Technology Isan Sakonnakhon Campus.

Conflicts of Interest: The authors declare that there is no conflict of interest regarding the publication of this article.

References

1. Pelissier, H. Recent developments in enantioselective organocatalytic michael reactions in aqueous media. *Current Organic Chemistry*. 2018, 22, 323-344.
2. Van Der Helm, M P.; Klemm, B.; Eelkema, R. Organocatalysis in aqueous media. *Nature Review Chemistry*. 2019, 3, 491-508.

3. Ren, Y.; Cai, C. Iodine catalysis in aqueous medium: An improved reaction system for knoevenagel and nitroaldol condensation. *Catalysis Letter*. 2007, 118, 134–138.
4. Gong, K.; He, Z.W.; Xu, Y. Green synthesis of 5–benzylidene rhodanine derivatives catalyzed by 1–butyl–3–methyl imidazolium hydroxide in water. *Monatshefte für Chemie*. 2008, 139, 913–915.
5. Aryanasab, F.; Ziyaei, A.H.; Mohammad, S.R. Dithiocarbamate as an efficient intermediate for the synthesis of 2–amino–1,3,4–thiadiazoles in water. *Tetrahedron Letter*. 2010, 51, 790–792.
6. Kidwai, M.; Singhal, K.; Kukreja, S. One–pot green synthesis for pyrimido [4,5–d] pyrimidine derivatives. *Zeitschrift für Naturforschung B*. 2007, 62b, 732–736.
7. Pravin, V.; Shinde, J.B.; Gujar, B. Silica in water: A potentially valuable reaction medium for the synthesis of pyrano [2,3–c]pyrazoles. *Bulletin of the Korean Chemical Society*. 2012, 33, 1345–1348.
8. Polshettiwar, V.; Varma, R.S. Biginelli reaction in aqueous medium: A greener and sustainable approach to substituted 3,4–dihydropyrimidin –2(1H)–ones. *Tetrahedron Letter*. 2007, 48,7343–7346.
9. Kumaravel, K.; Vasuki, V. Four component catalyst–free reaction in water synthesis of novel 2–amino–4–(5–hydroxy–3–methyl–1H–pyrazol–4–yl)–4H chromene–3 carbonitrile derivatives. *Green Chemistry*. 2009, 11, 1945–1947.
10. Ahadi, S.; Yasaei, Z.; Bazgir, A. A clean and one–pot synthesis of spiroindoline–pyranopyrazoles. *Journal of Heterocycle Chemistry*. 2010, 47, 1090–1094.
11. Taterao, M.P.; Ingale, S.A.; Srinivasan, K.V. Catalyst–free efficient synthesis of 2–aminothiazoles in water at ambient temperature. *Tetrahedron*. 2008, 64, 5019–5022.
12. Iwamoto, K.I.; Hamaya, M.; Hashimoto, N.; Kimura, H.; Suzuki, Y.; Sato, M. Benzoin reaction in water as an aqueous medium catalyzed by benzimidazolium salt. *Tetrahedron Lett*er. 2006, 47, 7175–7177.
13. Nair, V.; Vellalath, S.; Poonoth, M.; Mohan, R.; Suresh, E. *N*-heterocyclic carbene catalyzed reaction of enals and 1,2-dicarbonyl compounds: Stereoselective synthesis of spiroγ-butyrolactones. *Organic Letter*. 2006, *8*, 507-509.
14. Wang, X.N.; Zhang, Y.Y.; Ye, S. Enantioselective synthesis of spirocyclic oxindole-β-lactones via *N*-heterocyclic carbene-catalyzed cycloaddition of ketenes and isatins. *Advanced Synthesis & Catalysis.* 2010, 352, 1892-1895.
15. Sun, L.H.; Shen, L.T.; Ye, S. Highly diastereo- and enantioselective NHC-catalyzed [3+2] annulation of enals and isatins. *Chemistry Communication.* 2011, 47, 10136-10138.
16. Jiang, K.; Bhoopendra, T.; Chi, Y. Access to spirocyclic oxindoles via *N*-heterocyclic carbene-catalyzed reactions of enals and oxindole-derived α,β-unsaturated imines. *Organic Letter.* 2012, 14, 2382-2385.
17. Zhang, F.; Du, P.; Chen, J.; Wang, H.; Luo, Q.; Wan, X. Co-catalyzed synthesis of 1,4-dicarbonyl compounds using TBHP oxidant. *Organic Letter.* 2014, 16, 19322-1935.
18. Stetter, H. Catalyzed addition of aldehydes to activated double bonds-A new aynthetic approach. *Angewandte Chem*ie *International Edition.* 1976, 15, 639-647.
19. Leong, W.W.Y.; Chen, X.; Chi, Y.R. NHC-catalyzed reactions of enals with water as a solvent. *Green Chemistry.* 2013, 15, 1505-1508.
20. Stetter, H.; Schreckenberg, M. Addition of aliphatic aldehydes to activated double bonds. *Chemische Berichte*. 1974, 107, 2453.
21. Stetter, H. Catalyzed addition of aldehydes to activated double bonds-A new synthetic approach. *Angewandte Chem*ie *International Edition in English*. 1976, 15, 639–647.
22. Stetter, H.; Kuhlmann, H. Addition von aldehyde an aktivierte doppelbindungen-XII. *Tetrahedron*. 1977, 33, 353-356.
23. Novak, L.; Baan, G.; Marosfalvi, J.; Szantay, C. Application of carbonyl umpolung to prostaglandin synthesis I. Synthesis of 11-deoxy prostaglandin intermediates. *Tetrahedron Letter*. 1978, 19, 487-490.
24. Anjaiah, S.; Chandrasekhar, S.; Gree, R. Stetter reaction in room temperature ionic liquids and application to the synthesis of haloperidol. *Advanced Synthesis & Catalysis* 2004, 346, 1329-1334.
25. Phungpis, B.; Hahnvajanawong, V.; Theramongkol, P. Benzoin condensation and stetter reaction catalysed by *N*,*N*-dimethylbenzimidazolium iodide in [Bmim][OH]. *Oriental Journal of Chemistry.* 2014, 30, 933–939.

26. Stetter, H.; Schreckenberg, M. A new method for addition of aldehydes to activated double bonds, *Angewandte Chemie International Edition*. 1973, 12, 81.
27. Reutrakul, V.; Nimgirawath, S.; Panichanun, S.; Ratananukul, P. Addition reactions of α-(dimethylamino) nitriles with acrylonitrile: A simple synthesis of γ-ketonitriles. *Chemistry Letter*. 1979, 399-400.
28. Herman, H.; Schreckenberg, M. 1977, Process for Preparing Ketones, US Patent NO. 4014889.
29. Breslow, R. On the mechanism of thiamine action. IV.[1] Evidence from studies on model systems. *Journal of American Chemical Society.* 1958, 80, 3719-3726.
30. Stetter, H.; Kuhlmann, H. The catalyzed nucleophilicaddition of aldehydes to electrophilic double bonds. *Organic Reaction.* 1991, 40, 434.
31. Phungpis, B.; Hahnvajanawong, V. 1-Butyl-3-methylimidazolium bromide as a solvent and precatalyst for stetter reaction. *Asian Journal of Chemistry*. 2020, 32, 2028-2032.
32. Corey, E.J.; Zhang, F.Y. Mechanism and conditions for highly enantioselective epoxidation of α,β-enones using charge-accelerated catalysis by a rigid quaternary ammonium salt. *Organic Letter.* 1999, 1, 1287-1290.
33. Debiais, M.; Hamoud, A.; Drain, R.; Barthélémy, P.; Desvergnes, V. Bio-inspired NHC-organocatalyzed Stetter reaction in aqueous conditions. *RSC Advanced*. 2020, 10, 40709-40718.

JSTR
ASEAN Journal of Scientific and Technological Reports

Research article

The Differences of Precipitation Characteristics among GCMs over Southeast Asia under AR6 Climate Change Scenarios

Ketvara Sittichok[1*] and Chaiyapong Theppprasit[1]

[1] Department of Irrigation Engineering, Faculty of Engineering at Kampahengsaen Campus, Kasetsart University, Bangkok, 10900, Thailand; fengkrs@ku.ac.th
[1] Department of Irrigation Engineering, Faculty of Engineering at Kampahengsaen Campus, Kasetsart University, Bangkok, 10900, Thailand; fengcpth@ku.ac.th
* Correspondence: E-mail: fengkrs@ku.ac.th

Abstract: Southeast Asia is known globally as a highly vulnerable climate change region. Precipitation is the primary factor that impacts livelihood in this region due to recurring flood and drought incidents. Variables projections under climate change can be made using General Circulation Models (GCMs). An investigation of projected precipitation with the new phase of the model experiment, the Sixth Assessment Report (AR6), is worth to be considered. This study investigates the spatial distributions of variability, trend and conditions (wet/dry) of precipitations generated using 10 GCMs over the SEA under AR6 with four scenarios (SSP1-2.6, SSP2-4.5, SSP3-7.0, and SSP5-8). Three statistical methods, coefficient of variation (CV), Mann-Kendall test (MK) and standardized anomaly index (SAI), were calculated by grid cells. Significant differences among GCMs could be seen in the results. High precipitation variation with CV was indicated around the southern part of Indonesia and the Philippines oceans for six models, whereas only one model (MRI-ESM2) returned strong variation for mainland countries. A decreasing precipitation trend during the historical period could be observed in mainland countries with four GCMs. However, the SSP3-7.0 and SSP5-8.5 of most models presented precipitation increment. The extremely wet and dry ratio to all other years was calculated. Highly wet years higher than 10% were indicated in SSP5-8.5 with MPI-ESM1 occurring in most areas of the region, whereas other models gave 6-10% of highly wet occurrence. Drought situation occurred higher than 10% and could be seen with only three models with small areas under all scenarios.

Keywords; Climate Change; Coefficient of Variation; Mann-Kendall; Standardized Anomaly Index; Southeast Asia; Sixth Assessment Report

Citation:
Sittichok, K.; Theppprasit, S. The Differences of Precipitation Characteristics among GCMs over Southeast Asia under AR6 Climate Change Scenarios . *ASEAN J. Sci. Tech. Report.* **2022**, *25(1)*, 11-23. https://doi.org/10.55164/ajstr.v25i1.244632.

Received: July 12, 2021
Revised: December 20, 2021
Accepted: December 20, 2021
Available online: March 3, 2022

Publisher's Note:
This article is published and distributed under the terms of the Thaksin University.

1. Introduction

Southeast Asia (SEA) comprises eleven countries, which are: Indonesia, Myanmar, Thailand, Vietnam, Malaysia, Philippines, Laos, Cambodia, East Timor, Brunei and Singapore. This region is indicated as highly vulnerable to climate change [1,2]. SEA's livelihood mainly relies on agriculture. Therefore, meteorological changes, especially precipitation and temperatures, are

conducive to the growth of agricultural products that factor into the gross domestic product of various countries. These countries are indicated as vulnerable regions to climate change due to most people depending on natural resources [3]. A higher frequency of extreme events resulting in severe droughts and floods, including tropical cyclones, occur in this region, creating high-risk conditions. In addition, 563 million people of this region are located along coastlines around 173,251 kilometres that are at risk of rising sea levels and the impact of tropical storms. Further, this region is likely to face a more significant impact from climate change than the rest of the world [1].

The Intergovernmental Panel on Climate Change (IPCC) launched a new phase of the model experiment, the Sixth Assessment Report (AR6). Nine Shared Socioeconomic Pathways (SSPs) are indicated in the report with five high priority scenarios in Tier 1, comprising four groups (SSP1, SSP2, SSP3 and SSP5). SSP1 is a low challenges group presenting in Tier 1 with two scenarios; SSP1-1.9 and SSP1-2.6. These two scenarios reflect a 1.5 ^{0}C that is an ultimate goal under the Paris Agreement and a 2.0 ^{0}C presenting a sustainability corresponding to the previous scenario RCP 2.6. The middle of the road can be found in SSP2-4.5, presenting closely to the RCP4.5 of the AR5 scenario. SSP3-7.0 and SSP5-8.5 scenarios reflect a medium-high range, up to the highest level of AR6. SSP3-7.0 is in the regional rivalry of the socio-economic family, whereas SSP5-8.5 indicates a high emission scenario relating to the large use of fossil fuels of the 21st century [4].

To gain knowledge about climate change responses to climate systems. General Circulation Models (GCMs) that are the main tools for climate change works were employed. These models can develop climate projections related to future greenhouse gas emissions and socio-economic scenarios. The 50 GCMs and more than 20 institutions collaborate on the Coupled Model Intercomparison Project (CMIP6). For the 6th phase, the climate models, the atmosphere-ocean general circulation models (AOGCMs) and the Earth system models (ESM) calculate the future scenario projections using the concentration of greenhouse gases from all non-CO_2 [4]. Although the projection outputs generated from all GCMs mostly agree in the overview, the regional details among those GCMs should be considered. The differences between models result from various factors such as the model calculations, variability of climate systems and the implication of socio-economic relevance applied in the model. For these reasons, model variations can be noticeably observed; for example, some GCMs may result in dry conditions in a specific region while others may present wet incidents [5].

Precipitation fluctuation in both amount and trend on different temporal and spatial scales has been of great concern for policymakers given its impact on people's livelihood [6], especially in the SEA mentioned above. Drought and flood events are also strongly related to the magnitude of precipitation. An overview investigation of precipitation characteristics over this region should be worthy of notice for the new launch AR6 scenarios before the following model selection and downscaling process. Therefore, this study aims to investigate the differences of original GCM outputs to understand their precipitation characteristics: variations, trends and conditions under AR6 climate change scenarios. Ten available GCMs with only resolution around 100 km for all four scenarios in Tier 1 during 2015-2100 and historical simulations between 1850 and 2014 in the spatial scale of each grid cell were analyzed. Three statistical methods were employed in this study: coefficient of variation (CV), Mann-Kendall method (MK) and standardized anomaly Index (SAI). This research clearly defined the spatial differences of precipitation characteristics of all models and across the entire SEA.

2. Materials and Methods

2.1 Study area

Of the 11 countries in the SEA, 5 (Thailand, Burma, Laos, Cambodia, and Vietnam) are located on the mainland, an extension of the Asian continent. At the same time, the other 6 are island formations (Figure 1). The region is in a tropical zone, and similarities in climate can be found for all countries throughout the region. The agricultural sector is the main source of livelihood in most countries of this area, especially given that there has been a significant increase of land conversion from non-agricultural areas such as grasslands, forest areas and wetlands to cropland for higher yield productivities. Thus, these countries' GDPs have become even more vulnerable to climate change [1].

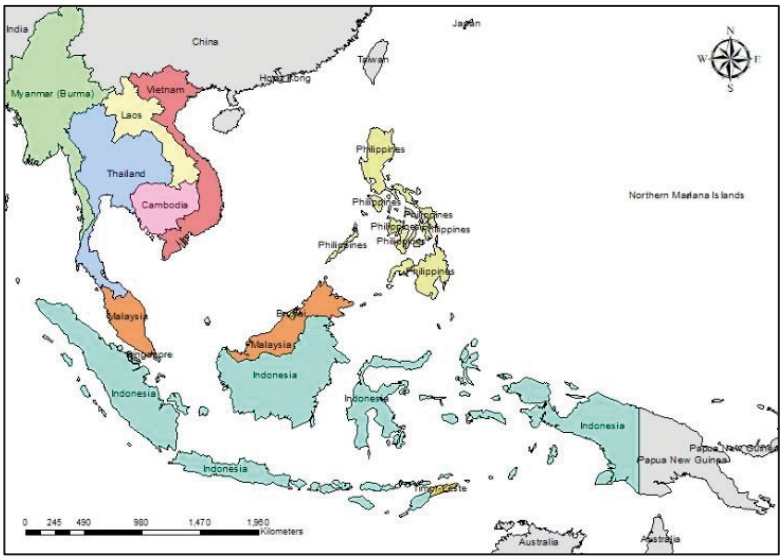

Figure 1. Countries in South East Asia

2.2 Data collection

Projected daily precipitation of four scenarios in Tier 1 (SSP1-2.6 SSP2-4.5 SSP3-7.0 and SSP5-8.5) during 2015-2100, including precipitation in the historical period (1850-2014) in CMIP6 generated from 10 GCMs were modelled. All selected GCMs are the Atmospheric-Ocean General Circulation Models (AOGCMs), which comprises biogeochemical function, for example, vegetation and some atmospheric chemistry in the model [4]. The differences among these 10 GCMs are the main components: land-ocean interactive dynamics, marine biological chemistry, and surface wave functions used to simulate atmospheric and hydrologic variables. The name of the models and their institutions are presented in Table 1. Only GCMs available for all four scenarios, including historical data, are considered in this study. These selected models have resolutions around 100 km. Only variant label of r1i1p1f1 where r, i, p and f refer to realization index, initialization index, physics index and forcing index respectively was selected.

Table 1 Selected GCMs used in this study

GCM	Institution	Abbreviation
CESM2-WACCM	National Center for Atmospheric Research, USA	CESM2
CMCC-CM2-SR5	Euro-Mediterranean Centre on Climate Change coupled climate model	CMCC-CM2
CMCC-ESM2	Euro-Mediterranean Centre on Climate Change coupled climate model	CMCC-ESM2
NorESM2-MM	Norwegian Earth System Model	NorESM2
TaiESM1	Taiwan Earth System Model	TaiESM1
MRI-ESM2-0	The Meteorological Research Institute, Japan	MRI-ESM2
GFDL-ESM4	Geophysical Fluid Dynamics Laboratory, USA	GFDL
INM-CM4-8	The Institute for Numerical Mathematics, Russia	INM-CM4
INM-CM5-0	The Institute for Numerical Mathematics, Russia	INM-CM5
MPI-ESM1-2-HR	The Max Planck Institute for Meteorology, Germany	MPI-ESM1

2.3 Statistical tests

This study employed three statistical methods widely used to estimate precipitation characteristics that were the coefficient of variation (CV), the Mann-Kendall test (MK) and the standardized anomaly index (SAI). The first and second methods were normally used to calculate variations and trends of precipitation based on the specific period. The last one can specify wet/dry years occurrences under the period of interest. Details of each method are presented below.

2.3.1 Coefficient of variation

The coefficient of variation (CV) is a statistic measure index used in this study to estimate rainfall variability. This index benefits to indicate which regions are facing the fluctuation of rainfall, leading to potentially high vulnerability for drought and water scarcity [7]. This method calculates the standard deviation of the rain averaged in a specific period. The CV range is between 0-100% and is classified into three groups. A region presents a CV value less than 20%, indicating low rainfall variability; 20-30% of CV and higher than 30% present medium and high rainfalls variability, respectively [8]. CV was widely used to investigate rainfall variability in various regions [9-11]. This indicator is computed as Equation 1, where $\boldsymbol{SD}$ and $\bar{\boldsymbol{X}}$ are standard deviation and mean values over the study period.

$$CV = \left(\frac{SD}{\bar{X}}\right) * 100 \tag{1}$$

2.3.2 Mann-Kendall test

The Mann-Kendall is the non-parametric statistical test for trend detection mostly used to examine increasing, decreasing or no-trend of rainfall time series. This method requires no prerequisite condition of the data and is normally applied to investigate the hydro-climatological data series in terms of spatial variation and temporal trends [12]. Many authors [13-15] have used this method to examine significant precipitation trends in different regions. The computation of the Mann-Kendall test considers n data time series containing two subsets of the data i and j where i = 1,2,3… n-1 and j = 1,2,3…n. These data are arranged in order time series and each one is compared to all subsequent data. Statistic S (Equation 2 and 3) is calculated and decreases if the data presented in a later period is lower than a data of a previous period and vice versa. The final set of S is all thus computational output.

$$S = \sum_{i=1}^{n-1} \sum_{j=i+1}^{n} sign(x_j - x_i) \tag{2}$$

$$sign(x_j - x_i) \begin{cases} +1 \; if \; (x_j - x_i) > 0 \\ 0 \quad if \; (x_j - x_i) = 0 \\ 0 \quad if \; (x_j - x_i) = 0 \end{cases} \tag{3}$$

Where x_i and x_j are annual precipitation of year i and j and $j > i$, respectively. n is the number of total data and $sign(x_j - x_i)$ is the result of equation 3 calculation. The standard normal statistic test (Z-test) is then calculated as Equation 4, whereas the variance of S can be computed using Equation 5

$$z \begin{cases} \frac{S-1}{\sqrt{Var(S)}} \; if \; S > 0 \\ 0 \; if \; S = 0 \\ \frac{S+1}{\sqrt{Var(S)}} \; if \; S < 0 \end{cases} \tag{4}$$

$$Var(S) = \frac{1}{18}[n(n-1)(2n+5) - \sum_{j=1}^{m} t_j(t_j - \;\; 1)(\;\; 2t_j + 5)] \tag{5}$$

Where n is the number of the tied group that is a zero difference between compared values and t_j is the number of data points in the t^{th} tied group. Positive / Negative Z value indicates an increasing/decreasing trend of precipitation.

2.3.3 Standardized Anomaly Index (SAI)

Standardized Anomaly Index (SAI) is commonly used to evaluate precipitation status in various areas [16-17, 10]. It was used to describe rainfall variability. The frequency of dry and wet incidents is also clarified by calculating annual rainfall events deviating from the average yearly rainfall in the study period. Negative\positive SAI values reflect less rainfall than normal, which is risky to drought\flood events. Equation 6 presents the method to compute SAI. x_i is the annual rainfall of year i and μ and δ is the average and standard deviation of long term rainfall period. SAI value can be classified into 7 groups indicated in Table 2.

$$SAI_i = \frac{(x_i - \mu)}{\delta} \tag{6}$$

Table 2 SAI classification

SAI	Category
2.0+	Extremely wet
1.5 to 1.9	Very wet
1.0 to 1.49	Moderately wet
-0.99 to 0.99	Near normal
-1.0 to -1.49	Moderately dry
-1.5 to -1.99	Severely dry
-2.0 and less	Extremely dry

3. Results and Discussion

Projected precipitation of ten GCMs according to AR6 climate change scenarios: SSP1-2.6, SSP2-4.5, SSP3-7.0 and SSP5-8.5, including historical simulation, were analyzed over the SEA region. Data in historical and scenarios simulations were considered during the 1850-2014 and 2015-2100 periods. Spatial precipitation variability, trend and condition grid by grid over the entire area are shown. The differences in precipitation characteristics among all ten models were revealed.

3.1 Precipitation variation of SEA under climate change scenarios

The coefficient of variation values (CV) of 10 GCMs with 5 scenarios (4 SSP (2015-2100) and historical simulations (1850-2014)) were calculated (Figure 2). CV was ranged in between 0-100% and then classified into three groups: Low (0-20%), Medium (20-30%) and High variation (>30%). Figure 2 presents all spatial distribution of CVs over SEA. During the historical period, high precipitation variation could be clearly seen in the six model outputs of CESM2, CMCC-CM2, CMCC-ESM2, NorESM2 TaiESM1 and MRI-ESM2. These models produced precipitation showing high variability in the southern and eastern parts of the region. In the south, high variability of precipitations had occurred in the Indian Ocean close to Indonesia. The North Pacific Ocean also exhibited high precipitation variation. The other models, GFDL, INM-CM4, INM-CM5, specified only a small area of high CV in the North Pacific Ocean. Only MPI-ESM1 presented high precipitation variability in the western and southern part of Thailand, west of Burma and some areas of the Philippines and Indonesia. Moderate precipitation variabilities were also presented with large regions of CESM2, CMCC-CM2, CMCC-ESM2, NorESM2 and TaiESM1and GFDL. CESM2 and NorESM2 simulated the moderate level in the area around the Philippine Sea, some parts of Vietnam, Indonesia and the Philippines; whereas CMCC-CM2, CMCC-ESM2, TaiESM1and GFDL exhibited moderate precipitation mostly in the South of SEA. Small areas of this level were also presented in INM-CM4, INC-CM5 and MPI-ESM1 located in the South of SEA.

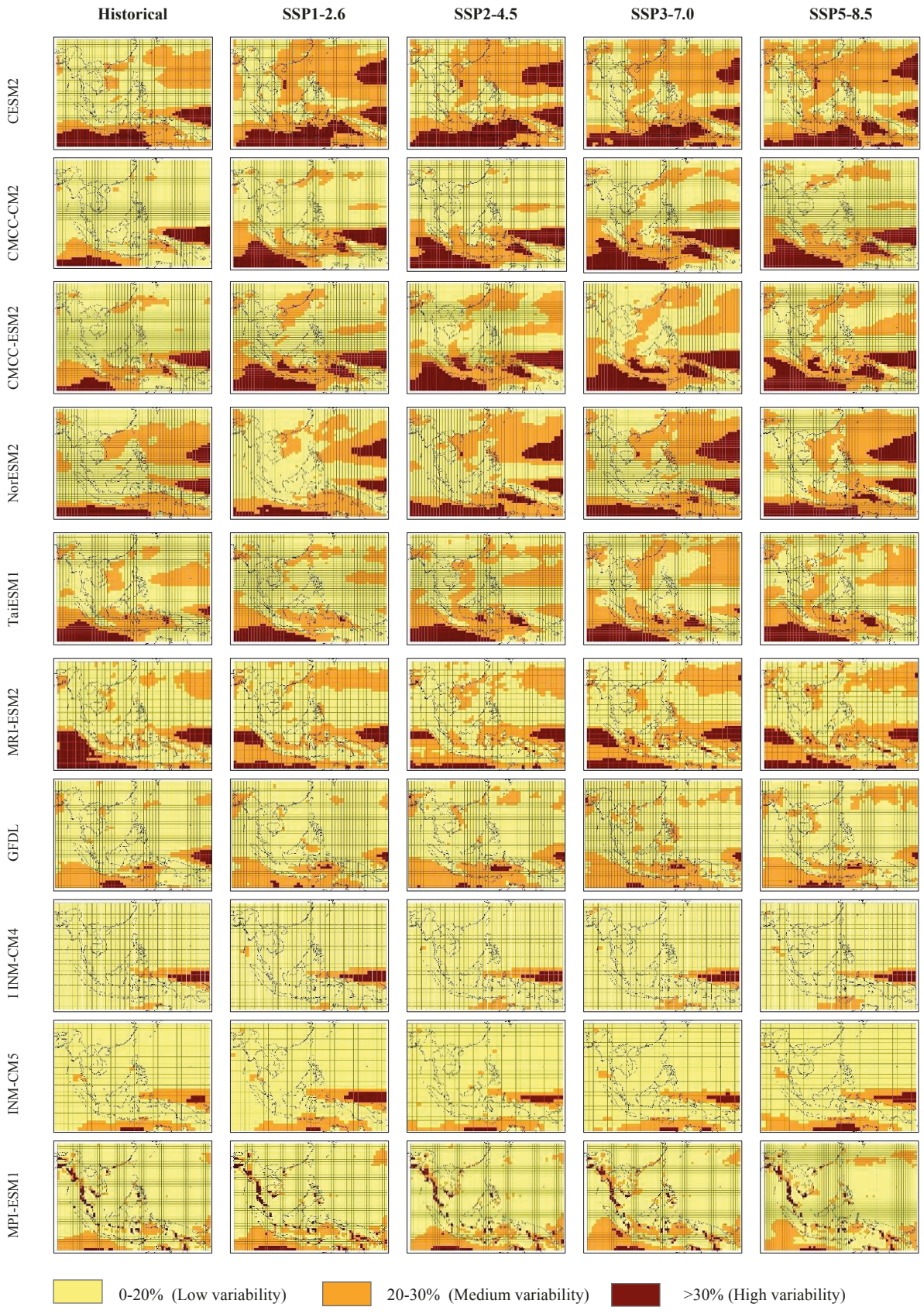

Figure 2. Spatial coefficient of rainfall variation over SEA (historical period: 1850-2014 / SSP: 2015-2100)

Projected precipitation under climate change scenarios using climate model strongly affected rainfall variability shown in CESM2 and NorESM2, especially for high levels of rainfall variation. CESM2 developed high rainfall variation in a larger area around the Philippines Sea and the Pacific Ocean in all SSP scenarios compared to the historical period showing no high variation around this area. NorESM2 also yielded similar results with a small area of high rainfall variation in these areas in the historical period. A larger coverage area could be seen for SSP scenarios. CMCC-CM2 and CMCC-ESM2 gave an increased range of CV around the Indian Ocean. A larger covering close to Indonesia could be noticeably found when four scenarios were forced into the models. Precipitation variation calculated from the other models during the historical period slightly differed from SSP scenarios.

In sum, if the spatial distribution of CVs were closely considered, it was found that GCMs could be divided into three groups. The first group, CESM2, CMCC-CM2, CMCC-ESM2, NorESM2, TaiESM1 and MRI-ESM2 mostly presented the highest CV in the same area with the same scenario. The second group was INM-CM4, INM-CM5 and GFDL showed a low level of CV in the large SEA area. Only small regions of the medium and high level of CV were found. Finally, MPI-ESM1 indicated a high variation of precipitation spread over in the mainland countries that were significantly different from others, as shown in Figure 2, with CV higher than 30% presenting in Thailand, Burma and some parts of Indonesia.

3.2 Precipitation trends of SEA under climate change scenarios

An overview of the spatial distribution of rainfall trends in SEA developed by 10 GCM models under historical and four SSP scenarios are shown in Figure 3. Statistical Z values were calculated for all grid cells across the region. Positive and negative values indicate an increase and decrease in rainfalls, respectively. The differences among the 10 model outputs could be noticed. In the historical simulations, CESM2 presented rainfall decreases in Burma, the North and the Northeast of Thailand, Laos, Cambodia, Vietnam and some parts of Malaysia and Indonesia similar to NorESM2, TaiESM1, MRI-ESM2, GFDL and INM-CM4. CMCC-CM2, CMCC-ESM2, INM-CM5 and MPI-ESM1 contradictorily showed rainfall increments in these countries.

Precipitation trends significantly changed when the models were applied with different scenarios. Increasing rainfalls were found in countries identified to have experienced rainfall decrease during historical periods (Burma, the North of Thailand, Laos, Cambodia, Vietnam, Malaysia, Indonesia, Brunei and Singapore) in CESM2 TaiESM1 and INM-CM4. In the scenario of SSP1-2.6, most models produced rainfall increases in most SEA countries except GFDL and MPI-ESM1. This event occurred in the Philippines, SEA and the Pacific. Increasing rainfalls for the entire region can be noticeably seen in TaiESM1 under SSP3-7.0 and SSP5-8.5, whereas SSP2-4.5 of this model and MPI-ESM1 under SSP1-2.6, SSP2-4.5 and SSP3-7.0 yielded rainfall decreases in most countries. These results were mostly consistent with [18], indicating a significant increase of precipitation under SSP5-8.5 rather than SSP2-4.5. All scenarios of MPI-ESM1exhibited a negative trend according to the Mann-Kendall test, while most of the Z results exhibited confidence intervals less than 90%.

3.3 SAI index of SEA rainfalls under climate change scenarios

SAI values of every year between 1850-2100 were calculated for all grid cells (Figures 4 and 5). SAI was initially categorized into seven classes. However, in this research it was modified to classify into three categories: very to extremely wet (SAI of higher than 1.5 to >2.0); severely to extremely dry (SAI of lower than -1.5 to <-2.0), and normal (SAI of -1.5 to 1.5) to mainly focus on extreme events of both wet and dry incidents. Percentages of events (a number of years) were calculated and compared to all years for the historical period (1850-2014: 165 years) and SSP scenarios (2015-2100: 86 years). Only extreme situations of both wet and dry events are explained below.

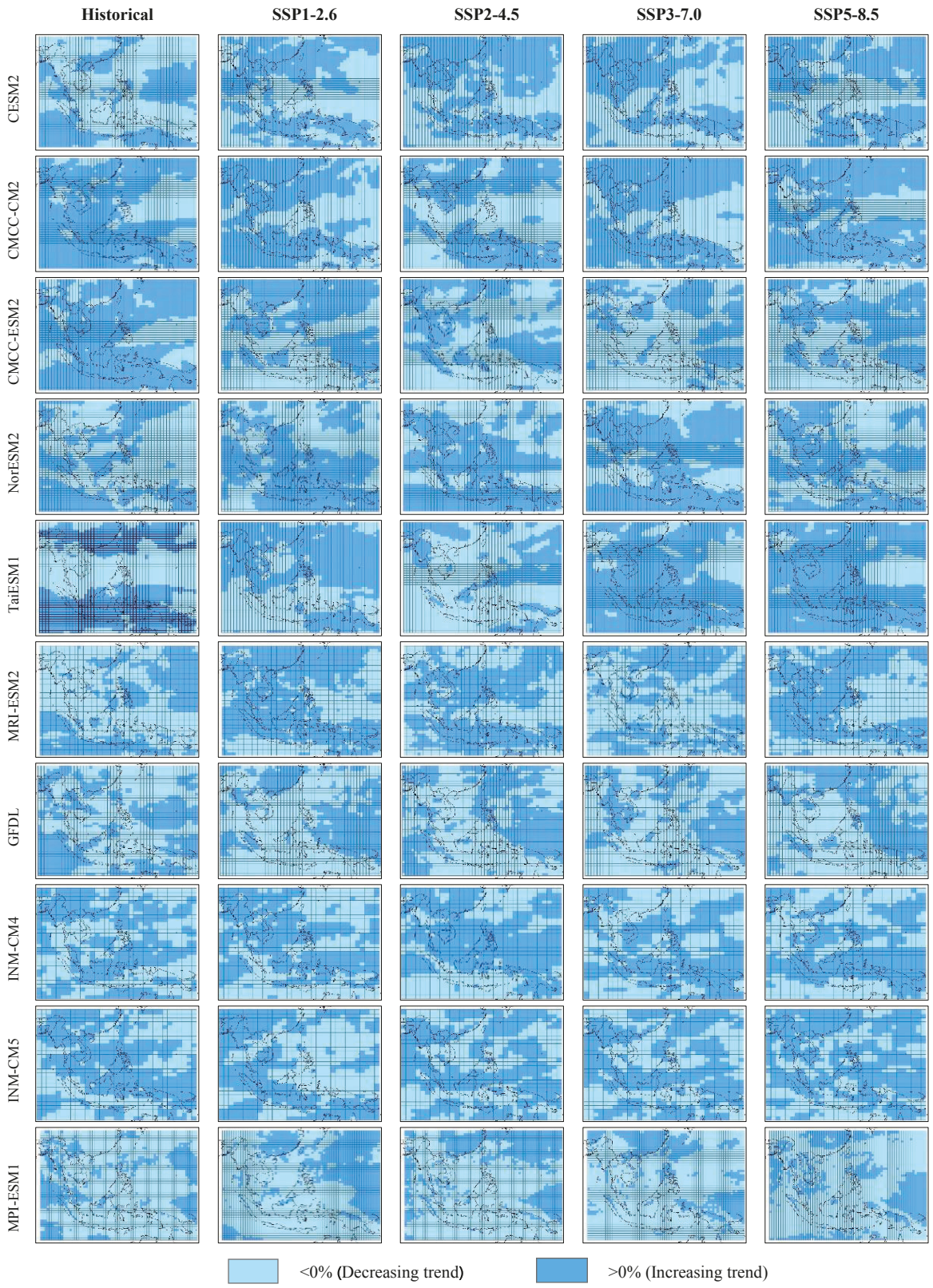

Figure 3. Spatial Mann-Kandell over SEA (historical period: 1850-2014 / SSP: 2015-2100)

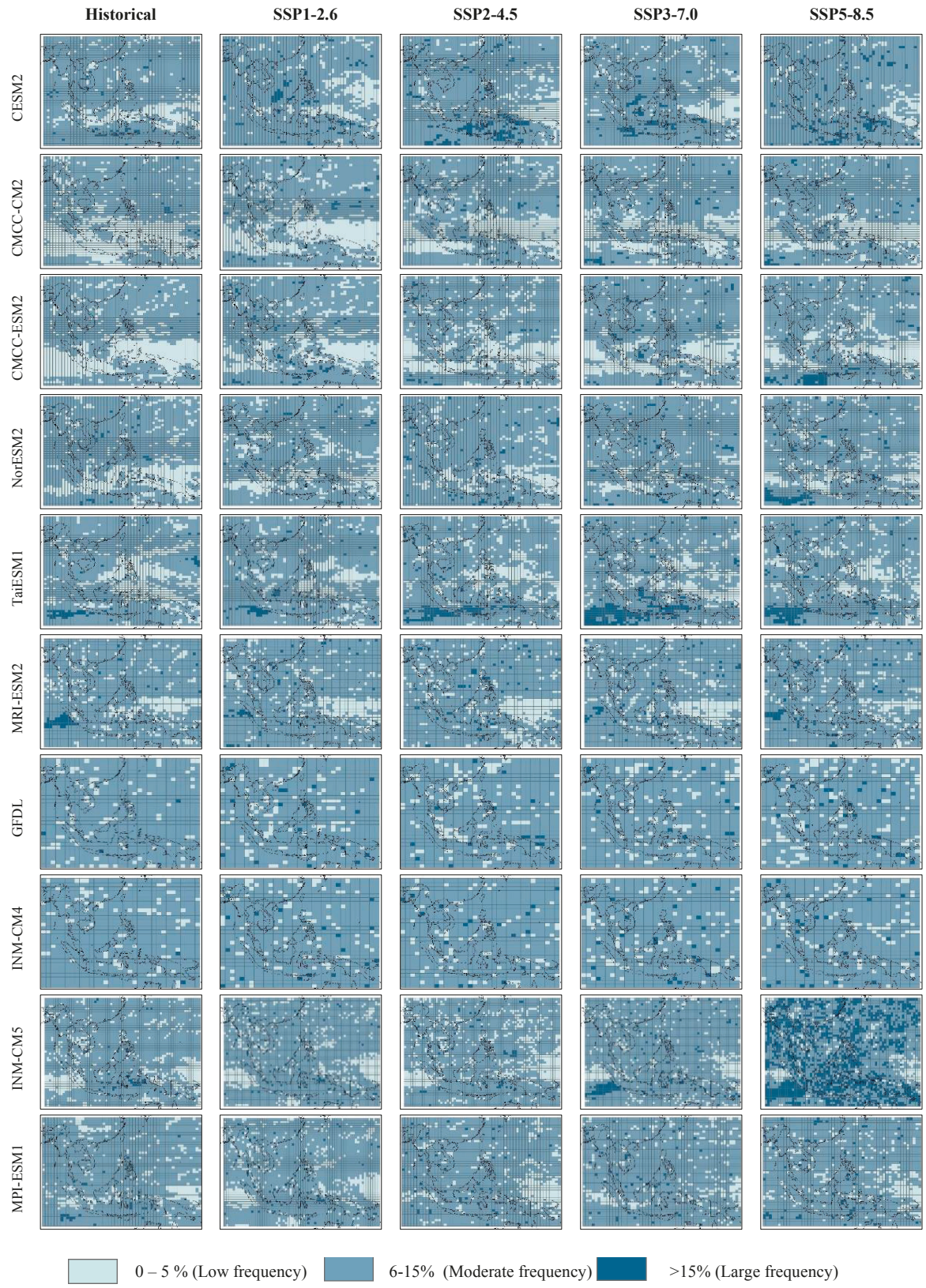

Figure 4. SAI very to extremely wet over SEA (historical period: 1850-2014 / SSP: 2015-2100)

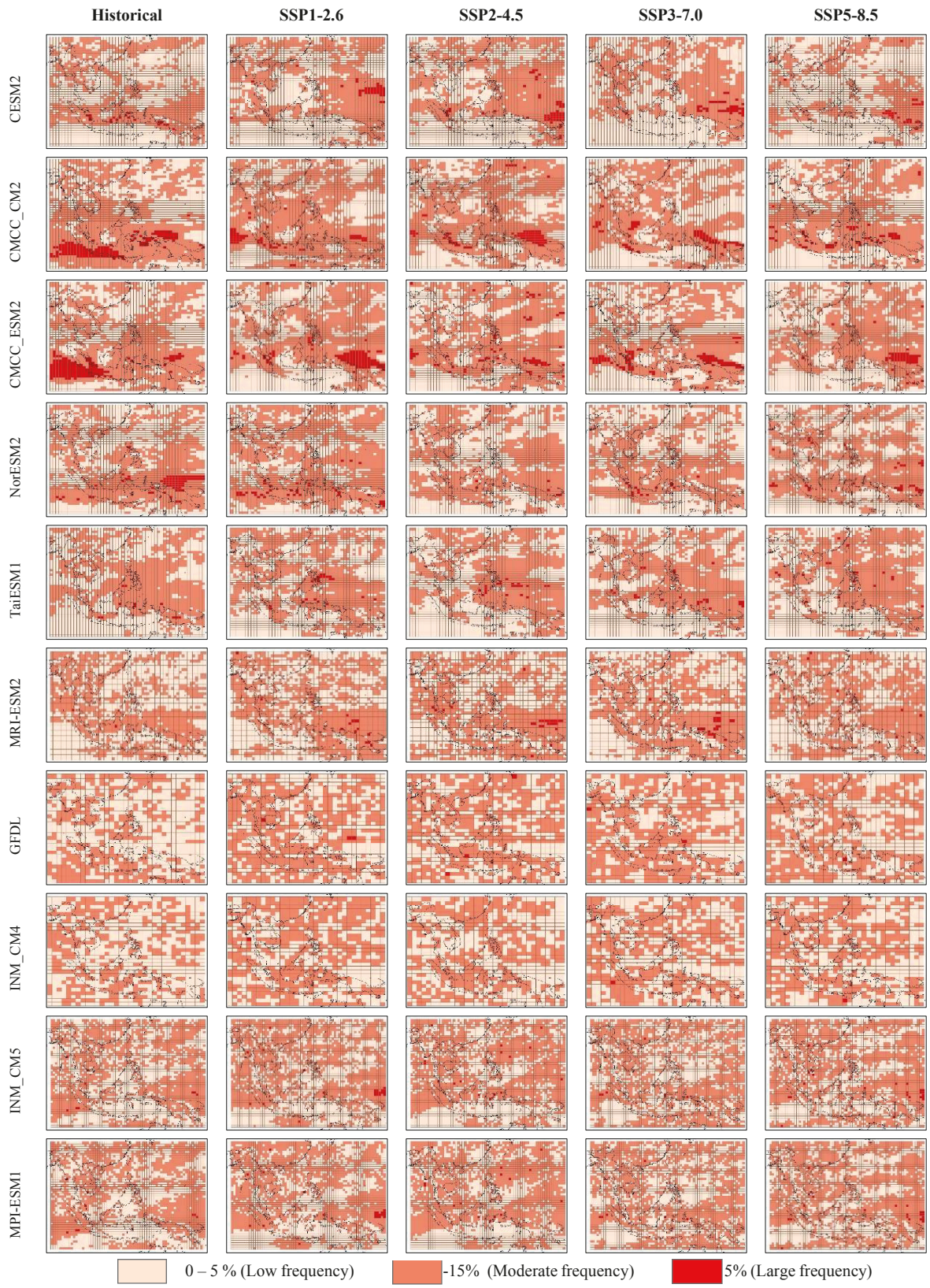

Figure 5. SAI severely to extremely dry over SEA (historical period: 1850-2014 / SSP: 2015-2100)

3.3.1 SAI-very to the extremely wet incident

The frequencies of rainfall conditions in very to extremely wet occurrences are shown in Figure 4. All precipitation simulations showed that very to extremely wet years often occurred in the range of 0-20% for all scenarios. However, most models simulated thefrequency of very to extremely wet occurrence for all over the region, around 6-15%, except the projection of INM-CM5 under SSP5-8.5, indicating this incident as more frequent than others. The differences of model simulation are noticeably presented. During the historical period, most countries faced extremely wet events in moderate frequency (6-15%) in various models except CESM2, CMCC-CM2, CMCC-ESM2 and NorESM2, showing a low-frequency level in most areas of Indonesia and the North Pacific Ocean. High precipitation events occurred with large frequency (>15%) in the Indian Ocean close to the West of Indonesia in TaiESM1 and MRI-ESM2.

Significant differences between historical periods and SSP scenarios were shown in various models. CESM2 exhibited a higher frequency of extreme events with more than 15% around the southern part of Indonesia with SSP2-4.5, SSP3-7.0 and SSP5-8.5, similar to TaiESM1. CMCC-ESM2 and NorESM2 presented a number of very-extreme wet with a high amount indicated in SSP5-8.5. Moderate frequency of these extreme events occurred covering most regions in GFDL and INM-CM4 in both historical period and SSP scenarios.

3.3.2 SAI-Severely to Extremely Dry conditions

A similar category of the events' frequency was also conducted with very to extremely dry conditions (Figure 5). Moderate frequency of drought conditions expanded all over the region for all models. CMCC-CM2, CMCC-ESM2, and NorESM2 historical simulations showed that extremely dry conditions often occurred around the South and West of Indonesia and the Indian Ocean. Countries in the mainland, for example, Thailand, Burma, Laos, Cambodia and Vietnam, mostly faced drought conditions during the historical period on a moderate scale (6-10%), resulting from most models.

According to climate change scenarios, SAI calculation showed a slight difference compared to the historical period. Moderate frequency of drought events occurred in large areas around the Philippines Oceans, whereas a small area of high frequency was also found for CESM2. CMCC-CM2 and CMCC-ESM2 gave a high frequency of drought conditions in the same area as CESM2. In contrast, the driest events around the South of Indonesia of these two models occurred in the historical period switched to the low and moderate frequency in all SSP scenarios. A large number of very to extremely dry incidents occurred across only a small area under climate change scenarios of NorESM2, TaiESM1 GFDL, MPR-ESM2 and MPI-ESM1.

4. Conclusions

Climate change's impact on various areas has been strongly evident, especially in Southeast Asia (SEA). The IPCC's sixth assessment report presents a future socio-economic projection of four scenarios for Tier1 with SSP1-2.6, SSP2-4.5, SSP3-7.0 and SSP5-8.5. This study investigated the difference of precipitation projection in spatial distribution under SSP scenarios and the historical period of ten models. These ten models had a spatial resolution of around 100 km with a variant label of r1i1p1f1. Variation, trend and condition of precipitations were analyzed using the coefficient of variation (CV), the Mann-Kendall test and Standardized Anomaly Index (SAI). Results revealed that significant differences between models were found. Six models (CESM2, CMCC-CM2, CMCC-ESM2, NorESM2 TaiESM1 and MRI-ESM2) clearly show high-moderate precipitation variation in the same area around the Indian Ocean and the North Pacific. These results were significantly different compared to the rest of the models. The Mann-Kendall test presented high variations among ten models. Eight models showed precipitation increments in most mainland countries for most scenarios except GFDL and MPR-ESM1. Finally, SAI was calculated for extremely wet and dry occurrences. The highest frequency of extremely wet events was seen with INM-CM5 under SSP5-8.5, whereas all models gave a majority range of extreme event occurrences around 6-10% of the study period. The increase of precipitation occurrences with extreme events in Southeast Asia were also found in [19]. Three models (CESM2, CMCC-CM2 and CMCC-ESM2) noticeably presented a high frequency of dry situation in variance from other models, which predominately showed only a low-moderate frequency of drought. The results of this study showed the differences among all ten models. Some models can be categorized in the same group whereas other GCMs presented significant differences. [20] also mentioned the performance difference among GCMs with different metrics. Therefore, researchers should pay more attention to selecting the output of

GCMs for continuing working on climate change areas. Considering a large number of GCMs or multi-model ensembles were recommended. This should notify researchers for model selection in the next step of local study on precipitation under climate change scenarios.

5. Acknowledgements

This study was supported by the Faculty of Engineering at Kamphaengsaen campus, Kasetsart University, Thailand. Also, the authors (s) would like to thank Dr. Winai Chaowiwat, a senior researcher (water resources engineering) at Hydro-Information Institute, for the valuable knowledge.

Author Contributions:

Funding: This research received no external funding

Conflicts of Interest: The authors declare no conflict of interest.

References

1. Asian Development Bank. The Economics of Climate Change in Southeast Asia: A Regional Review 2009; ISBN 978-971-561-787-1.
2. Hijioka, Y.; Lin, E.; Pereira, J.J.; Corlette, R.T.; Cui, X.; Insarov, G.E.; Lasco, R.D.; Lindgren, E.; Surjan, A. Asia. In: Climate Change: Impacts, Adaptation, and Vulnerability. Part B: Regional Aspects. Contribution of Working Group II to the Fifth Assessment Report of Intergovernment Panel on Climate Change 2014.
3. National Intelligence Council. Southeast Asia: The Impact of Climate Change to 2030: Geopolitical Implications. Conference Report CR 2010-02 January 2010.
4. Meinshausen, M.; Nicholls, Z.R.J.; Lewis, J.; Gidden, M.J.; Vogel, E.; Freund, M.; Beyerle, U.; Gessner, C.; Nauels, A.; Bauer, N.; Canadell, J.G.; Daniel, J.S.; John, A.; Krummel, P.B.; Luderer, G.; Meinshausen, N.; Montzka, S.A.; Rayner, P.J.; Reimann, S.; Smith, S.J.; Berg, M.; Velders, G.J.M.; Vollmer, M.K.; Wang, R.H.J. The shared socio-economic pathway (SSP) greenhouse gas concentration and their extensions to 2500. *Geoscientific Model Development.* 2020, 13, 3571-3605.
5. Fajardo, J.; Corcoran, D.; Roehrdanz, P.R.; Hannah, L.; Marquet P.A. GCM compareR: a web application to assess differences and assist in the selection of general circulation models for climate change research. *Methods in Ecology and Evolution.* 2020, 11, 656-663.
6. Raty, O.; Raisanen, J.; Ylhaisi, J. Evaluation of delta change and bias correction methods for future daily precipitation: intermodel cross-validation using Ensemble simulations. *Climate Dynamics.* 2014; 42, 2287-2303.
7. Charles J. V.; Douglas, E.M.; Green, P.A.; Revenga, C. Geospatial indicators of emerging water stress: an application to Africa. *Ambio.* 2005, *34*(3), 230-236.
8. Bekele, F.; Mosisa, N.; Terefe, D. Analysis of current rainfall variability and trends over Bale-Zone, South Eastern Highland of Ethiopia. *SF Journal of Global Warming.* 2017, 1:2.
9. Pujiastuti, I.; Nurjani, E. Rainfall pattern variability as climate change impact in the Wallacea Region. IOP Conf. Series: *Earth and Environmental Sciences.* 2017, 148. 012023.
10. Eshetu, G.; Johansson, T.; Garedew, W. Rainfall trend and variability analysis in Setema-Gatira area of Jimma, Southwestern, Ethiopia. *African Journal of Agricultural Research*. 2016, *11*(32), 3037-3045.
11. Archite, M.; Caloiero, T.; Walega, A.; Krakauer, N.; Hartanim T. Analysis of the spatiotemporal annual rainfall variability in the Wadi Cheliff Basin (Algeria) over the period 1970 to 2018. *Water.* 2021, 13, 1477.
12. John, A.S.; Brema, J. Rainfall trend analysis by Mann-Kendall test for Vamanapuram River basin, Kerala. *International Jounral of Civil Engineering and Technology*. 2018, *9*(13), 1549-1556.
13. Hussain, F.; Nabi, G.; Boota, M.W. Rainfall trend analysis by using the Mann-Kendall test & Sen's slope estimates: a case study of district Chakwak rain gauge, Barani area, Northern Punjab province, Pakistan. *Science International (Lahore).* 2015, *27*(4), 3159-3165.
14. Gadedjisso-Tossou, A.; Adjegan, K.L.; Kablan, A.K.M. Rainfall and temperature trend analysis by Mann-Kendall test and significance for rainfed cereal yields in Northern Togo. *Sci.* 2021, *3*(17). 1-20.
15. Ahmad, I.; Tang, D.; Wang, T.; Wang, M.; Wagan, B. Precipitation trends over time using Mann-Kendall and Spearman's rho tests in Swat River basin, Pakistan. *Advances in Meteorology*. 2015, 431860.

16. Koudahe, K.; Kayode, A.J.; Samson, A.O.; Adebola, A.A.; Djaman, K. Trend analysis in standardized precipitation index and standardized anomaly index in the context of climate change in Southern Togo. *Atmospheric and Climate Sciences.* 2017, 7, 401-423.
17. Bayable, G.; Amare, G.; Alemu, G.; Gashaw, T. Spatiotemporal variability and trends of rainfall and its association with Pacific Ocean Sea surface temperature in West Harerge zone, Eastern Ethiopia. *Environmental Systems Research*. 2021, *10*(7). 1-21.
18. Supharatid, S.; Nafung, J.; Aribarg, T. Projected changes in temperature and precipitation over mainland Southeast Asia by CMIP6 models. *Journal of Water and Climate Change.* 2021, doi.10.2166/wcc.2021.015.
19. Ge, F.; Zhu, S.; Luo, H.; Zhi, X.; Wang, H. Future changes in precipitation extremes over Southeast Asia: insights from CMIP6 multi-model ensemble. *Environmental Research.* 2021, 16, 024013.
20. Lqbal, Z.; Shahid, S.; Ahmed, K.; Wang, X. Evaluation of CIMP6 GCM rainfall in mainland Souteast Asia. *Atmospheric Research.* 2021, doi.10.1016/j.atmosres.2021.105525.

JSTR
ASEAN Journal of Scientific and Technological Reports

Research article

Production Line Process Improvement with Process Reengineering – A Case Study In Garment Factory

Yanin Palasri[1] and Somjai Boonsiri[2]

[1] Department of Mathematics and Computer Science, Faculty of Science, Chulalongkorn University, Bangkok, 10330; 6278008023@student.chula.ac.th
[2]Department of Mathematics and Computer Science, Faculty of Science, Chulalongkorn University; somjai.b@chula.ac.th
* Correspondence: E-mail: somjai.b@chula.ac.th

Abstract: ABC is struggling to reach daily production objectives and has low productivity, which is one of the productline line process problem. Business Process Reengineering (BPR) employs process redesign heuristics to enhance an existing production line process using an assessment technique and fit-gap analysis. The simulation tool is used to model the production line process redesign. After adopting the provided approach and conducting the simulation, the company's production productivity and service level increased by about 45%. The required simulation resulted in critical measurements such as manufacturing capacity and lead-time. This research demonstrates the redesign production line process that must be followed to archive this artefact.

Keywords: business process reengineering; fit-gap analysis; production line process; redesign heuristics

Citation: Palasri, Y.; Boonsiri, S. Production Line Process Improvement With Process Reengineering – A Case Study In Garment Factory. *ASEAN J. Sci. Tech. Report.* **2022**, *25*,(1), 24-35. https://doi.org/10.55164/ajstr.v25i1.244708

Article history:
Received: July 27, 2021
Revised: December 13, 2021
Accepted: December 16, 2021
Available online: March 3, 2022

Publisher's Note:
This article is published and distributed under the terms of the Thaksin University.

1. Introduction

Nowadays, the garment and textile industries are one of the important business sectors that drives Thailand's GDP and export revenue growth every year [1,2]. Many Computer Integrated Manufacturing Systems are widely distributed in the manufacturing industry. It aids in the standardisation of the production line process and increases efficiency to a certain extent. The existing management information systems face difficulties in keeping up with the fast-changing pace of the complex business models and the diversified customer needs [3]. With the emergence of new technologies such as Enterprise Resource Planning (ERP) software, it is widely used among medium to large businesses' scale. The various benefits have been provided to the organisation for the post-implementation, such as reducing the production cost, increasing service quality, and raising process efficiency in the long run [4].

In this research, the case of ABC garment manufacturing company is brought up to study about production line process. ABC garment manufacturing is a company whose subsidiaries manufacture men's and women's clothing for export to Europe, Canada, Japan, the U.S.A., and Russia. The company has factories in Thailand and Vietnam. The existing production line process and business operations of Thailand's manufacturing are overly reliant on reports and redundant procedures, resulting in missed daily output. It is expected that

Enterprise Resource Planning (ERP) software can facilitate the production process complexity and eliminate redundant tasks. The assessment approach and fit-gap analysis have been applied in this research. However, the ERP software implementation consumes longer time than expected with the analysis result. Plus, the standard functions of ERP software do not support the business requirements, and a customised program is required. Therefore, we have changed the approach to applying the Business Process Reengineering (BPR) as the proposed methodology based on our new analysis described in Section 4.

Following the suggested methodology and solution definition, the simulation tool is used to model the new redesign production process to determine its efficacy. To ensure efficiency, manufacturing capacity, lead time, and daily production target achievement are considered critical measurements of the expected outcome.

2. Current Issues

It is dedicated to manufacturing original equipment manufacturers or OEM for the top world brand name. In addition, garment manufacturing is a vast process. All operations are done in different departments in a garment factory. Also, the production line process is a sequential process starting from designing, sampling, laying, marking, cutting, stitching, checking, finishing, pressing, and packaging [5]. Therefore, the garment industry required adaptable and flexible technology to track and control the entire production line process. The QR code has been used for monitoring every production step, and the in-house program is developed as the core back-end system connected to the Oracle Database. On the other hand, this firm has suffered from low productivities, resulting in the inability to meet the daily output target. The problems were analysed using the cause-effect diagram, as shown in Figure 1.

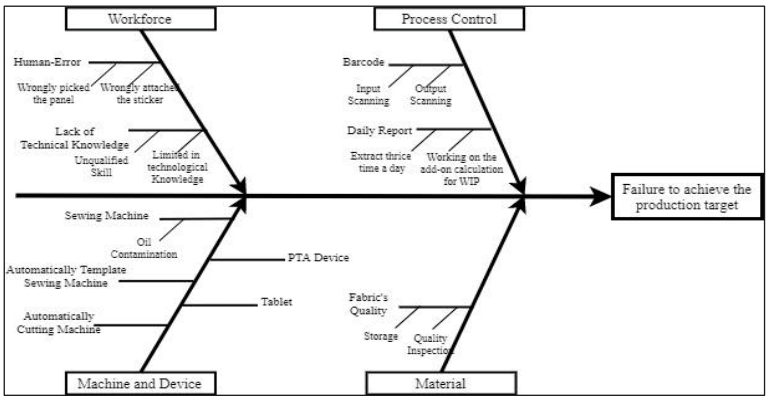

Figure 1. Cause-Effect Diagram

From Figure 1, many possible causes were identified as the root causes of the problem in the production line process, such as lack of worker's awareness, lack of technical knowledge, oil contamination from the sewing machine, and time-consuming manual calculation of the daily report. The officer and the foreman who mainly control the production line process have relied too heavily on the report.

3. Related Work

The main purpose of the literature review is to bring up the prominent point of each related work and discuss, based on the authors' perspective, that could support the core objective of this research. The authors have concluded the strong point and summarised it in the below section

A). Improvement of shirt making production through lean manufacturing – Identify the issues that occurred in the garment industry**.**

The most important aspect of this literature study is constructing a cause-effect diagram to identify prevalent difficulties in the garment business. The main factors that affect the garment industry are labour

rigidity, instability, political changes, regulations, informality, low productivity and low competitiveness [6]. This review has brought up the case study of a small company that manufactures the prima cotton polo shirts. It is found that this company suffers from the product's delivery to customers, and the problem was analysed using an Ishikawa diagram (Cause-Effect diagram).

B). The Dependency of the department in the garment industry – Identify the dependency of department and workstation in the garment industry

The activity diagrams have represented the business process of garment manufacturing. The problems become more evident when the researchers model the strategic dependencies between departments, the services they offer, and the constraint they impose on each other [3]. In such a case, the researchers have decomposed the business processes of garment manufacturers. They derive the dependencies among different departments by applying the i* modeling framework and a service-oriented approach.

The i* model has been specially developed based on the early requirements in this literature. There are two basic models in the i*framework: the strategic dependency (SD) model and the strategic rationale (SR) model. The strategic dependence illustrates the connection between different actors in achieving goals, performing tasks, and providing resources. Through understanding the dependencies between actors, the enhancements and weaknesses of goals and tasks could be analysed [3]. As a result of this literature research, the authors used the i* model to deconstruct the production line process and capture the diagram displayed in section 4, Figure 3.

C). Evaluation of Transportation Reservation Management Module Usage in ERP system at PT. XYZ – Apply fit-gap analysis & technology acceptance model to the research

This literature carried out the Fit gap analysis method to understand and compare installed systems (TRM) with existing requirements. Then, Technology Acceptance Methodology (TAM) model was applied. It is expected that TAM can identify the factors that can influence user behaviour in accepting and using the system TRM at PT.XYZ [7]. Fit Gap analysis has been conducted after receiving the input data from PT.XYZ company. Five columns have been identified: Business requirement, describe existing solution, priority, degree to fit, gap description and new capabilities. After performing Fit Gap Analysis, the TAM has been used to find out the user's acceptance towards the system TRM. The results of the TAM calculation will be compared with the hypothesis that the authors have previously determined [7].

In short, the fit-gap analysis and TAM model have carried out that the features of the TRM system are still not following the requirement or the system design request and many features need to be developed. Therefore, the authors have foreseen the practical use and advantage of the two methodologies; therefore, fit-gap analysis is selected to be applied as one of the research methodologies. In the TAM model and the authors' perspective, the tool is more involved in people behaviour than the process flow itself.

4. Research Methodology

The research methodology has been developed based on business process management (BPM). The BPM is the discipline of improving a business process from end to end by analysing it, modelling how it works in different scenarios, executing improvements, monitoring the improved process and continually optimising it [8]. Referring to the business process management textbook [9], the process consists of process discovery, analysis, process redesign, process implementation, process monitoring, and control.

A). Process Discovery

The As-Is production line process in ABC garment manufacturing is identified by the creation of the production process flow, as shown in Figure 2. After the planning process is done by the planning/IT/IE

department, the fabric will be issued out from the warehouse and directly sent to the 5LAS process, as displayed in Figure 2.

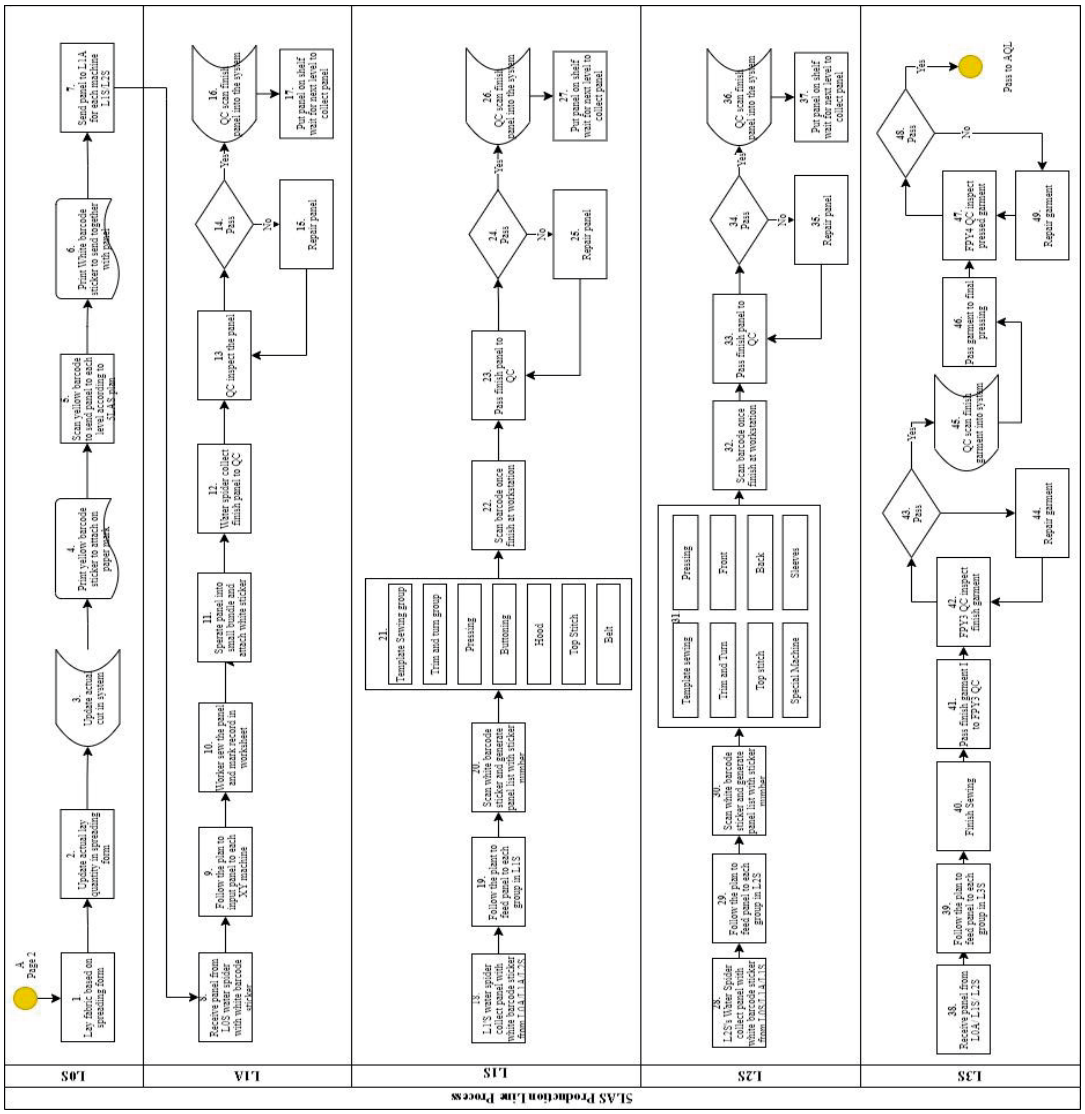

Figure 2. 5LAS Production Line Process

B). Process Analysis

In the process analysis, two tools have been applied: Cause-Effect diagram and Fit-gap analysis. The Cause-Effect diagram is used to identify the root causes of the existing production process problem as described in Figure 1. After the critical issues have been identified, the fit-gap analysis will address how well the system under consideration fits the proposed solution.

C). Process Redesign

Once the fit-gap analysis of each problem area is identified in Table 1, we will know the gap between the As-Is and To-Be production line processes. Two solutions are proposed:

- Develop a customised program to auto-generate the report, including the manual calculation which the officer currently does
- Redesign the production process based on the Business Process Reengineering (BPR) – Redesign heuristics

Firstly, the core production process in ABC garment manufacturing is the 5LAS process. The standard function of ERP software to generate the report automatically does not support the production process complexity. Therefore, the customised program has been proposed to develop the ERP software as the new capacity to reduce or eliminate these gaps. However, the customised program is required to create on ERP software, and the implementation takes a long time as a year based. Hence, we have shifted the plan of ERP software implementation to propose another solution.

Another proposed solution is to redesign the production process based on Business Process Reengineering (BPR). It is a process in which the enterprise can significantly improve some key aspects of the enterprise's performance, such as cost, quality, service, and speed [10]. We have redesigned the production process based on the redesign heuristics and adjusted some parameters from the enterprise's performance. The new production process is tested and simulated using [11]. The OXCLOSE clothing style's production process is brought up to be a case study of the production process and redesign in this research.

D). Process Implementation

The last step is to simulate the redesign production process of clothing styles H06_OXCLOSE, a made-to-order from ABC's customer, to ensure that the proposed solution improves the current production process. The simulation input consists of process flow, resources, and the initial value of decision parameters.

E). Process Monitoring and Controlling

After the simulation, the production capacity and lead time of each OXCLOSE's clothing part from the As-Is/To-Be production process are compared. We expect the production capacity to increase with the comparison and the production lead time decreases, respectively.

5. Experimental Details

A). Process Analysis and Fit Gap Analysis

Referring to the literature review, the concept of the dependency of the department in each garment company [3] has been applied to the production line process. Each clothing style has a different 5LAS production line process flow in which currently this process is managed and controlled by the officer. We have applied the model and analysis approaches covering a different perspective of the production process flow. However, each clothing style's 5LAS production line process is differently considered by the dependency among the workstations, goals, and dependency relationship modelling process. Therefore, we can't model the standardised 5LAS production line process template. Instead, a high-level of the overall production process has been constructed in Figure 3.

The dependency tasks of each department are represented in Figure 3. It consists of five departments: Planning/IT/IE (Industrial Engineering), MIM (Merchandising), planner maker, warehouse, OB/TPE and two core processes: L0A and 5LAS. The diagram starts with the MIM department receiving the order confirmation from the planning department. Then, the MIM department will create the SO (Sales Order) and BOM (Bill of Materials) in the system. This indicates the dependency among two departments that the MIM department must wait until it receives the order confirmation from the planning department. The dependence is well described by the symbol of the connector connected between two departments

After getting essential data for analysis, we have conducted the fit-gap analysis template shown in below table:

Table 1. Fit Gap Analysis of ERP Software Implementation

		ERP Software Implementation		Business Process Reenginerring	
Problem Area	*Existing Solution*	*Gap between existing & new*	*New Capacity needed to reduce or eliminate gap*	*Gap between existing & new*	*New Capacity needed to reduce or eliminate gap*
Relied too heavily on the report. The operation can't start until the report is generated	Most of the officers and workers felt indifferent toward the number of current reports as they have continued doing the same operation.	The process of each clothing style is very complex to automate on the system, also the standard function of ERP software is not supporting such kind of process complexity.	The new customized program is required to develop on the ERP software to support the process variety and complexity.	To apply the automation - one of the re-design heuristics approach. Data sharing (Intranets, ERP) Similarly to the proposed solution of ERP implementation. The standard function of ERP may not support the clothing style complexity	The new customized program is required to develop on the ERP software to support the process variety and complexity.
Fail to achieve daily production target	The officer and foreman need to work closely to the workers. They have monitored and controlled the production process by QR code tracking and manually update the daily report to identify which process/ step is delayed which possibly causing the slowdown in entire production process	The external device such as QR code scanner and QR code reader needs to connect to ERP system. The cost of infrastructure's setting and maintenance may high. Also as mentioned in point no#1, the process of each clothing style is too complex to automatically generate from the system in which the manual calculation is the process after the report is generated.	The new customized program is required develop on the ERP software to support the process variety, complexity, and manual calculation.	Once the production process is re-designed based on the re-design heuristics approach. The new production process is required to test the effectiveness using the simulation model or tool.	Define the simulation approach (Simulation tool/model, expected result and result measurement) as it is required to prove the new production process efficiency
Low productivity	The management team has set up weekly meeting for the workers who work in the assembly process. The purposes are to brainstorm, share and gather the idea about the causes of the low productivity	N/A	N/A		

From Table 1, we have proposed two solutions: ERP software implementation and business process reengineering. In each solution, the gaps of the proposed solutions are identified in column "Gap between existing & new", and the new capacity has been suggested to eliminate the gap of the new solution. It can be seen from Table 1 that the ERP implementation solution is required a new customised program to support the process complexity. Moreover, the ERP implementation and custom program development takes a long time, like a year-base. Hence, we have dropped this proposed solution and focus more on the business process reengineering solution

B). Design the new process

The Business Process Reengineering (BPR) is selected as the new approach to solving the current problems in ABC Manufacturing's production process. OXCLOSE clothing style is made to order that contains production process complexity. The OXCLOSE consists of 11 clothing parts, and each part will be embodied at the end of the production process. As per process analysis, we detected some parameters that reduce production process efficiency. One of the OXCLOSE's clothing parts, the hat, consists of many dependency

work and sub-process. It is the relationship in which a task relies on one or more tasks to be performed in a certain order before it is marked complete. We have created a histogram in Figure 4 to describe each clothing part's production standard time's frequency. It can be that there are two clothing parts of Collar and Hat with standard time; 6.86 and 14.11 min respectively contained the most time-consumed production process. Hence, the collar and hat's clothing parts are the key process that require the BPR consideration.

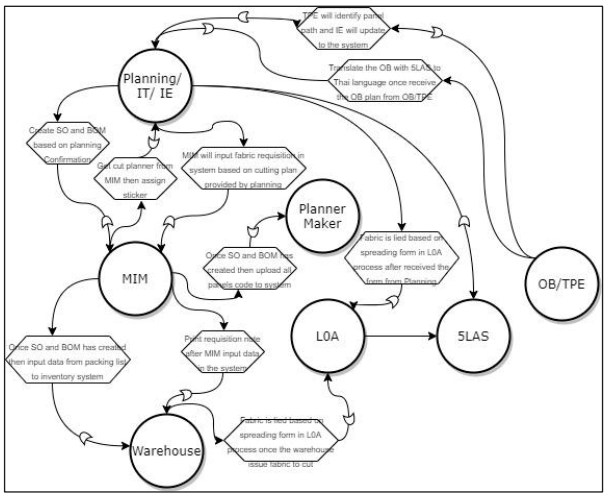

Figure 3. Dependency of departments in ABC garment manufacturing company

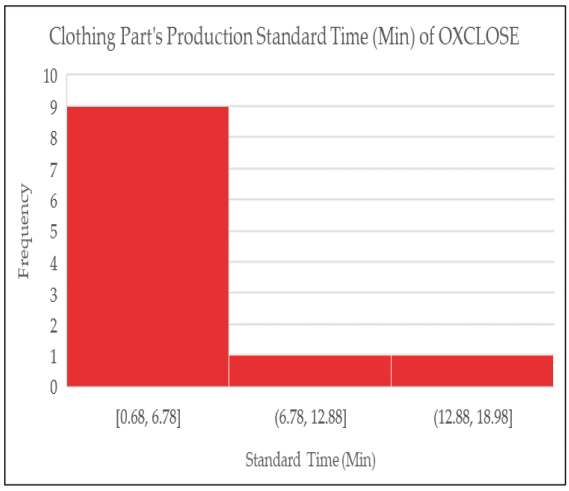

Figure 4. Clothing Part's Production Standard Time (Min) of OXCLOSE

Table 2. OXCLOSE_7 Subprocesses flow panel

Clothing Part	Step Sequences					
	1	2	3	4	5	6
Hoodie Piece 2 (CHO)	B12	B61	B31			
Hoodie Piece 1 (SHD)	B12	B61				
Hoodie Lining (174)	B12	B31	B61			
Collar (P1)	B12	B31	B41	B12	B51	
Bottom Collar (UCL)	B13	B31				
Flap Pocket (HIW)	B13	B21	B31	B41		
Sleeve Straps (P10)	B21	B31	B41			
Placket Piece (FAC)	B41					
Front Placket's Hoodie (HFF)	B12					
Placket Base (HFN)	B12	B31				
Hat (109)²	B13	B21	B31	B61	B51	B71

Hat $(109)^2$ = SHD+CHO+HFN+HFF+174

The redesign heuristics [12] are applied with the current production process of the OXCLOSE clothing style. As per the investigation, 5LAS and sub-process in L1S are redesigned as below:

- Task Elimination – Collar base activity in the L1S process is eliminated. This activity is unnecessary for the operation and has no additional value in increasing processing speed [13] as it can be completed earlier.

- Resequencing the 7 sub processes in the L1S process, the tasks with lots of dependency work would have started first because the dependency work takes more time than others.
- Parallelism – The individual tasks that do not require a dependency process can proceed parallel with other workstations.

Resource Optimisation – The number of resources is allocated based on the number of dependency tasks of the clothing parts. Resource sharing is applied for the clothing parts that contain fewer processes

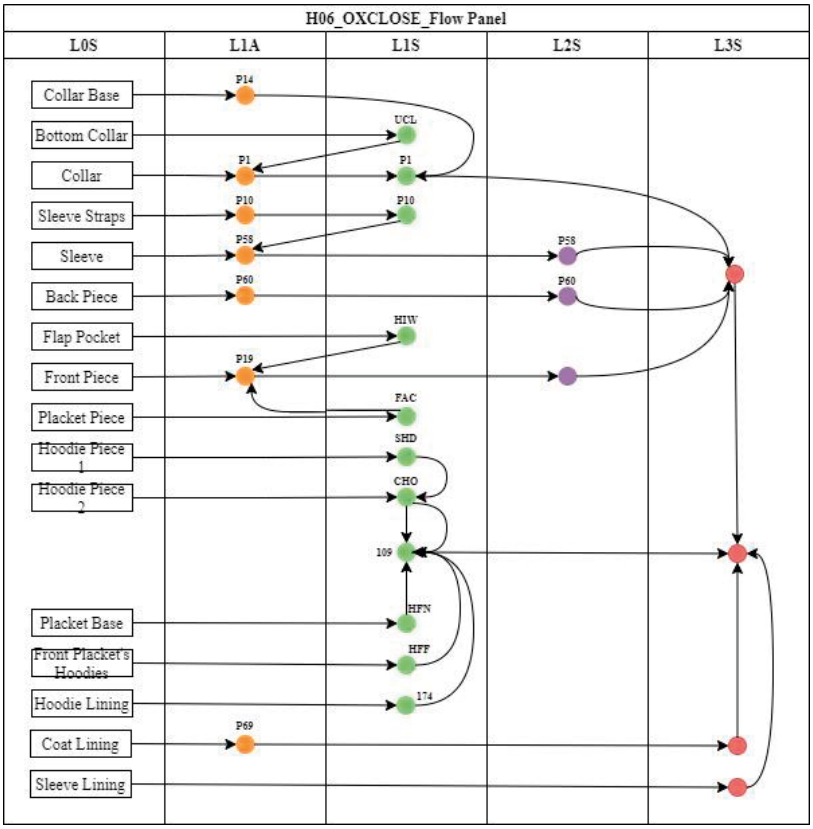

Figure 5. OXCLOSE_5LAS flow panel

The L1S process consists of 7 sub-processes: B1X, B21, B31, B41, B51, B61, and B71, which Table 2 represents the redesign work sequence of OXCLOSE clothing style. The clothing parts highlighted in yellow can be proceeded in parallel. Also, the clothing part of the collar (P1) and flap pocket (HIW) could have started first. Since both processes contain multiple dependency work in sub-process.

C). Test with New Process

Two production line processes are mainly redesigned: the 5LAS process and 7 sub-processes in the L1S process (One of the 5LAS processes). We have first tested the redesign of 7 sub-processes and then followed by the overview of the 5LAS process. The assumption is that if the redesign of the sub-process gives a good result, the production lead time of the entire 5LAS product should be decreased.

6. Result and Discussion

Table 4 shows the new production capacity of each clothing part and the production lead time of each workstation in the redesign L1S process. Table 3 depicts the current standard time calculation and production capacity for OXCLOSE's L1S clothing part process.

Table 3. Current production capacity of each clothing part and the standard time calculation

Clothing Part	Std. Time (Min)/ Piece	No. of Piece/ Hour
Hoodie Piece 2 (CHO)	3.97	15
Hoodie Piece 1 (CHO)	2.15	27
Hoodie Lining (174)	4.1	14
Collar (P1)	6.86	8
Bottom Collar (UCL)	0.68	87
Flap Pocket (HIW)	2.68	22
Sleeve Straps (P10)	2.67	22
Placket Piece (FAC)	2.53	23
Front Placket's Hoodie (HFF)	0.82	72
Placket Base (HFN)	0.79	75
Hat (109)	14.11	4
Total standard time and total pieces produced in 1 hr	**41.36** (Min)	**369**

Table 4. New production capacity of each clothing part and the

Clothing Part	Std. Time (Min)/ Piece	No. of Piece/ Hour
Hoodie Piece 2 (CHO)*	3.58	29
Hoodie Piece 1 (CHO)*	2.09	33
Hoodie Lining (174)*	4.06	27
Collar (P1)***	6.51	17
Bottom Collar (UCL)**	0.92	63
Flap Pocket (HIW)*	2.39	24
Sleeve Straps (P10)**	2.02	47
Placket Piece (FAC)	2.53	23
Front Placket's Hoodie (HFF)*	1.21	66
Placket Base (HFN)**	1.39	62
Hat (109)***	14.05	8
Total standard time and total pieces produced in 1 hr	**40.75** (Min)	**399**

Redesigned heuristics [12] on clothing parts has led to increased production capacity and a shorter manufacturing lead time. From Table 3 and Table 4, the average production capacity of each clothing part is increased by 45%. After applying the redesign process, the current output subtracts the number of new outputs to get the differentiated amount. Then, add up the group of differentiated amounts together and divide by each clothing part's count.

Benchmarking

To see the advantage of the new process, standard time and production capacity's comparison are made between the existing and unique production process. These two variables are the important keys to disclose the new process efficiency. According to Soontorn (2016), the business process reengineering (BPR) of unnecessary process elimination and modification is applied to the computer service centre. Based on Soontorn's finding, the cycle time for service processes (day/working time) is reduced from 2.57 to 1.36 day/working time. The new process reduced 6 unnecessary steps, and these approaches decreased cycle time and waiting time as per expectation. Immawan (2018) claims that key performance indicator (KPI) is one of the measurement tools to assist the comparison between the old and new business processes. He also included production capacity as the main variable in KPI measurement.

The asterisk (*) in each clothing part means this clothing part applied the redesign process where (*) Parallel Tasks, (**) Resource Optimisation, (***) Resequencing Task.

In parallel tasks (*), we have set each L1S'sub process in the simulation tool to run the clothing part parallelly. In other words, Hoodie lining, Hoodie piece 1, Hoodie piece 2 and Flap pocket are simultaneously run. The standard time of some clothing part has slightly decreased because the dependency among each sub-process is removed.

In resource optimisation (**), we have re-allocated the worker in each sub-process with the centralisation to avoid overloading one group and another group waiting for work [14]. For example, the clothing part of the front placket's hoodie and placket base, B12's sub-process, is the first workstation of both clothing parts, containing a few processes. Hence, shared resources between these clothing parts are applied to the B12 workstation. As a result, the production capacity decreases, and the standard time increases, respectively. However, it doesn't impact the entire production process much.

For the case of the bottom collar and sleeve straps, B31's sub-process is the second workstation of both clothing parts. Regarding resource optimisation, we intend to increase the production capacity of the sleeve straps because OXCLOSE clothing style requires 2 pieces of sleeve straps per clothing. Therefore, we have set the shared resources and the allocation rule in the B31's sub-process of the simulation tools. As a result, the sleeve straps production capacity increases, whereas the bottom cars decrease.

Lastly, since collar and hat contain more sub-processes than others and require input from other processes such as L1A and within L1S itself, they should have started the tasks immediately once all components are ready at the workstation. Plus, these two clothing parts are considered the top priority to start the process. The production capacity of both clothing parts is increased according to the increase in other components such as hoodie pieces 1, 2 and hoodie lining, etc.

Best Practices

To guide the process improvement action continuously, we suggest the new production process of OXCLOSE clothing style to the factory's manager since the new process provides the improvement of standard time and production capacity. It can substitute the current production process in the long run. In addition, we did some more studies about continuous process improvement. Plan-Do-Check-Act (PDCA) cycle is one of the most popular tools [17]. It is a four-step model of carrying out change as the cycle should be repeated again and again for continuous improvement. However, in the scope of this research, we focus only on the business process reengineering (BPR) as one of the methodologies to solve the core problems. It provided us with the expected quantitative results. In future work, we will continue to study how to improve the process continuously by using the PDCA tool

Author Contributions: The authors conceived and designed the new production line process by applying the re-designed heuristics guideline. In addiontion, the simulation tool (BPSimulator) has been used to simulate the new production process in order to prove its efficiency. After the simulation, the expected results are given with an increase in production capacity and decrease in production lead time. With the quantitative results, it is proved that Business Process Regineering (BPR) and the selected re-designed heuristics are the most appropriated approach to improve the current production line process. The ABC garment manufacturing company can follow this approach and apply to ABC garment manufacturing's current L1S process.

Findings

Process discovery and process analysis are the main principles of this research. Process discovery is an initial step that provides a baseline for process improvements and identifies key problem areas by business process reengineering (BPR). The garment manufacturing process is very complex and lots of dependency tasks are required, especially from the production process of fabric to the finished product. It is crucial to break down the process into a detailed level. Besides, the process analysis tool also enables you to understand the health of different operations within a business to improve process efficiency, identify the detrimental elements in operation, and overcome obstacles. Without a proper analysis, it will be a waste of time and effort to solve the wrong problems or switch from one software to another. Hence, the researcher should consider these two processes as the highest priority at the beginning of the research.

Conflicts of Interest: The authors declare no conflict of interest.

7. Conclusions

This paper focuses on the 5LAS process improvement by using the cause and effect diagram to identify the core problems in the production process. After that, the fit-gap analysis is performed to discover the best fit solution. The redesign heuristics to the existing production line process is the conclusion and the concept is applied. The new process is being constructed using the simulation tool to model the new production process. The simulation result shows the increasing production capacity and slightly decreased production lead time of the clothing style OXCLOSE, which meets the objective of this research paper. In future work, we have planned to study the ERP software implementation to overcome the low productivity problems such as the behavior of relying too heavily on the report and manual work caused by the report. Due to the current circumstance of the Covid—19 pandemic, ABC Manufacturing has brought up a new protocol to create a hygienic workplace. All workers must be fully vaccinated and tested for Covide-19 every week. With this protocol, it has been reported that no workers are infected with the disease for 3-4 months. However, a contingency plan is still required during this pandemic. Per suggestion, to compensate for infected workers during the pandemic, the manufacturing workers should be trained in multitasking to pay for the lack of workers in some clothing's tasks activity.

References

1. How to Calculate Efficiency. (n.d.). Accessed July 07, 2021, from https://best-excel-tutorial.com/59-tips-and-tricks/313-efficiency.
2. Investment, T. B. (2016). Thailand: TextileIndustry. Accesses July 07,2021, from https://www.boi.go.th/index.php?page=business_opportunities_detail&topic_id=117531.
3. Z. Xu, H. Zhao, S. L. Tan.; L. Liu, "Service-Driven Migrating of Enterprise Information Systems: A Case Study," 2012 19th Asia-Pacific Software Engineering Conference, 2012, pp. 127-136, doi: 10.1109/APSEC.2012.123.
4. Costello, L. (2018, February 21). Advantages and Benefits of ERP Software Solutions. Accessed July 07,2021, from https://terillium.com/benefits-of-erp/.
5. Textileblog. (2020, August 17). Garment Manufacturing Process: Step by Step Section Wise. Accessed July 07,2021, from https://www.textileblog.com/garment-manufacturing-process-step-by-step/.
6. K. Bautista-Calderon, D. Padilla-Reyes, F. Maradiegue-Tuesta and J. Alvarez-Merino, "Improvement of shirt making production through lean manufacturing," 2019 IEEE Sciences and Humanities International Research Conference (SHIRCON), 2019, pp. 1-4, doi: 10.1109/SHIRCON48091.2019.9024864.

7. F. Jingga, S. Cornelius, Alfin.; N. Limantara, "Evaluation of Transportation Reservation Management Module Usage in ERP System at PT. XYZ (a case study approach using Fit Gap Analysis and Technology Acceptance Model)," 2019 International Conference on Information Management and Technology (ICIMTech), 2019, pp. 266-271, doi: 10.1109/ICIMTech.2019.8843776.
8. K.Pratt, M. (2020, September). Business Process Management (BPM). Accessed July 07,2021, from https://searchcio.techtarget. com/definition/business-process-management.
9. Weske, M. (2007). Business process management: concepts, languages, architectures. Springer.
10. Y. -j. Miao, "How Does the Enterprise Implement Business Process Reengineering Management," 2010 International Conference on E-Business and E-Government, 2010, pp. 4100-4102, doi: 10.1109/ICEE.2010.1029.
11. The simulation tools. [Online]. Accessed June 2021, from https://www.bpsimulator.com.
12. Mansar, Selma.; Reijers, H.. (2007). Best practices in business process redesign: use and impact. Business Process Management Journal. 13. 193-213. 10.1108/14637150710740455.
13. Somphanpae, Salinthip & Boonsiri, Somjai. (2016). Business Process Improvement Using Adjustable Parameters on Simulation–A Case Study in Restaurant Business. Journal of Advances in Information Technology. 232-238. 10.12720/jait.7.4.232-238.
14. Dumas,M. [Marlon Dumas].(2014, April 14).Business Process Management – Lecture 7: Process Redesign [Video]. Youtube. https://www.youtube.com/watch?v=mIJLneu8_go.
15. Phiphopsuthipaiboon, Soontorn & Boonsiri, Somjai. (2016). Business Process Reengineering–A Case Study on Computer Center Service. MATEC Web of Conferences. 81. 06006. 10.1051/matecconf/20168106006.
16. Immawan, Taufiq & Asmarawati, Citra & Cahyo, Winda. (2018). Business Process Reengineering in a Sago Production Process. 1-5. 10.1109/ICSTC.2018.8528602.
17. What is Continuous Process Improvement. (2020, June 24). Accessed December 06, 2021, from https://www.solvexia.com /blog/what-is-continuous-process-improvement.

JSTR
ASEAN Journal of Scientific and Technological Reports

Research article

Efficacy of Oral Toltrazuril in Newborn Piglet

Pitchayapa Saracharoen[1] and Supaporn Somrup[2*]

[1] Faculty of Technology Community Development, Thaksin University, Phatthalung, 93210 Thailand, Pitchayapa1632542@gmail.com
[2] Faculty of Technology Community Development, Thaksin University,Phatthalung, 93210 Thailand, supaporn.vet@gmail.com
* Corresponding author: E-mail: supaporn.vet@gmail.com

Abstract: Drug in piglets has a protective effect against dysentery. The aims of this study were determined the efficacy of toltrazuril in newborn-piglets. In 2 piglets of 819 piglets were divided into 2 groups. Baycox® drug group, using 446 piglets. Zurilguard® drug by using 373 piglets by adding a dose of toltrazuril antibiotic 1 ml. by oral suspension. It was found that the weaned weight of the Baycox® and Zurilguard® was found no significant difference ($P > 0.05$). The percentage of farrowing crate damage for the Baycox® of drugs had 10.23 % (39/407). In Zurilguard®, there was a percentage of farrowing crate damage at 3.18 % (14/359). As a result, percentages of farrowing crate damage were significantly different in both groups ($P < 0.05$). Efficacy from FCS indicated that Baycox® was more effective at returning piglets to diarrhea FCS 3 in newborn-piglets 39.24% (175/446) pigs at 7 day 43.64% (182/417) pigs at 14 day 24.27 % (100/412) weaned 25.80% (105/407). FCS indicated that Zurilguard® was more effective at returning piglets to FCS-3. In newborn-piglets 33.51% (125/373) piglets 7 days 37.82% (138/366) at piglets 14 days 58.96 % (214/363) weaned 42.82% (153/359). Zurilguard® had a lower rate of returning of FCS-3 in newborn-piglets and pig at 7 day than the Baycox® but rate of return of FCS-3 in pig at 14 day and weaned pigs more than Baycox®. In conclusion of oral toltrazuril that found efficacy of Zurilguard® for mortality rate of newborn-piglets to weaning in 21 days more than Baycox®.

Keywords: Antibiotic, Baycox®, Toltrazuril, Zurilguard®

Citation:
Saracharoen, P.; Somrup, S.; Efficacy of Oral Toltrazuril in New born Piglets. *ASEAN J. Sci. Tech. Report.* **2022**, 25(1), 36-40. https://doi.org/10.55164/ajstr.v25i1.244250.

Article history:
Received: May 27, 2021
Revused: December 22, 2021
Accepted: December 22, 2021
Available online: March 3, 2022

Publisher's Note:
This article is published and distributed under the terms of the Thaksin University.

1. Introduction

The most common problem in piglets after birth is diarrhoea. This occurs for many reasons, such as diarrhoea from *Escherichia coli* (E. *coli*) diarrhoea, infectious disease in piglets known as "PED" This causes a wide range of losses, starting from mortality, scraping, stunting, shedding, and causing ongoing problems to nursery and finishing pigs. It makes it easy to get infected and get sick with respiratory issues. There is a mortality rate and scrapped higher than Effective normal growth and lower food efficiency. Use more time to sell until the party is sold. There is a higher cost of production. The result is Farm owners have decreased profits. [1-2] Swine dysentery is caused by a protozoan virus called *Isospora suis*, which causes the small intestine wall cells to be destroyed or damaged. All economic animals, Including wild animals, can become infected. The prevalence of the disease will be higher when a bird or mammal comes together. The oocyte of dysentery is resistant to the environment. They can stay outside for months and are difficult to destroy with disinfectants. Which makes

it difficult to control. The severity of the disease depends on the strain of coccidiosis.[3] The type of animals involved, symptoms. They range from asymptomatic infection to severe intestinal infection. Some piglets die due to infection. It harmed production efficiency. Therefore, it is the reason for the efforts to find a preventive measure. The control of dysentery in pigs is a drug application program to cover the problem period (metaphylactic program) and treatment program. [1] The purpose of this study is to study the efficacy of Toltrazuril in newborn piglets between the Baycox® and Zurilguard® for controlling diarrhoea in the piglet.

2. Materials and Methods

Animals used in the study, Two piglets group, were tested for a total of 819 piglets. The experiments were divided into 2 groups and the piglets were weighed. It is divided into 4 age periods: first 7 days of delivery, 14 days, and weaning. Group 1: Baycox® 446 Baycox® feeders were administered to piglets in a volume of 1 millilitre one day after the birth of piglets. Group 2: Zurilguard® 373 Zurilguard® feeders were administered to piglets in a dose of 1 millilitre one day after the birth of piglets. Record of experimental results, mean first stillbirth (number of piglet/ sow), represent live birth (number of piglet/sow), mean piglet weight Percentage of maternity damage and average piglet ADG (gram). Animal license approval code U1-01120-2558.

With the following calculation methods

1. Average newborn (number of piglet/ sow)

$$= \frac{\text{number of firstborn}}{\text{Number of sows}}$$

2. Average piglet (number of piglet/ sow)

$$= \frac{\text{Piglets live}}{\text{Number of sows}}$$

3. Piglet average weight

$$= \frac{\text{Piglet weight}}{\text{Number of piglets}}$$

4. Percentage damaged in maternity envelope

$$= \frac{\text{Damaged maternity envelope}}{\text{Number of piglets weaned}}$$

5. ADG Average piglet (gram)

$$= \frac{\text{Mean weaned piglet} - \text{average first stillborn piglet weight}}{\text{Weaning age}} \times 100$$

Statistical analysis of data

The 819 piglets were collected in two groups: 446 Baycox® piglets. The experimental group of 373 Zurilguard® were evaluated for Fecal consistency score at 7-day birth, 14-day age and weaning. According to the symptoms of diarrhoea, as follows Fecal consistency score chart. The statistical variance was analyzed and compared the mean differences between the groups using the Indipendent-Samples T-Test is used by SPSS.

3. Results and Discussion

A study comparing Toltrazuril in two species of newborn piglets, newborn piglets total 819 using Baycox® and Zurilguard®. The experiment was classified into two groups: Group 1, Baycox®, Total newborn piglets are 446, Total piglets are 40. Testing by filling up Baycox® in newborn piglets by oral suspension 1 millilitre after the piglets were born 1 day. Group 2, Zurilguard® Total newborn piglets are 373, Total piglets are 34 testing by filling up Zurilguard® in newborn piglets by mouth 1 millilitre after the piglets were born 1 day of 373 Zurilguard® drugs, a total of 34 sows after the piglet was born 1 day.

The result found that both the sampling group of medicine group 1 and group 2 affected the weight of piglets until growing to a weaning state. That found no difference in statistical significance ($P > 0.05$)

Table 1. Growth efficiency of newborn piglets to weaning in 21 days.

Data	Newborn piglets group		p-value
	Baycox®	Zurilguard®	
Number of piglets alive (piglets)	446	373	-
Birth weight (kg)	1.65 ± 0.33	1.60 ± 0.22	0.15
Weight 7 days aging (kg)	2.95 ± .053	3.30 ± 0.60	0.23
Weight 14 days aging (kg)	4.99 ± 1.09	3.42 ± 0.92	0.10
Weaning weight (kg)	7.14 ± 1.11	5.84 ± 1.06	0.83
ADG (gram)	261..62 ± 52.89	202.58 ± 48.15	0.55
Number of piglets weaned (piglets)	407	395	-

Note: Group 1; Baycox®), Group 2; Zurilguard®.

Table 2. The mortality rate of newborn piglets to weaning in 21 days.

Data	Newborn piglets group		p-value
	Baycox®	Zurilguard®	
Number of piglets alive (piglets)	446	373	-
7 days old death (percent)	0.70 ± 0.94[a]	0.21 ± 0.48[b]	0.00
14 days old death (percent)	0.13 ± 0.40	0.09 ± 0.29	0.27
Weaning death (percent)	0.13 ± 0.33	0.12 ± 0.33	0.85
Weaning age (days)	21	21	-
Number of piglets weaned (piglets)	407	359	
Number of piglets weaned (piglets)	39	14	-
Damaged maternity envelope			
(body)Percentage damaged in maternity envelope	10.23 ± 17.19 [a]	3.18 ± 5.18[b]	0.02

Note: Group 1; Baycox®, Group 2; Zurilguard®.
[a, b :] different in statistical significance ($P < 0.05$)

The result was found that birth rate damage of using Baycox® has shown the rate as 10.23% (39/407) and the case of Zurilguard® has shown the birth rate's damage as 3.18% (14/359). Both experimental groups are different in statistical significance ($P < 0.05$).


0 = Normal feces


1 = Soft faeces


2 = Mild faeces


3 = Severe feces

Figure 1. Faecal consistency score [4]

Table 3. Faecal consistency score (FCS) in the piglet.

Age of piglet	Number of piglet	Present of diarrhea	FCS 0	FCS 1	FCS 2	FCS 3
Baycox®						
First birth	446	59.87	-	40.13	20.65	39.22
7 days	417	43.64	-	29.91	26.45	43.64
14 days	412	24.27	49.52	26.21	-	24.27
weaning	407	25.80	64.86	9.34	-	25.80
Zurilguard®						
First birth	373	47.72	-	52.28	14.21	33.51
7 days	366	57.38	7.65	34.97	19.56	37.82
14 days	363	67.77	23.69	8.54	8.86	58.96
weaning	359	42.62	27.30	30.08	-	42.62

Toltrazuril was studied in premature piglets between Baycox ® and Zurilguard ® from stillbirth to weaning piglets. Has resulted in piglets after adding the drug, there is no rate of coccidiosis. Having a lower incidence of diarrhoea is consistent with Pipat et al. [5]. It was reported that the filling of Toltrazuril in the stillborn piglets was as a medicine filling to prevent dysentery (*Isospora suis*) and reduce the diarrhoea rate in piglets. The filling of the drug effectively prevented coccidiosis and piglets with diarrhoea.

4. Conclusions

The efficiency of Baycox ® helps the piglets have got better from diarrhoea. The piglet sampling group has gotten diarrhoea before filling up Baycox®, counted as 59.87%. After filling up Baycox® for 7 days until weaning, the piglets have acquired diarrhoea, counted as 31.24%. The piglets have not got diarrhoea as 68.76%. The piglets have died from being laid on by other piglets counted as 5 piglets. The piglets have been weak, small and have a flatulence total of 34 piglets calculated as 10.23%. The efficiency of Zurilguad® has very well benefits on growth and the rate of death from diarrhoea in the piglet group. The piglet sampling group has gotten diarrhoea before filling up Zurilguard®, counted as 47.72%. After filling up Zurilguard® for 7 days until weaning, the piglet has acquired diarrhoea, counted as 55.92%. The piglet has not got diarrhoea calculated as 44.08% and the piglet has died from being laid on from other piglets counted as 4 piglets. The piglets have been weak, small and have a flatulence total of 10 piglets counted as 3.18%. However, protocols of metaphylactic treatment with 5% toltrazuril (15 mg/kg) in naturally infected, extensively reared beef calves from birth to 1 year of age. It found fewer oocysts were excreted in the treated group for up to 75 days and at 150 days of age ($p < 0.05$). In the final stage of the study, significant differences. [6] Zurilguard® can treat and control Isospora suis in newborn piglets [7] while Baycox ® against neonatal Isospora suis-coccidiosis in synchronous piglets. However, Baycox 5% Suspension is indicated for use against neonatal Isospora suis-coccidiosis in piglets product by Bayer. The recommended dosage of toltrazuril is 20 mg per kg. [8] But Zurilguard® product by Pharmatech, there are different brands. In subsequent studies, faeces should be examined to confirm the presence of parasite eggs in the laboratory and the health assessment of pigs in other systems.

5. Acknowledgements

Thank you to Farmers Southern for financial support.

Author Contributions:

Funding:

Conflicts of Interest:

References

1. Wat Namkang, knowledge of coccidiosis 2010, betterpharma Publisher.
2. Supot Methiyaphan, Ladda Tongwongsa, Jirawayuchot, Prateep Pemayotin. March 1991 ,Cock disease of piglets in Thailand. *Animal Science* Year 42 Volume 1: pp. 21-37.
3. Cossidiosis in Piglets with Toltuazuril in a Special Oral Suapension. Proceedings of the 13 th IPVS Congress; pp. 256-257.
4. Estefania Perez-Calvo, Alfian N. Wicaksono, Ester Canet, Emma Daulton, Waldemar Ens, Ulrich Hoeller, Viviane Verlhac, Pietro Celi, James A. Covington. The measurement of volatile organic compounds in faeces of piglets as a tool to assess gastrointestinal functionality.
5. Pipat Arunpimat,Nion Rattanapop, Waraporn Pimprapi. Semtember – December 2013 , A study on the efficacy of Toltrazuril in the symposium for sympathy in upcountry step studios . Year 23 *Veterinary Journal* No. 3: pp. 132-137.
6. Efficiency of 5% toltrazuril in the metaphylactic treatment of coccidiosis in naturally infected and extensively reared beef calves. Reginato CZ, D'ambroso Fernandes F, Sangioni LA, Vogel FSF. Reginato CZ, et al. Trop Anim Health Prod. 2021 May 17; 53(2): 329. doi: 10.1007/s11250-021-02770-8. Trop Anim Health Prod. 2021. PMID: 34002297.
7. Agromed co., Zurilguard® [Online]. [2012]. Available from: http://agromed.co.th/index.php/product/product_detail/20. [2021, Dec 23].
8. Vet contact. Baycox® - Pig, Poultry and Piglets [Online]. [2021]. Available from: https://www.vetcotact.com/en/art.php?a=54&t. [2021, Dec 23].

JSTR
ASEAN Journal of Scientific and Technological Reports

Research article

Design and Development of Saline Infusion Administration System Using IoT

Nuth Otanasap[1] *, Veerapong Kanchanawongkul[2] and Chanintorn Chalermsuk[3]

[1] Department of Computer Engineering, Faculty of Engineering, Southeast Asia University, Bangkok, 10160, Thailand; nuto@sau.ac.th
[2] Department of Mechanical Engineering, Faculty of Engineering, Southeast Asia University, Bangkok, 10160, Thailand; veerapongk@sau.ac.th
[3] Department of Computer Science, Faculty of Arts and Sciences, Southeast Asia University, Bangkok, 10160, Thailand; chanintornc@sau.ac.th
* Correspondence: nuto@sau.ac.th

Abstract: According to the current deficiency of medical personnel due to many COVID-19 patients today, the workload of nurses and caregivers increases. One of the costliest tasks for healthcare professionals is monitoring and controlling the administration of saline solutions to bedridden patients. This research aims to develop a monitoring and regulating system to conduct the saline solution to patients using IoT technology. The Arduino UNO R3 and Node MCU ESP8266 microcontroller board are used as a processor to receive the saline weight input from the load cell and control the saline flow rate by the servo motor arm. The developed system can also be remotely monitored and controlled online via Wi-Fi, Internet, and cloud computing with mobile and web applications developed by Flutter. From the results of trying that determine the saline flow rate with different periods, it was found that the system was able to control the flow rate for the specified time with a total meantime accuracy of 88.47%. It was also found that the accuracy rate would increase if the flow rate were set for a short period, while the accuracy rate would decrease if the flow rate were set for a long time. The experiment revealed that the developed prototype system could monitor, alert, and automatically control the flow rate of saline administration to patients as the specified objectives.

Keywords: Saline Infusion; Saline Controlling; IoT

Citation:
Otanasap, N.; Kanchanawongkul, V.; Chalermsuk, C. Design and Development of Saline Infusion Administration System Using IoT. *ASEAN J. Sci. Tech. Report.* **2022**, *25(1)*, 41-49. https://doi.org/10.55164/ajstr.v25i1.244460

Article history:
Received: June 25, 2021
Revised: December 4, 2021
Accepted: February 23, 2022
Available online: March 3, 2022

Publisher's Note:
This article is published and distributed under the terms of the Thaksin University.

1. Introduction

According to the ageing society of many countries and the Covid-19 epidemic, the number of patients increases continuously. As a result, it exceeds the ability of nurses and caregivers. Reducing the workload of healthcare workers is therefore essential. Monitoring and controlling the administration of saline to patients is one of the nurses' tasks that pose a considerable burden. Thus, the researchers aim to develop a system that can automatically monitor and control saline administration to reduce the workload of healthcare professionals. In addition, with the development of Internet of Things (IoT) technology, it is possible to develop sensor-based monitoring and reverse-control with actuators through the Internet, mobile applications, and cloud computing.

Furthermore, the ability to automatically adjust the saline flow rate according to the doctor's prescription and monitor and alert the active status via

a mobile application reduces the burden on caregivers. Another factor is the price which must be more cost-effective and less expensive than the digital infusion pumps available in the market. Examples of digital infusion pumps available on the market cost about $240 to $300. The proposed system can also collect the patient's history and behaviour data to reduce the workload and care benefits.

2. Related Works

A literature review on the development of IoT-based saline monitoring and control systems revealed that, in addition to using IR sensors to detect saline water content. We also found that load cell [1-3], ultrasonic sensor [4-5], tilt sensor [6], level sensor [7], and flow sensor [8] were used to perform the functions of detecting the volume and flow rate of saline from a bottle. However, the developed system can only detect the amount of saline and notify the nurse or caregiver [1-5], [8-9], primarily through mobile applications, and output only through the LCD [5, 7]. In contrast, some systems, in addition to detecting the amount of saline, can also control the saline flow rate according to the doctor's prescription [7-8]. However, in the system that can control the flow rate, it was found that the nurse had to set the saline drip-rate manually. The system can automatically adjust the saline drip rate, but caregivers must also monitor whether the physician directs the saline infusion time. Furthermore, systems using solenoid valves to control flow rate require that the saline flows directly through the device, potentially contaminating germs or foreign matter [7]. While the research performed a servomotor control method [8], the caregiver had to calculate the saline drip rate to control the saline depletion at the doctor's schedule. The system cannot control the rate of saline administration to the patient within the amount of time the doctor can determine. Another essential prerequisite for developing IoT-based saline monitoring and control systems is when the patient goes to the bathroom or other cases where the saline flow or drip rate is abnormal. Most systems cannot detect vibrations both from the patient's body and from the surrounding equipment, which affects the abnormal flow of the saline solution. Only research studies [6] can address this problem with tile sensors. Moreover, to prevent blood flow backwards during the saline container is empty, the operation needs to hold the saline flow when the container is almost blank. Only the [8] system can squeeze the saline tube to prevent the backflow of blood. Also, most systems fail to demonstrate the validity of the trials to monitor and control saline administration by a physician-prescribed system. This research focuses on designing and developing an automatic monitor and control saline feeding and adjusting the saline flow rate system. Additionally, nurses or caregivers can monitor the flow rate and residual saline volume through a mobile application. As well as to prevent abnormal saline flow rates from patient movement, the system can detect abnormal flow rates from distorted weight signals from the load cell. In addition, if the saline content in the container is less than 5% weight from the original volume, or there is severe vibration of the container detected by the load cell, the system will squeeze the saline line to prevent the backflow of blood the saline tube.

3. Materials and Methods

Responsible for the objectives of this research, the research team has designed a system that focuses on enabling the system to respond to IoT-based operations. The ESP8266 Node MCU and Arduino UNO R3 are used as the central processing unit, enabling integration with cloud computing via a Wi-Fi network. For the principle of operation of the system, initialize the beginning load of the patient saline container or bag to define the initial saline substances by the Load Cell, Shear type as 10Kg measured load and 1.0 ±0.15 mV/V measured output. The HX711 amplifier module amplifies the signal received from the load cell and forwards it to the Arduino UNO R3. The traceability status information is sent to the ESP8266-12E Node MCU to deliver cloud computing. Firebase and Mongo DB are used in this development. Firebase, a Google service, is used for online notifications. MongoDB, private cloud storage, is chosen for data management and patient data security. This research developed both mobile applications and web applications for the user interface. Flutter is used to create mobile applications that can run on either Android or iOS platforms. The servo motor is commanded by the Arduino UNO R3 board and is used to steer the saline tube's compression or repose to increase or decrease the saline flow rate, respectively.

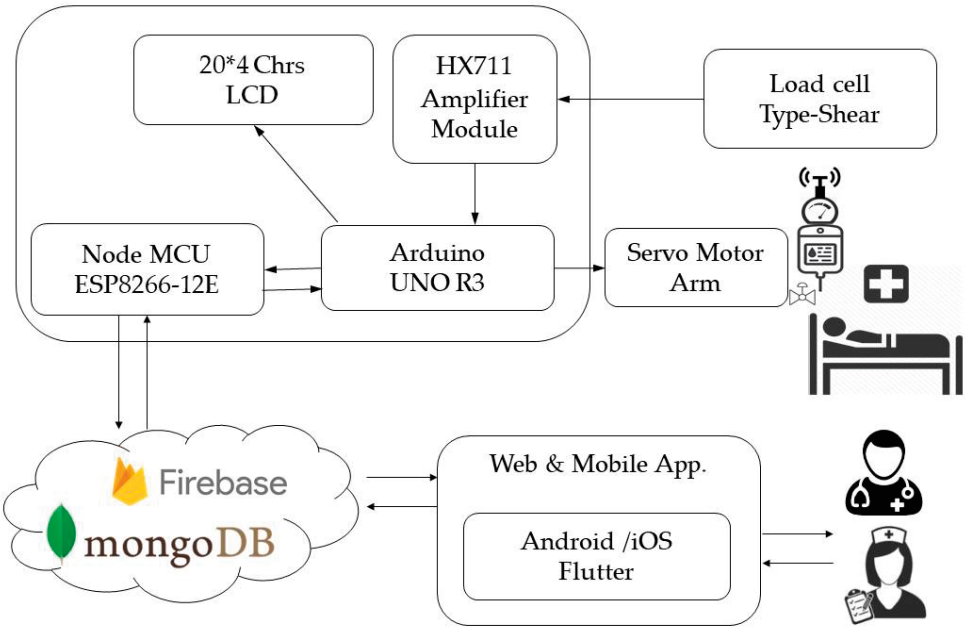

Figure 1. System Framework

Figure 2 shows an algorithm to observe and regulate the flow rate of saline solution as prescribed by the physician. It starts with determining the weight of the saline bag due to the various initial packaging and volume of the saline solution as *Init_Wt*. The nurse or caregiver will then select an order to determine the duration of the saline solution, such as 1, 3, 5, or 8 hours directed by the doctor, then transfer to minutes as *Infusion_Time*. Then determine the final weight for the saline drainage stop as *Stop_Wt*. The flow rate is calculated based on the lost weight by the initial weight divided by the infusion time determined in the previous step.

$$Flow\_Rate = Init\_Wt\ (g.)/Infusion\_Time\ (min.), \tag{1}$$

The system then determines the degree of the servomotor arm that compresses the saline tube so that the saline solution flow rate is relative to the required time. The system then calculates the weight of the lost brine from the previously lost weight minus the weight of the brine imported from the load cell at that time. In addition, the system determines the average flow rate as a basis for detecting possible abnormal flows. The normalized flow rate average as *Norm_Flow* is calculated by the previous mean plus standard deviation. The system then compares the weight lost from the flow with the flow rate. If the weight loss as *Curr_Flow_Wt* from the flow is greater than the flow rate as *Flow_Rate*, then the brine flow is too high, the servomotor arm is forced to squeeze the tube more to reduce the flow rate. Conversely, if the weight lost from the flow is less than the flow rate, then the brine flow is too small, the servomotor arm is forced to squeeze the tubeless to increase the flow rate.

In addition, if the load cell vibrates signal occurs by comparing the current flow weight with average normal flow, which means an abnormality. The system will command the servo motor arm to squeeze the tube to stop the saline flow for safety reasons. The system will repeat the above process until the saline is 5% or less, depending on the requirement. Finally, the system will instruct the servo motor arm to squeeze the saline tube to stop flowing for safety and prevent backflow of blood. Then, the system will send a notification to the caregiver or nurse for further action.

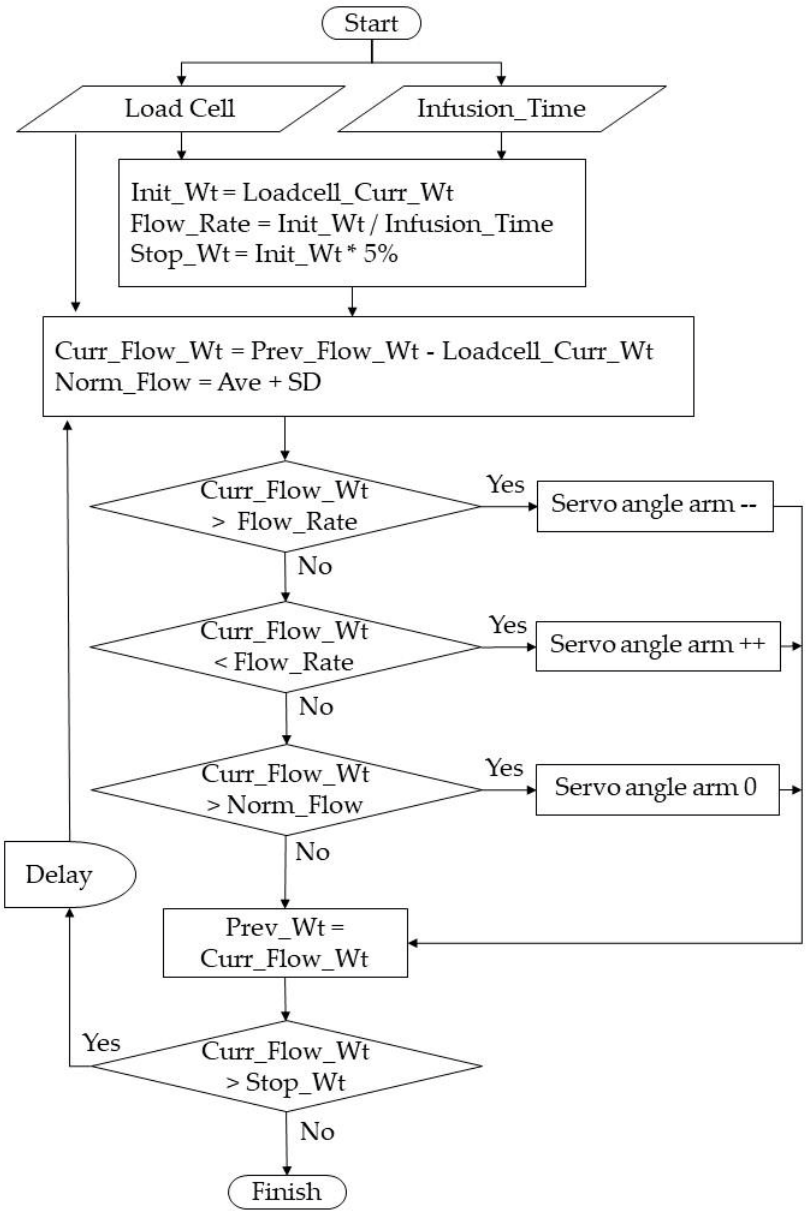

Figure 2. Algorithm to observe and regulate the flow rate of saline solution

Refer to Figure 3; the use case diagram illustrates the functions that doctors and nurses can access to the system. It consists of the following functions: *Add, Find, & Update User Profile* are functions where users can add, search, and update patient information. *Doctor's Orders* is a function that which the doctor can order the detail of saline solution, such as the type of saline solution and the duration. In addition, the nurse can take the doctor's orders from this function. *Saline Status Display* is a function that users of both doctors and nurses can track the flow status of saline solution. Furthermore, users can also receive notifications in case of abnormalities or saline depletion from the *Saline Monitor & Notification* function. To assign access rights to the system, the user must log in and deactivate from the *Login/ Logout* function.

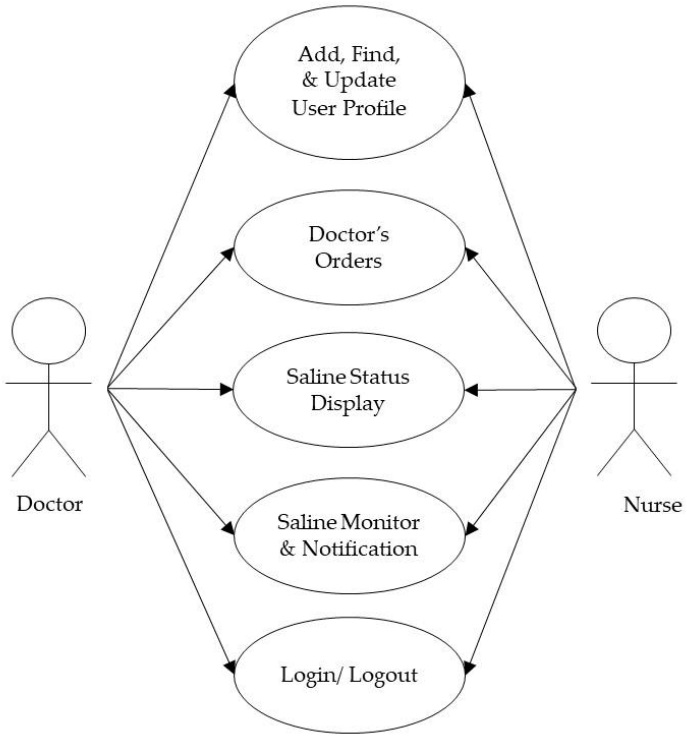

Figure 3. Use-case Diagram

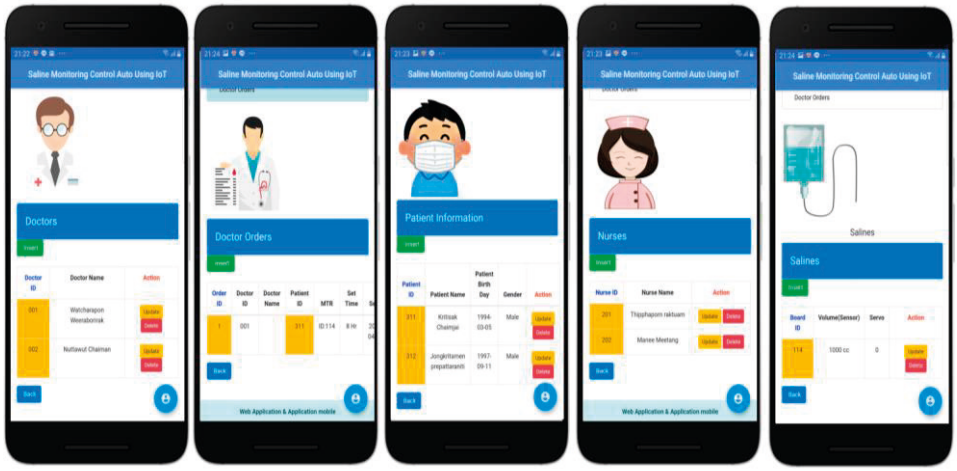

(a) (b) (c) (d) (e)

Figure 4. Example UI of Mobile Application

Figure 4 presents an example of a mobile user interface that allows nurses or caregivers to monitor, control saline administration and receive system notifications through a mobile application as follows: (a) UI for physicians to access the system, (b) UI for doctor's orders for saline solution, (c) UI showing patient information, (d) UI for nurses to access the system and work records; and (e) UI for monitoring and alerting in the event of anomalies. Not only can doctors and nurses use the system via the mobile application, but they also use the system via the web application.

An example of a web application interface is shown in figure 5. The interface shows the doctor's instructions and details and the status of saline administration to each patient.

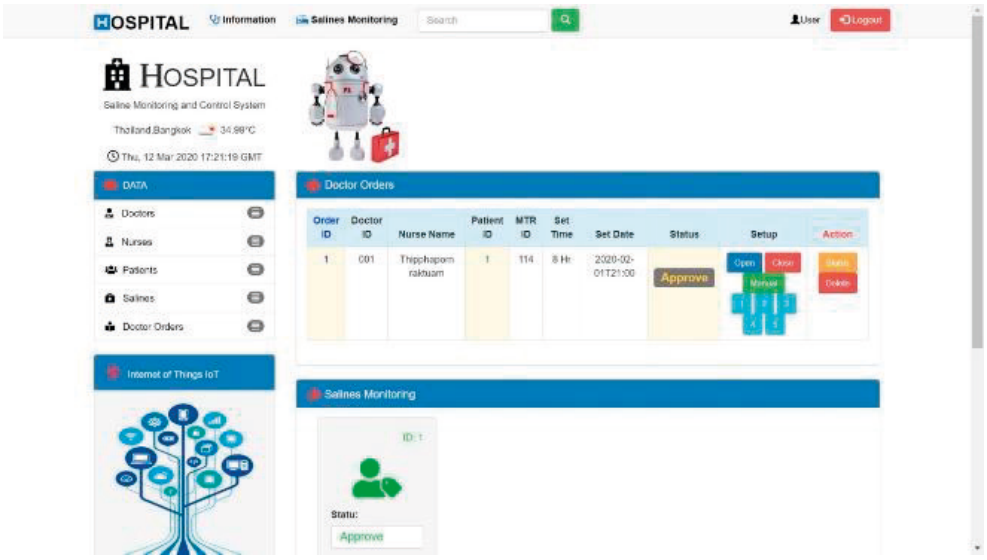

Figure 5. Example UI of Web application

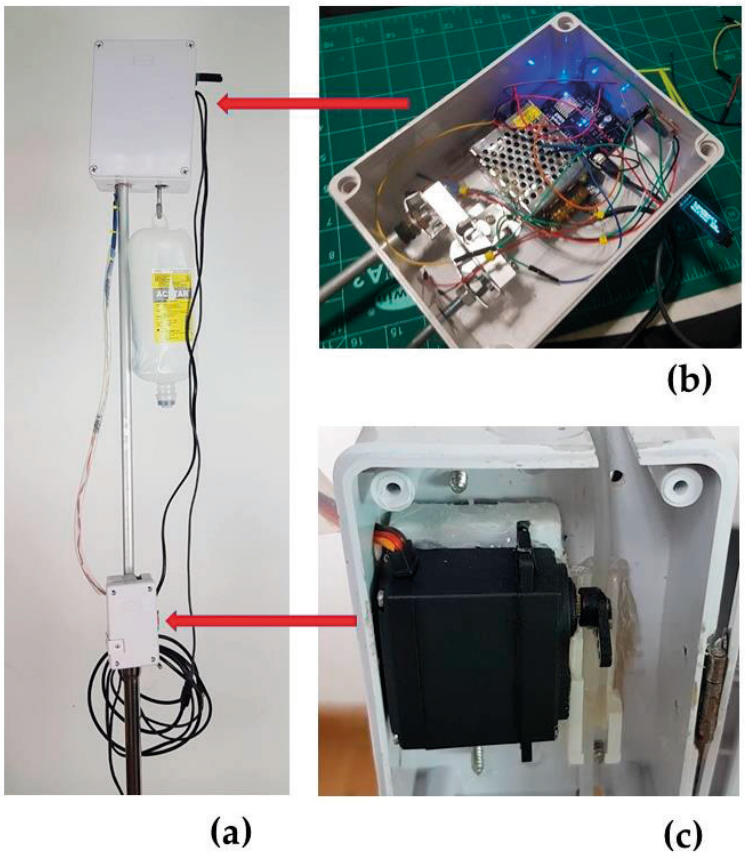

Figure 6. Hardware prototype of the developed system

Refer to Figure 6; It represents the hardware prototype of the system (a). The upper box (b) contains a Load cell Type-Sher for hanging the saline solution bag. The load cell is connected to the HX711 Amplifier Module to amplify the weight signal and forward it to the Arduino UNO R3 board to process and control the compression or release of the saline flow rate by the servo motor arm stored in the lower box (c). It can also display the weight of saline solution via 20*4 Characters LCD. The saline weight data is transmitted from the

Arduino UNO R3 to the Node MCU ESP8266-12E connected to the Internet via a Wi-Fi network, further forwarding the data to the cloud as detailed in (b).

4. Results and Discussion

An experimental simulation was created by hanging a 1000 mL saline bag on a load cell. Then, the experimental set was divided into five batches, each of which was assigned a different saline end time. Since the experiment used a 1000 mL or 1000 g saline size excluding package weight to avoid excessive saline flow and demonstrate that the system can determine the minute time, the duration of the first set of experiments was established (A) settles a time of 150 minutes or two and a half hours. The second set (B) is scheduled for 240 minutes or 4 hours, the third (C) is designed for 360 minutes or 6 hours, the fourth (D) is designed for 540 minutes or 9 hours, and the last set (E) is scheduled 900 minutes or 15 hours. Prolonged time intervals are intended only to respond to cases where the doctor wants to keep the vein open (KVO) to prevent blood clots. Then create a timer and record since the brine started flowing. The servomotor arm squeezes the brine tube to stop the flow until the brine solution is reduced to less than 5% of the starting weight. Each set of trials performed five trials for a total of 25 attempts. The results of the experiment are exhibited in Table 1.

Table 1. Comparison of the flow rate controlling of the saline solution at the specified various time

No.	Test Set (min.)					
	A (150)	**B (240)**	**C (360)**	**D (540)**	**E (900)**	**Total**
1	149.46	228.18	308.18	538.21	941.25	
2	144.14	228.33	409.58	579.62	836.67	
3	144.57	242.9	329.86	628.33	941.25	
4	146.93	240.17	329.84	580.38	836.67	
5	139.58	251.17	337.96	579.23	836.67	
$\bar{x}$	**144.94**	**238.15**	**343.08**	**581.15**	**878.50**	**437.17**
SD	**3.67**	**9.90**	**38.78**	**31.92**	**57.28**	**28.31**
Min.	139.58	228.18	308.18	538.21	836.67	
Max.	149.46	251.17	409.58	628.33	941.25	
Err. (min.)	**5.06**	**1.85**	**16.92**	**41.15**	**21.50**	**17.30**
Err. (%)	**3.38%**	**1.23%**	**11.28%**	**27.44%**	**14.33%**	**11.53%**

Table 1 and Figure 7 show the result of the (A-E) test set marks at the specified time compared to the experimentations. The results of the experiments consisted of mean, standard deviation, time-tolerance mean, and percentage of meantime error for each test set of different specified times. The results showed that the first test (A) was assigned to drain the saline solution within 150 min; the system was able to do so in a mean time of 144.94 min (± 3.67 min) with a meantime error of 5.06 min or 3.38%. The second group (B) results were determined to complete the saline solution within 240 minutes. The system achieved an average of 238.15 minutes (± 9.90 minutes), with an average time error of 1.85 minutes or 1.23%. Results of the third experiment (C) were determined to release the saline solution to be discharged entirely within 360 minutes; the system achieved a mean time of 343.08 minutes (± 38.78 minutes), a mean time error of 16.92 minutes, or an error of 11.28%. Additionally, in the third trial (D), which was timed to deplete the saline solution at 540 min, the system achieved a mean time of 581.15 min (± 31.92 min) with a mean time error of 41.15 min or 27.44%. The last set of experiments (E) was scheduled to run out of saline in 900 minutes. However, the system was able to do it in an average time of 878.50 minutes (± 57.28 minutes), with a mean time error of 21.50 minutes, or 11.53%. All trials' total meantime error was 11.53% (± 10.41%). Thus, it can be concluded that the system is accurate in controlling the flow rate of the brine solution to the required accuracy of 88.47% (± 10.41%). It was also found that in the experimental results, shorter flow intervals resulted in fewer errors. Conversely, setting a longer interval for the flow will also result in more errors.

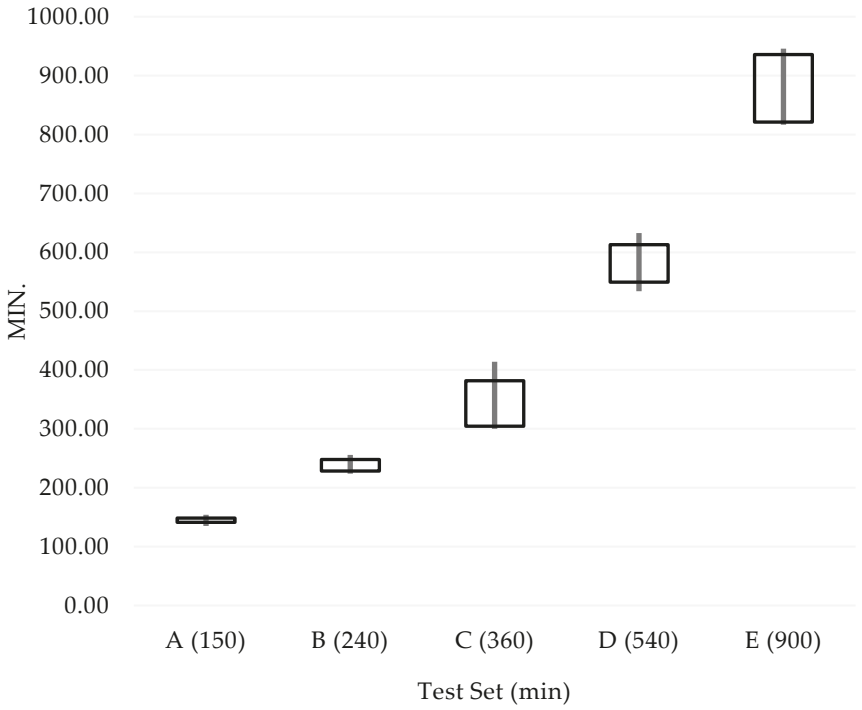

Figure 7. Schemes follow the same formatting.

5. Conclusions

The design, development, and experimentation of the monitoring and control system for saline solution in this time can be used as a prototype system. In addition, this system can work according to the specified purpose of reducing the workload of nurses or caregivers via web and mobile apps and can also automatically control and adjust the amount of saline solution to patients. Including equipment used for both load cells, servo motors and microcontroller boards are generally cheaper than commercially available devices with approximately 200 USD. It can also be monitored and commanded via the cloud, a capability that surpasses any commercially available device today. However, researchers and developers can also use the prototype system to improve the working algorithm to improve accuracy and optimize the saline solution to be more consistent and reduce errors that keep getting less.

6. Acknowledgements

Thanks to Southeast Asia University for facilitating both the location and the facilities. Therefore, this project was completed.

Author Contributions: Conceptualization, Otanasap. N. and Kanchanawongkul. V.; methodology, Otanasap. N. and Chalermsuk. V.; software, Otanasap. N. and Chalermsuk. V.; validation, Otanasap. N., Kanchanawongkul. V. and Chalermsuk. V.; formal analysis, Otanasap. N.; investigation, Otanasap. N.; resources, Otanasap. N. and Kanchanawongkul. V.; data curation, Otanasap. N.; writing—original draft preparation, Otanasap. N.; writing—review and editing, Otanasap. N. and Kanchanawongkul. V.; visualization, Otanasap. N. and Chalermsuk. V.; supervision, Otanasap. N.; project administration, Otanasap. N.; funding acquisition, Otanasap. N. All authors have read and agreed to the published version of the manuscript.

Funding:

Conflicts of Interest: The authors declare no conflict of interest.

References

1. Amith Raj, N.; Bhavana, K. P.; Narasimha Murthy, B.; Sneha, V.; Benni, N. S. IoT Based Electronic Valve for Quantitative Control of Saline Flow and Patient Monitoring. *International Journal of Scientific Research and Review* 2019, *7*(3), 2088-2092.
2. Kulkarni, T.; Devare, M. A.; Zende, S.; Yadav, S.; Biradar, A. Design and Development a Model for Saline Monitoring System. *International Journal of Engineering Applied Sciences and Technology* 2020,5(1), ISSN No. 2455-2143, 497-501.
3. Umchid, S.; Kongsomboom, P.; Buttongdee, M. Design and development of a monitoring system for saline administration. *In Proceedings of the World Congress on Engineering* 2018, Vol. 1, pp. 4-6.
4. Hossain, S.; Sharmin, S.; Faruk, T.; Islam, M. K. Low-Cost Digitization of Infusion Pump for Real-time Automated Flow Rate Monitoring and Warning. *In 2019 2nd International Conference on Innovation in Engineering and Technology (ICIET)* 2019. (1-5). IEEE.
5. Sunil, G.; Aluvala, S.; Reddy, G. R.; Sreeharika, V.; Sindhu, P.; Keerthana, S. (2020, December). IoT based saline level monitoring system. *In IOP Conference Series: Materials Science and Engineering* 2020, 981(3), 032095. IOP Publishing.
6. Malleswari, B. N.; Venkataram, N. Smart saline level monitoring system using IOT. *International Journal of Engineering & Technology* 2018, 7(2.7), 817-819.
7. Radhakrishnan, R.; Ramesh, J. Smart Fluid Level Monitoring and Controlling System. *International Journal of Scientific Research and Engineering Development* 2020, 3(2), 522-525.
8. Rashid, H.; Shekha, S.; Reza, S. T.; Ahmed, I. U.; Newaz, Q.; & Rasheduzzaman, M. A low cost automated fluid control device using smart phone for medical application. *In 2017 International Conference on Electrical, Computer and Communication Engineering (ECCE)* 2017, 809-814. IEEE.
9. Deshmukh, R.; Jadhav, K.; Borude, T.; Lanke, H.; Wagholi, J. I.; Darokar, P. M. A Survey Paper on Patient Health and Saline Level Monitoring System using IoT. *International Journal of Engineering Research & Technology (IJERT)* 2019, *8(11)*, 807-809.

JSTR
ASEAN Journal of Scientific and Technological Reports

Research article

CO_2 decomposition using the coaxial dielectric barrier discharge: effect of mixed gas and double outer electrodes

Nikom Rattanarojanakul[1]* Somyos Srikhongrak[2], Witoon Nulek[3] and Yutthana Tirawanichakul[4]

[1] Department of Physics and General Science, Faculty of Science and Technology, Rambhai Barni Rajabhat University, Chanthaburi, 22000, Thailand; nikom.p@rbru.ac.th
[2] Department of Physics and General Science, Faculty of Science and Technology, Rambhai Barni Rajabhat University, Chanthaburi, 22000, Thailand; somyos.s@rbru.ac.th
[3] Department of Physics and General Science, Faculty of Science and Technology, Rambhai Barni Rajabhat University, Chanthaburi, 22000, Thailand; witoon.n@rbru.ac.th
[4] Department of Physics, Faculty of Science, Prince of Songkla University, Songkhla, 90112, Thailand; yutthana.t@psu.ac.th
* Correspondence: nikom.p@rbru.ac.th

Citation:
Rattanarojanakul, N.; Srikhongrak, S.; Nuleg, W.; Tirawanichakul, Y. CO_2 decomposition using the coaxial dielectric barrier discharge: effect of additive gas and double outer electrodes. *ASEAN J. Sci. Tech. Report*. **2022**, *25(1)*, 50-59. https://doi.org/10.55164/ajstr.v25i1.244790.

Article history:
Received: August 7, 2021
Revised : February 9, 2022
Accepted: February 11, 2022
Available online: March 29, 2022

Publisher's Note:
This article is published and distributed under the terms of the Thaksin University.

Abstract: This work has studied CO_2 decomposition through the dielectric barrier discharge (DBD). The configuration of the DBD reactor was performed as a coaxial DBD tube. The dielectric barrier was made of a quartz tube with 1 mm thickness, while an outer electrode was made of a copper flat sheet wrapping around a quartz tube. The coaxial axis was made of stainless steel rod to be an inner electrode. The power source was applied by the alternative current (AC) high voltage with 7.8 kHz of frequency to both electrodes of the plasma reactor. The experiment was conducted on various conditions such as a mixed gas ratio, discharge gap, applied voltage, outer electrode length, two outer electrodes, and gas flow rate. The results showed that CO_2 conversion was decreased when CO_2 concentration increased. Similarly, the increase of gas flow rate also caused the decrease of CO_2 conversion. Whilst the increase of an applied voltage causes the CO_2 conversion clearly increased. Similarly, the CO_2:Ar ratio of 60%:40% achieved 30% of CO_2 conversion. Furthermore, the high percentage of CO_2 conversion of 47.2% has been obtained from a 1.3 mm discharge gap with 40 ml/min of gas flow rate.

Keywords: Gas conversions; DBD reactor; Pollution control; Gas discharges; Greenhouse Gases

1. Introduction

The dielectric barrier discharges (DBDs) are well-known for the generation of ionized gases and have been employed for several applications such as greenhouse gas decomposition, gas conversion, pollution control, ozone synthesis, excimer laser, material, and film surface modifications, etc. CO_2 gas is a part of greenhouse gases and has been attracting to the global warming and climate change on the earth, which can be more emitted from the transportations, burning of all fossil fuels, and also had presented in the natural gas and biogas [1-3]. However

CO_2 gas is one of the additive gases in the process of methane conversion into hydrocarbon gases [4-8]. The chemical bond of CO_2 is very strong and hard to be dissociated. To break the bond of C-O, the temperature has to be used at least at 1,500 ℃ for the thermolysis process, resulting in the huge power consumption. However, plasma technologies have been adopted to avoid the use of such high temperatures. Many geometries were configured for plasma-assisted reforming such as an arc discharge, glow discharge, corona discharge, dielectric barrier discharge (DBD), radio frequency (RF) discharge, etc. [9-18]. The reactions of plasma chemistry for CO_2 decomposition can be seen in Eq. 1 and Eq. 2, after the process of CO_2 decomposition, this CO_2 is converted into CO and O_2 [19-21]. Similarly, Eq. 1 and Eq. 2 confirm that CO and O_2 are the main product, where ΔH is the enthalpy of the reaction. However, O_2 can be formed by the recombination of O radicals, and similarly, CO_2 also has been reformed by the recombination of CO with O radicals and O_2 with C radicals [9, 22]. CO gas product is utilized for hydrocarbon fuel synthesis (e.g. methanol, ethanol, and acetic acid synthesis) and the mineral and metal industries (e.g. smelting and refining processing).

$$CO_2 \rightarrow CO + \frac{1}{2}O_2, \Delta H = 2.9 \text{ eV} \quad (1)$$

$$CO_2 \rightarrow CO + O, \Delta H = 5.5 \text{ eV} \quad (2)$$

Furthermore, it can be considered in the unit of Joule [23].

$$CO_2 \rightarrow CO + O, \Delta H = 529.8 \text{ kJ/mol} \quad (3)$$

The DBD plasmas have been utilized for a long time for surface modifications, gas treatment, chemical synthesis, etc. The characteristic of DBDs can initiate plasma reactions in low energy consumption and low temperature in the atmosphere. Whilst gas temperature can remain low, the electron temperature is high. These electrons have high energy in the range of 1-10 eV, in which it has enough energy to break the chemical bonds of gas molecules directly [9, 11, 24-28].

CO_2 conversion using a DBD reactor was operated under various conditions such as gas flow rate, gas temperature, power frequency, and power input [29]. The previous results indicated that the increase of input power and gas temperature could raise the conversion rate, while the increase of flow rate caused the conversion to decrease. In support, Indarto, A. et al. [9] had reported the review article for greenhouse gas and toxic gas decompositions via plasma technologies. In summary, they suggested that the advantage process should be the combined or new alternative process. In addition, other reports [9, 12, 14, 21] have also suggested and presented that noble gas (such as He, Ar, Kr, xe) contained in gas feeding or placing a solid catalyst in plasma zone can raise the rate of the gas conversion and product yield.

Furthermore, CO_2 was utilized in the process of CH_4 reforming to produce hydrogen and hydrocarbon fuels. A recent article from Tao, X. et al. [8] has reported the reviewed article for the opportunity of CH_4-CO_2 reforming in different methods and processes. They have suggested that it is included by three factors to achieve high performance, there are reactor configuration, electron density, and plasma temperature. These factors caused the high plasma and electron densities to elevate the gas dissociation and produce more ions and neutron species.

This work represented CO_2 decomposition via the coaxial DBD applying by AC high voltage with high frequency under several conditions such as CO_2 mixed with Ar to increase an electron density [12, 14, 21], applied voltage, gas flow rate, discharge gap and discharge volume (length of outer electrode and outer electrode numbers). Which was operated in the atmosphere and the room temperature.

2. Materials and Methods

2.1. Experimental configuration

The experimental diagram is represented in Figure 1 consisting of CO_2 and Ar gas tanks, gas regulator, valve, flow meter, mixer unit, needle valve, coaxial DBD reactor, bubble flow meter, high

voltage power source, resistor (R_{limit} = 1.5 kΩ), measuring capacitor (C_m = 10 nF), high voltage (HV) probe (Tektronix, P6015A), voltage probe, Oscilloscope (Tektronix, TDS3014B) and Gas analyzer (Geotech, Biogas Check). Coaxial DBD reactor was fabricated from quartz tube, Teflon insulator, Aluminum flat sheet, and stainless steel rod. A quartz tube with a thickness of 1 mm and an inner diameter of 12 mm was provided for a chamber. Teflon insulator is used for closing both sides of a quartz tube and fixing the inner electrode in the middle of a quartz tube. An aluminum flat sheet is wrapped around a quartz tube to set as an outer electrode, while stainless steel rod is placed inside of a quartz tube to be an inner electrode. Especially, Figure 2 has been illustrated the different installations for one outer electrode (A), two outer electrodes to increase the discharge volume (B), and the cross-section of the reactor (C).

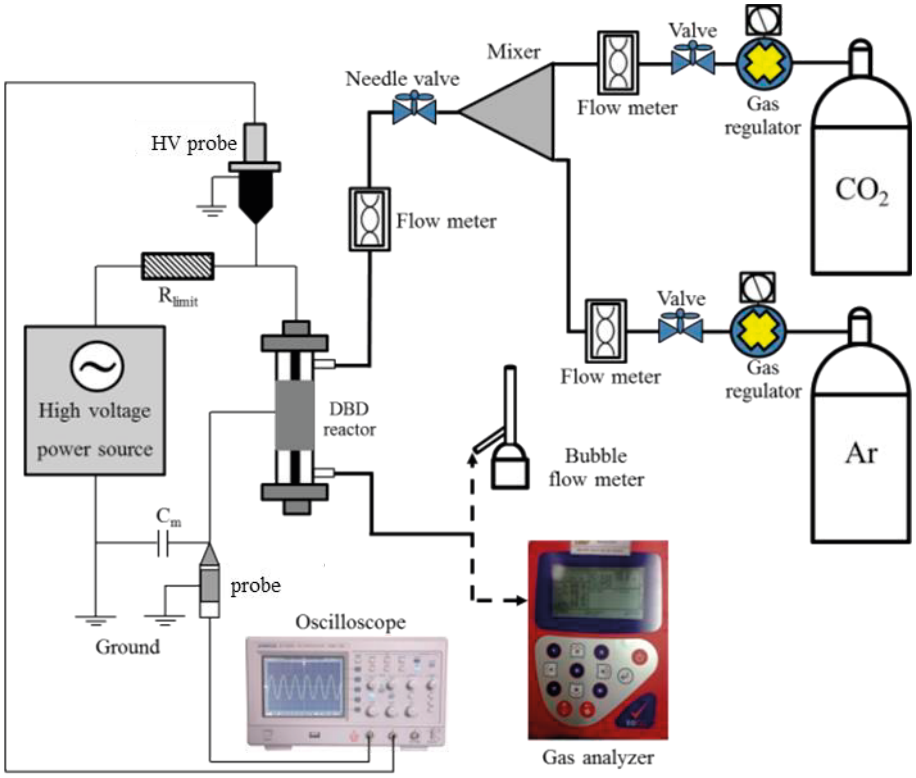

Figure 1. Experimental diagram and setup.

Figure 2. Reactor configuration for one outer electrode (A), two outer electrodes (B), and the cross-section of the reactor (C).

2.2. Operating and Measurement Methods

The concentration of CO_2 gas before and after the reaction process through the coaxial DBD reactor was investigated by a Gas analyzer instrument (Geotech, Biogas Check), this instrument consists of a gas detector for CH_4, CO_2, O_2, and H_2S. Inlet gas flow was controlled and measured by a needle valve and flow meter, respectively, while outlet gas flow was measured by the bubble flow meter. The

applied voltage used for plasma generation is measured by the HV probe. Furthermore, charge transfer can be measured from the voltage across C_m by using a voltage probe. These parameters of applied voltage and charge transfer were utilized to calculate the power consumption by Q-U Lissajous plotting [30].

2.3. Analysis and Calculation Methods

The results will be analyzed such as CO_2 conversion (χ_{conv}), O_2 selectivity (O_{2s}), power consumption, and conversion efficiency to propose the performance for the system of CO_2 decomposition. The formulas for gas analysis are rewritten from Danhua, M. et al. [24] and Paulusen, S. et al. [29]as shown in the following equation.

$$\chi_{conv}\ (\%) = \frac{CO_2 \text{ converted (mol)}}{CO_2 \text{ input (mol)}} \times 100 \tag{4}$$

$$O_{2s}\ (\%) = \frac{O_2 \text{ product (mol)}}{CO_2 \text{ converted (mol)}} \times 100 \tag{5}$$

Whilst O_2 selectivity (O_{2s}) was calculated by Eq.5 because this O_2 molecule reformed from CO_2 dissociation. In the case of power consumption (P_E) and the conversion efficiency (η_{conv}), it can be adopted from Wang, S. et al. [10] and Phuengkum, N. et al. [30] as shown below.

$$P_E\ (W) = f \cdot C_m \int_0^T U_t du_c \tag{6}$$

$$\eta_{conv}(\%/W) = \frac{CO_2 \text{ conversion (\%)}}{P_E\ (W)} \tag{7}$$

In Eq. 6, parameters were included the power source frequency (f = 7.8 kHz), measuring capacitor (C_m = 10 nF), applied voltage (U_t) and voltage across C_m (u_c).

3. Results and Discussion

3.1. Effect of CO_2 concentrations

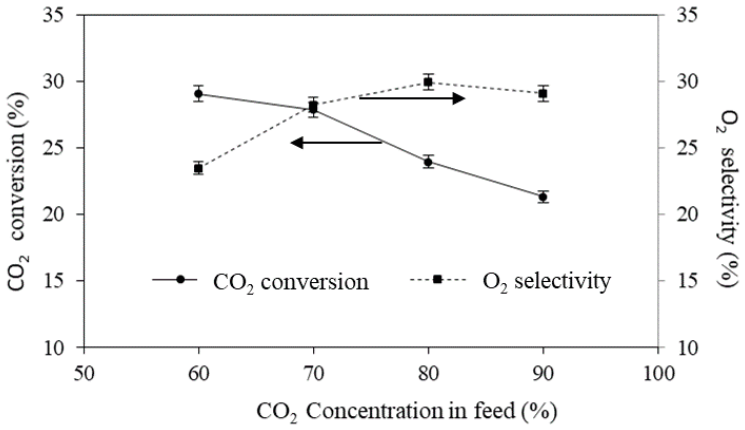

Figure 3. Effect of CO_2 diluted in Ar on CO_2 conversion and O_2 selectivity.

CO_2 gas was diluted by Ar gas, the percentage of CO_2 concentration was varied from 60% to 90%. The operating condition consists of 50 ml/min of gas flow rate, 1.30 mm of discharge gap, 8 cm of outer electrode length, and applied voltage was 8 kV. The result is shown in Figure 3, it has indicated that the increase of CO_2 concentration causes CO_2 conversion to decrease. On the other hand, O_2 selectivity which is the gas product has higher increased at 80% of CO_2 concentration.

3.2. Effect of outer electrode length and applied voltage

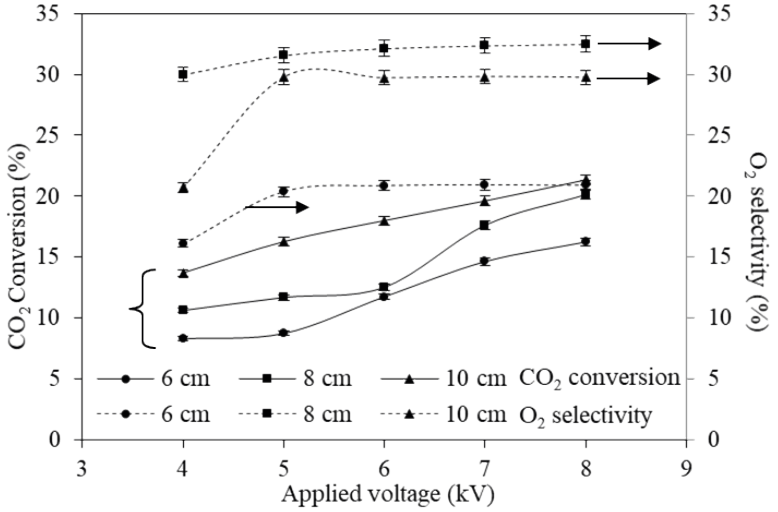

Figure 4. Effect of outer electrode length and applied voltage on CO_2 conversion and O_2 selectivity at 1.3 mm of discharge gap.

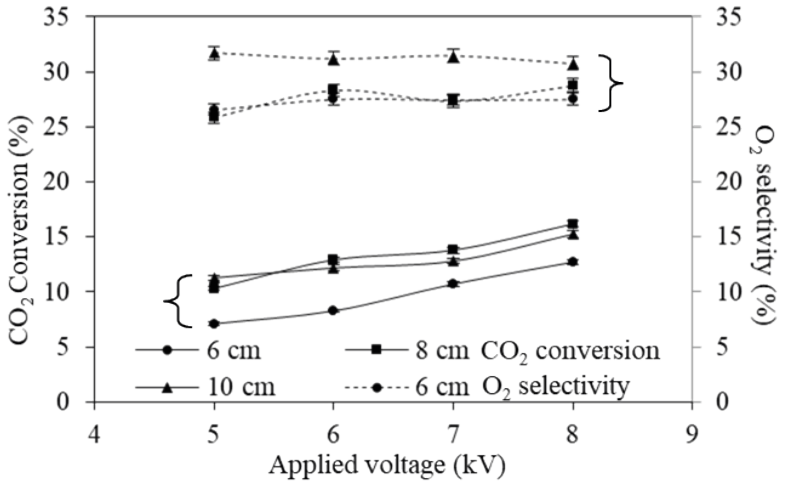

Figure 5. Effect of outer electrode length and applied voltage on CO_2 conversion and O_2 selectivity at 2.8 mm of discharge gap.

The experimental condition was conducted by 80 ml/min of gas flow rate and 60%:40% of CO_2:Ar ratio. These conditions have operated on two discharge gaps; there are 1.3 mm (Figure 4) and 2.8 mm (Figure 5), respectively. Figure 4 shows that the highest conversion of CO_2 can be achieved from the longest outer electrode. When the discharge gap is considered, 1.3 mm of discharge gap can raise CO_2 conversion higher than 15% for 8 cm and 10 cm of outer electrode lengths. In contrast, when the discharge gap was set at 2.8 mm (in Figure 5), the result has represented that it cannot raise CO_2 conversion to 15% for all of the outer electrode lengths. However, Figure 4 had been shown that 10 cm of outer electrode length can achieve higher CO_2 conversion than all of it. Whilst O_2 product was considered in terms of O_2 selectivity, Figure 4 and Figure 5 have indicated that O_2 selectivity was slightly changed after 5 kV of applied voltage. Indeed, it was implied that the high conversion of CO_2 can't raise the O_2 selectivity directly. As the gas product of CO_2 plasma consists of CO, O_2, and O_3, when O_2 selectivity was decreased it seems that the O_3 product might be increased. Because the O_3 forming can become from the recombination of O_2 molecules with O radicals.

3.3. Effect of discharge gap and plasma volume

The discharge gap is varied as 0.4 mm, 1.3 mm, and 2.8 mm, the length of the outer electrode was 8 cm, gas flow rate and CO_2:Ar ratio were 50 ml/min and 80%:20%, respectively. The free space between one outer electrode and another outer electrode was 8 cm as shown in Figure 2B to configure the two outer electrodes to increase the plasma volume. the result In Figure 6 has obviously indicated that the highest conversion of CO_2 can be obtained from the two outer electrodes with 1.3 mm of discharge gap (1.3 mm, 2OE). For O_2 selectivity, the result in Figure 7 has shown that O_2 selectivity from the 1.3 mm discharge gap with two outer electrodes (1.3 mm, 2OE) and 0.4 mm discharge gap has downward trended, while CO_2 conversion was increasing. However, the result in Figure 6 and Figure 7 have represented that the highest conversion of CO_2 and lowest O_2 selectivity can be achieved from a 1.3 mm discharge gap with two outer electrodes.

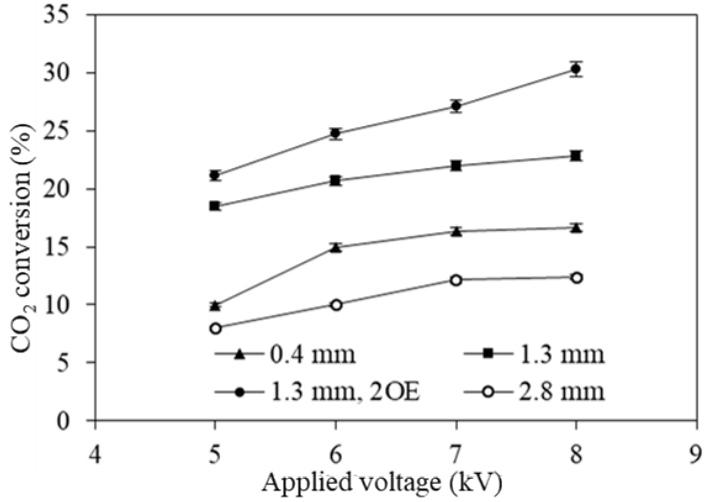

Figure 6. Effect of discharge gap and two outer electrodes (1.3 mm, 2 OE) on CO_2 conversion.

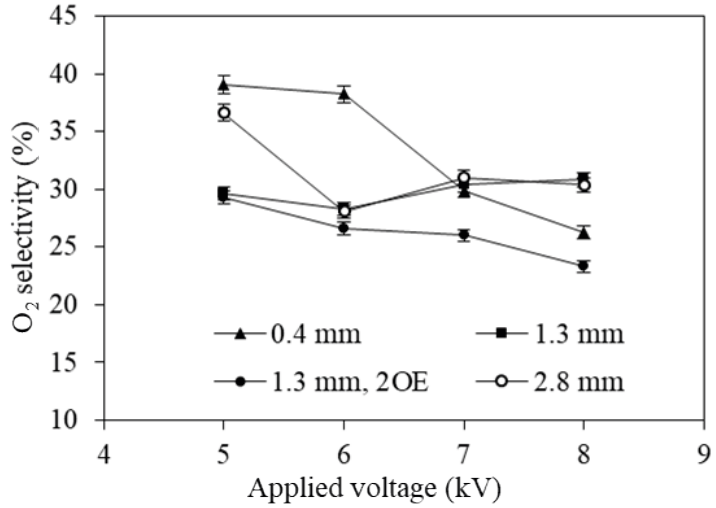

Figure 7. Effect of discharge gap and two outer electrodes (1.3 mm, 2 OE) on O_2 selectivity.

3.4. Effect of feeding flow rate

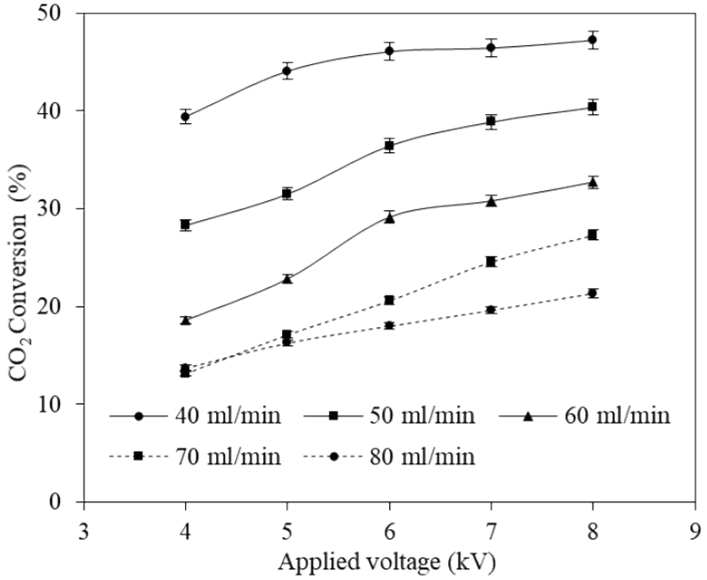

Figure 8. Effect of gas flow rate and applied voltage on CO_2 conversion and O_2 selectivity.

The experiment was conducted through the condition of 1.3 mm discharge gap, 60%:40% of CO_2:Ar ratio, 10 cm of outer electrode length. Whilst the feeding flow rate is varied from 40 ml/min to 80 ml/min. The result is shown in Figure 8, it has clearly present that the high flow rate causes the conversion CO_2 to decrease, while the low flow rate raises the percentage of CO_2 conversion. The highest conversion of CO_2 was obtained at 40 ml/min and gradually increased with increasing applied voltage.

3.5. Power consumption and conversion efficiency

The results were computed by Eq. 6 and Eq. 7 and have represented in Figure 9 and Figure 10 for the power consumption and conversion efficiency, respectively. In Figure 9, the results have shown that increasing of applied voltage causes the power consumption to increase for all conditions, while igure 10 has been showing the conversion efficiency was decreased when an applied voltage increased. However, the result has indicated that the high efficiency of CO_2 conversion can be achieved at a 1.3 mm discharge gap and 1.3 mm discharge gap with two outer electrodes. In contrast, the 2.8 mm discharge gap has shown a negative result of the power consumption and the conversion efficiency, there is high power consumption and low conversion efficiency.

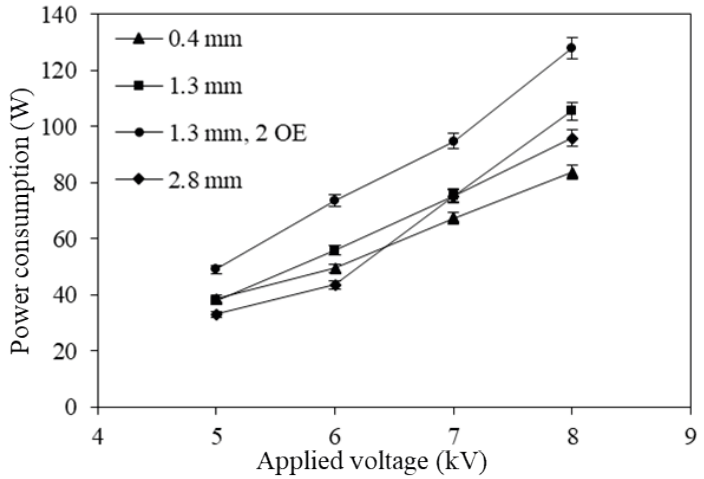

Figure 9. Power consumption versus applied voltage for each discharge gap.

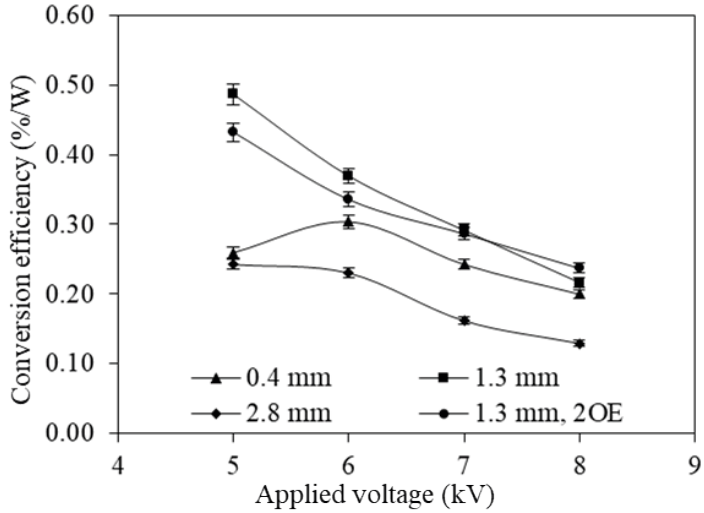

Figure 10. Conversion efficiency versus applied voltage for each discharge gap.

4. Conclusions

In summary, this work obviously exhibited that the use of the longest outer electrode at 10 cm and two outer electrodes with a 1.3 mm discharge gap could improve the performance of the coaxial DBD reactor and enhance the percentage of CO_2 conversion. In similarity, the increased applied voltage, low flow rate of gas feeding, and low CO_2 concentration can also raise the CO_2 conversion. It is clear that the highest percentage of CO_2 conversion was achieved at a 1.3 mm discharge gap with two outer electrodes, while its conversion efficiency was found to be lower than that of one outer electrode. In addition, this work can elevate the CO_2 conversion up to 47.2% at 10 cm of outer electrode length with a 1.3 mm discharge gap and 60%: 40% of the CO_2:Ar ratio with 40 ml/min of gas flow rate.

5. Acknowledgements

The authors would like to acknowledge to Faculty of Science and Technology and Rambhai Barni Rajabhat University for their support. Assist. Prof. Dr. Laemthong Chuenchom is thanked for proofreading the revised manuscript.

Author Contributions: IV characteristics of CO_2 and O_2 dielectric barrier discharges

Funding:

Conflicts of Interest:

References

[1] Guangyin, Z.; Youcai, Z. *Pollution Control and Resource Recovery for Sewage Sludge*, Guangyin, Z., Youcai, Z., Eds.; Butterworth-Heinemann, 2017; pp. 352-275.

[2] Da Costa Gomez, C. *The Biogas Handbook*, Wellinger, A., Murphy, J., Baxter, D., Eds.; Woodhead Publishing, 2013; pp. 1-16.

[3] Lyon, D. R. *Environmental and Health Issues in Unconventional Oil and Gas Development*, Kaden, D., Rose, T., Eds.; Elsevier, 2016; pp. 33-48.

[4] Rueangjitt, N.; Akarawitoo, C.; Chavadej, S. Production of Hydrogen-Rich Syngas from Biogas Reforming with Partial Oxidation Using a Multi-Stage AC Gliding Arc System. *Plasma Chemistry and Plasma Processing* 2012, pp. 583-596.

[5] Kroker, T.; Kolb, T.; Schenk, A.; Krawczyk, K.; Mlotek, M.; Gericke, K.-H. Catalytic Conversion of Simulated Biogas Mixtures to Synthesis Gas in a Fluidized Bed Reactor Supported by a DBD. *Plasma Chemistry and Plasma Processing* 2012, pp. 1-18.

[6] Kolb, T.; Kroker, T.; Voigt, J.; Gericke, K.-H. Wet Conversion of Methane and Carbon Dioxide in a DBD Reactor. *Plasma Chemistry and Plasma Processing* 2012, pp. 1-17.

[7] Qi, W.; Huiling, S.; Binhang, Y.; Yong, J.; Yi, C. Steam enhanced carbon dioxide reforming of methane in DBD plasma reactor. *International Journal of Hydrogen Energy* 2011, pp. 8301-8306.

[8] Tao, X.; Bai, M.; Li, X.; Long, H.; Shang, S.; Yin, Y.; Dai, X. CH_4-CO_2 reforming by plasma – challenges and opportunities. *Progress in Energy and Combustion Science* 2011, pp. 113-124.

[9] Indarto, A.; Choi, J.-W.; Lee, H.; Song, H. K. Decomposition of greenhouse gases by plasma. *Environmental Chemistry Letters* 2008, pp. 215-222.

[10] Wang, S.; Zhang, Y.; Liu, X.; Wang, X. Enhancement of CO_2 Conversion Rate and Conversion Efficiency by Homogeneous Discharges. *Plasma Chemistry and Plasma Processing* 2012, pp. 979-989.

[11] Lee, D.; Kim, K.-T.; Song, Y.-H.; Kang, W.; Jo, S. Mapping Plasma Chemistry in Hydrocarbon Fuel Processing Processes. *Plasma Chemistry and Plasma Processing* 2012, pp. 1-21.

[12] Indarto, A.; Yang, D> R.; Choi, J.-W.; Lee, H.; Song, H. K. Gliding arc plasma processing of CO_2 conversion. *Journal of Hazardous Materials* 2007, pp. 309-315.

[13] Babaie, M.; Davari, P.; Talebizadeh, P.; Zare, F.; Rahimzadeh, H.; Ristovski, Z.; Brown, R. Performance evaluation of non-thermal plasma on particulate matter, ozone and CO_2 correlation for diesel exhaust emission reduction. *Chemical Engineering Journal* 2015, pp. 240-248.

[14] Wen, Y.; Jiang, X. Decomposition of CO_2 Using Pulsed Corona Discharges Combined with Catalyst. *Plasma Chemistry and Plasma Processing* 2001, pp. 665-678.

[15] Yoshida, K.; Rajanikanth, B. S.; Okubo, M. NO_x Reduction and Desorption Studies Under Electric Discharge Plasma Using a Simulated Gas Mixture: A Case Study on the Effect of Corona Electrodes. *Plasma Science and Technology* 2009, pp. 327-333.

[16] Xiang, L.; Xumei, T.; Yongxiang, Y. An Atmospheric-Pressure Glow-Discharge Plasma Jet and Its Application. *IEEE Transaction on Plasma Science* 2009, pp. 759-763.

[17] Chang, M. D.; Jian, H. Y.; Bruno, C. Decomposition of toluene in a gliding arc discharge plasma reactor. *Plasma Sources Science and Technology* 2007, pp. 791-799.

[18] Xu, S.; Khalaf, P.; Martin, P.; Christopher, W. J. CO_2 dissociation in a packed-bed plasma reactor: Effects of operating conditions. *Plasma Science and Technology* 2018, Volume 27, pp. 1-13.

[19] Fridman, A. *Plasma Chemistry*, Cambridge University Press: New York, 2008; p. 978.

[20] Spencer, L.; Gallimore, A. Efficiency of CO_2 Dissociation in a Radio-Frequency Discharge. *Plasma Chemistry and Plasma Processing* 2011, pp. 79-89.

[21] Mei, D.; Zhu, X.; Wu, C.; Ashford, B.; Williams, P. T.; Tu, X. Plasma-photocatalytic conversion of CO_2 at low temperatures: Understanding the synergistic effect of plasma-catalysis. *Applied Catalysis B: Environmental* 2016, Volume 182, pp. 525-532.

[22] Yu, Q.; Kong, M.; Liu, T.; Fei, J.; Zheng, X. Characteristics of the Decomposition of CO_2 in a Dielectric Packed-Bed Plasma Reactor. *Plasma Chemistry and Plasma Processing* 2012, pp. 153-163.

[23] Zheng, G.; Jiang, J.; Wu, Y.; Zhang, R.; Hou, H. The Mutual Conversion of CO_2 and CO in Dielectric Barrier Discharge (DBD). *Plasma Chemistry and Plasma Processing* 2003, pp. 59-68.

[24] Danhua, M.; Xinbo, Z.; Ya-Ling, H.; Joseph, D. Y.; Xin, T. Plasma-assisted conversion of CO_2 in a dielectric barrier discharge reactor: understanding the effect of packing materials. *Plasma Sources Science and Technology* 2015, Volume 24, pp. 1-10.

[25] Tendero, C.; Tixier, C.; Tristant P.; Desmaison, J.; Leprince, P. Atmospheric pressure plasmas: A review. *Spectrochimica Acta Part B: Atomic Spectroscopy* 2006, pp. 2-30.

[26] Wagenaars, E.; Brandenburg, R.; Brok, W. J. M.; Bowden, M. D.; Wagner, H.-E. Experimental and modelling investigations of a dielectric barrier discharge in low-pressure argon. *Journal of Physics D: Applied Physics* 2006, pp. 700-711.

[27] Wagner, H. E.; Brandenburg, R.; Kozlov, K. V.; Sonnenfeld, A.; Michel, P.; Behnke, J. F. The barrier discharge: basic properties and applications to surface treatment. *Vacuum* 2003, pp. 417-436. doi:10.1016/S0042-207X(02)00765-0.

[28] Kogelschatz, U. Dielectric-Barrier Discharges: Their History, Discharge Physics, and Industrial Applications. *Plasma Chemistry and Plasma Processing* 2003, pp. 1-46.

[29] Paulusen, S.; Verheyde, B.; Tu, X.; Bie, C. D.; Martens, T.; Petrovic D.; Bogaerts, A.; ; Sels, B. Conversion of carbon dioxide to value-added chemicals in atmospheric pressure dielectric barrier discharges. *Plasma Sources Science and Technology*, 2010; Volume 19, pp. 1-6.

[30] Phuengkum, N.; Tirawanichakul, Y. Physics applications: IV characteristics of CO_2 and O_2 dielectric Barrier discharges. *2011 IEEE Colloquium on Humanities, Science and Engineering (CHUSER)* 2011, pp. 805-808.

JSTR
ASEAN Journal of Scientific and Technological Reports

Research article

Effect of Decomposed-Stone Dust on Properties of Concrete

Chookiat Choosakul[1] Khwanchiwa Yongsata[2]* and Sunun Monkaew[3]

[1] Division of Civil Engineering, College of Industrial Technology and Management, Rajamanagala University of Technology Srivijaya, Nokhon Si Thammarat, 80210, Thailand; chookiat56@yahoo.com
[2] Division of Technology Engineering, Faculty of Engineering and Technology, Rajamanagala University of Technology Srivijaya, Trang, 92150, Thailand; khwanchiwa.y@rmutsv.ac.th
[3] Division of Civil Engineering, Faculty of Engineering, Rajamanagala University of Technology Phra Nakhon, Bangkok, 10800, Thailand; sunun.m@rmutp.ac.th
* Correspondence: E-mail: khwanchiwa.y@rmutsv.ac.th

Abstract: The objective focused on the study of shrinkage behavior of concrete using Decomposed-Stone Dust to replace Portland cement type 1 in the ratio of 10, 15, and 20 percent by weight of binder as well as designing compressive strength at 280 kg/cm^2. Testing the formation time, shrinkage behavior, and compressive strength of concrete was compared with the concrete using Portland cement type 1. The study found that the concrete using Decomposed Stone Dust was an increased formation period in accordance with the amount of replaced Decomposed-Stone Dust. Autogenous shrinkage, dry shrinkage, and compressive strength of concrete mixed with Decomposed-Stone Dust were less than control concrete. In all mixing ratios, the ratio of 20% replacement of Portland cement dust was the most suitable for this study. The initial formation time was 155 minutes. The final formation period was 305 minutes. The autogenous shrinkage was 312 microns, the dry shrinkage was 699 microns and compressive strength was 286 kg/cm^2 respectively at age 28 days.

Keywords: Shrinkage Concrete, Compressive Strength, Decomposed-Stone Dust, Natural Pozzolan

Citation:
Choosakul, C.; Yongsata, K., Monkaew, S. Effect of Decomposed-Stone Dust on Properties of Concrete. *ASEAN J. Sci. Tech. Report.* **2022**, *25(1)*, 60-68. https://doi.org/10.55164/ajstr.v25i1.244118

Article history:
Received: May 7, 2021
Revised: February 10, 2022
Accepted: February 23, 2022
Available online: March 29, 2022

Publisher's Note:
This article is published and distributed under the terms of the Thaksin University.

1. Introduction

Decomposed stone is a raw material found in volcanic, granite, feldspar, or kaolin sites. Thailand found several sources of decaying stone. However, the most popular sources used in the ceramics industry are Lampang, Lopburi, Kanchanaburi, and Phetchaburi, as known as the trade name of it in Pottery Stone. In general, the main mineral structure of a decaying stone consists of quarts and mica. (White Mica; $K_2O{\cdot}3Al_2O_3{\cdot}6SiO_2{\cdot}H_2O$). Quarts are highly fireproof with no stickiness, including incapable of melting. On the other hand, mica has properties like kaolin by quality of being sticky. Because of that quality, it improves the flow conditions of decomposed stone, the decomposed stone's melting point is about 1,150-1,300 °C. Decomposed stone is a mineral that yields silica, alumina, and potash in the optimum ratio with the chemical composition in the structure as shown in Table 1 [1] Decomposed stone dust is obtained by crushing the rock, which has properties containing Class N pozzolans [2] as ASTM C 618 [3].

From the study of [2], it was found that decomposed stone dust can be used as a substitute for type 1 Portland cement in mortars for construction and plastering work. The mortar mixed with 25% of the decomposed stone dust had the highest compressive strength. Mortar mixed with 20% of the decomposed stone dust had the highest tensile strength. According to a study of [4] in high-strength concrete, the decomposed stone dust can be used as a substitute for the Portland cement type 1 to a ratio of 10% with a compressive strength of 517 kg/cm^2 at age 28 days.

Table 1. The amount of chemical elements in the structure of decomposed stone

Chemical composition (%)	Lampang [1]	Lopburi [1]	Surat Thani [2]
SiO_2	76.61	75.88	30.07
Al_2O_3	13.09	11.69	19.86
Fe_2O_3	0.35	0.81	13.67
SO_3	-	-	6.29
MgO	0.01	< 0.01	2.47
CaO	0.15	0.20	16.78
Na_2O	5.20	3.67	1.31
K_2O	1.59	4.74	2.12
TiO_2	0.05	0.13	-
P_2O_5	< 0.01	< 0.01	0.21
MnO_2	0.02	0.01	-
Cr_2O_5	0.01	<0.01	-
LOI	3.92	3.67	5.80

The cracking from the concrete shrinkage is one of the problems with the concrete structures. This is because cracks affect the stability and beauty of the structure. Cracking concrete allows the water or other substances to penetrate the concrete surface and react with the water and reinforcement. Resulting in the reinforcement rusting reduced cross-sectional area. That resalt influenced to be decreasing of the tensile strength of the reinforcing steel, including increasing of the deflection and will affect the problem of using the building in the long-term. Concrete cracking usually occurs in early concrete life by having low-strength concrete shrinkage cracking, which has a complex mechanism. It depends on many factors: including independent contraction shrinkage rate pull creep conditions of retention elastic modulus [5-6]. There are many types of concrete shrinkage. The contraction that has a great effect on cracking is auto genius contraction and dry shrinkage. The cracking caused by the concrete shrinkage is the result of the automatic shrinkage and the dry shrinkage that are coexist. Shrinkage of concrete alone cannot cause concrete to crack. But if the recoil is retained, whether it is retaining from the internal reinforcement or an external structure. All cause a seizure within the concrete when the concrete is retained, a tension unit is created. When the tensile strength unit is greater than the concrete tensile strength, the concrete will crack [7].

2. Materials and Methods

2.1 Research materials

2.1.1 Binder

This research was using Portland Cement Type 1, SCG brand of Siam Cement Company Limited, produced in accordance with TIS 15, Volume 1 [8] and decomposed stone dust from rotted stone wells in DonSak district Suratthani Province by using decomposed stone material to grind thoroughly.

2.1.2 Aggregates

Coarse aggregates using limestone with the maximum size of 3/8 inch, the value of 2.77, water absorption of 0.49%, the weight of 1,512 kg/m^3, and fineness modulus (FM) is 7.47. The fine aggregate used coarse sand with specific gravity (Saturated Surface Dry) of 2.60, water absorption of 0.48%, unit weight of 1,590 kg/m^3 and FM is 3.10. Both types of aggregates are aggregate grading in accordance with standard ASTM C33 [9].

2.2. Mixture design and sample preparation

Concrete sample preparation by replacing the decomposed stone dust material to replace Portland Cement Type 1at a ratio of 10, 15, and 20% by weight of the binder. Design concrete mix according to standards ACI 211.1-91 [10] .The maximum compressive strength is determined at the age of 28days (fc′) equals 280 kg/cm ^{2}which is suitable for medium-sized buildings and as it is used for most low rise structural buildings [11]. The concrete mixing design is shown in Table 2.

Table 2. Concrete Mixing Designs in This Study

Code	Content (kg/m^3)				
	Cement	**DSD**	**Sand**	**Rock**	**Water**
OPC	420	0.00	866	924	162
DSD10	375	42	866	924	162
DSD15	357	63	866	924	162
DSD20	336	84	866	924	162

Note :OPC = Concrete mixed with Ordinary Portland Cement Type1
DSD10 = Concrete mixed with Decomposed Stone Dust 10%

2.3 Test method

2.3.1 Fineness of decomposed stone dust test by sieve number 325 according to ASTM C430 [12].

2.3.2 ***Setting time of concrete*** was sifted through a No.4 sieve and placed into a cube-shaped formwork and size 15 x 15 x 15 centimeter by tested in accordance to ASTM C403 [13]. Test for the collapse value of fresh concrete was according to ASTM C143 [14].

2.3.3 Dry shrinkage test by applying from the ASTM C596 [15]. The model was removed at 24 hours and then, incubated in water for 7 days. The temperature during incubation was 30 ± 2 °C. When the curing has finished, then removed the sample from the water and dried the surface with a cloth. The length of the sample was taken against a standard fixed-length metal rod. Which is the default length the incubated parts were taken in the air, the average temperature was 30 ± 2 °C. The length of the sample was taken against a standard fixed-length metal rod. The air curing life was 7 to 28 days to determine the percentage of dry shrinkage over the curing life. Also, the values measured at different ages were used to calculate the percentage of dry shrinkage.

2.3.4 Autogenous shrinkage test is compliant ASTM C157 [16] measured for the shrinkage of concrete bar sizes 7.5 x 7.5 x 28.5 centimeter. Test by removing the 24 -hour old model and measuring the initial length samples are aged for 1 day, then incubated by plastic wrap for 1 to 28 days and stored in the incubation room. The shrinkage measurement was started as an applied method from the same standard used for the dry shrinkage measurement.

2.3.5 The compressive strength test with cylinder 15 × 30 centimeter mold. The samples were demolded 24 hours after casting. The cylinder was tested at the age of 7 days, 14 days, and up to 28 days monitoring stag after the wet curing process at the curing tank in accordance with procedures according to ASTM C39 [17]. The compressive strength reported in this article is the average obtained from 3 test samples.

3. Results and Discussion

3.1 Fineness of decomposed stone dust

Resolution test results of decomposed stone dust It was found that the average percentage of retention on a wet sieve No. 325 standard sieve was 27.70%. The obtained values are within the criteria specified by ASTM C618 [3], which must be less than 34%.

3.2 Setting time of concrete

Table 3shows the time of the formation of concrete samples. The results showed that the increase in the decomposed stone dust resulted in an increased time of formation. Due to the increased replacement of pozzolanic materials, the cement content is low, resulting in an increased formation time, C_3S will decrease with the decrease of Portland cement. This substance allows concrete to be formed in a short time. It relates to the research of [18].

Table 3. Setting Time and Slump of fresh concrete blended with decomposed stone dust

Code	Setting Time (min)			Slump (cm)
	Initial	Finished	Elapsed	
OPC	119	268	149	8
DSD10	127	274	147	10.5
DSD15	140	289	149	11.5
DSD20	155	305	150	12

3.3 Dry shrinkage

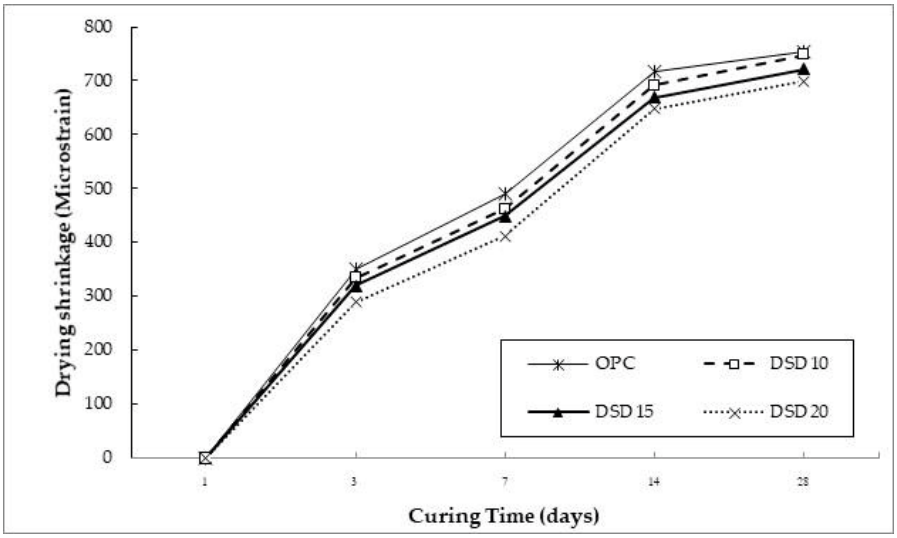

Figure 1. Dry shrinkage of concrete

Figure 1 shows the dry shinkage of concrete was found that concrete mixed with decomposed stone dust tends to shrink less than control concrete, the shrinkage of concrete increased with the increase in curing time for both controlled concrete and decomposed stone dust mixture. The contraction rate occurs rapidly at the beginning. And begin to decline over time. This is because, initially, large volumes of free water could easily be moved outside through the capillary channel until the water content in the gel structure and calcium silicate hydrate (C-S-H) is released, but the evacuation capacity is very low [19]. Due to the structure of the gel

and the C-S-H (Restrained) to be used at an increased time. Increased hydration results in an increased amount of C-S-H in concrete, that is, the capillary cavity is smaller, water or moisture makes it difficult to move. Up results in, therefore the shrinkage rate is lower until the shrinkage is stable.

3. 4Autogenous shrinkage

The autogenous shrinkage behavior of concrete mixed with decomposed stone dust compared with control concrete overall is presented in Figure 2. It can be seen that concrete containing decomposed stone dust had lower shrinkage than control concrete. The shrinkage value decreased as the amount of cement replacement with decomposed stone dust increased. Increasing the percentage of replacing cement with decomposed stone dust is equivalent to reduce the amount of cement in the concrete. As a result, the hydration reaction decreases, and the free water content in the concrete increases, Thus, causing the shrinkage of autogenous [20].

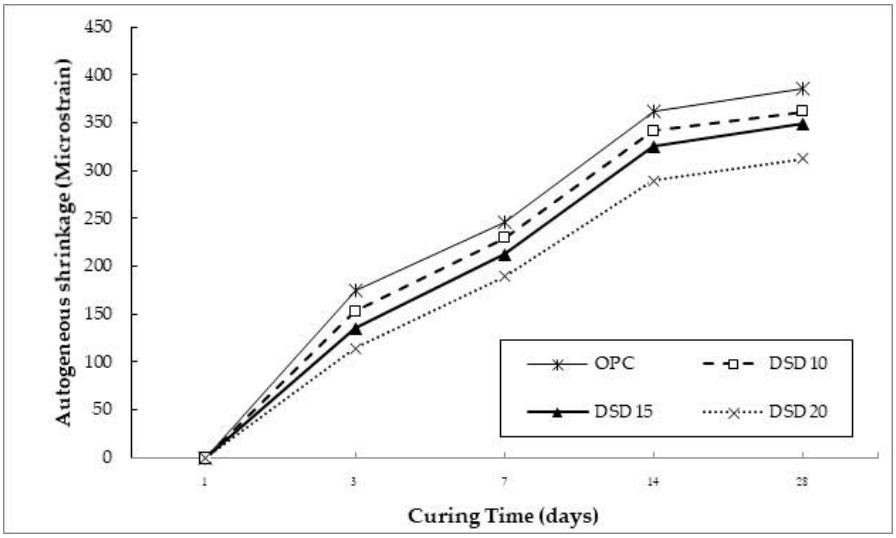

Figure 2. Autogenous shrinkage of concrete

3.5 Compressive Strength

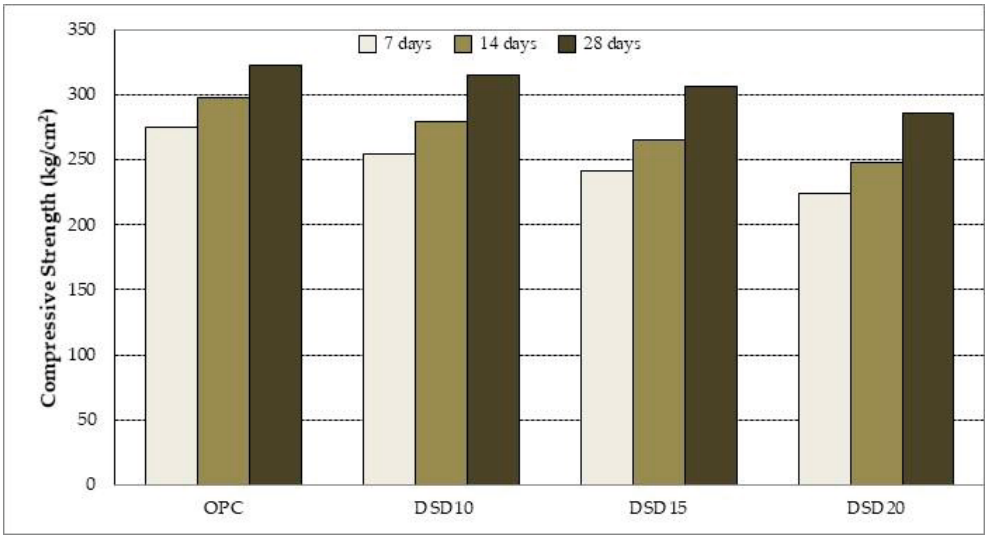

Figure 3. Compressive Strength of concrete

Figure 3 shows the results of testing the compressive strength of concrete. Increasing the amount of decomposed stone dust will reduce the compressive strength of concrete. Developing the compressive strength of concrete with curing age, it can be seen that the control concrete develops regularly. But in the concrete mix with decomposed stone dust, the early compressive strength development is relatively lower because of the absence of pozzolanic reaction, but after 14 days the compressive strength development rate will be higher. This is because the pozzolanic reaction develops more as the curing age increases [21]. For replacement of 10% and 15% of decomposed stone dust gives compressive strength close to those of OPC at 28 days.

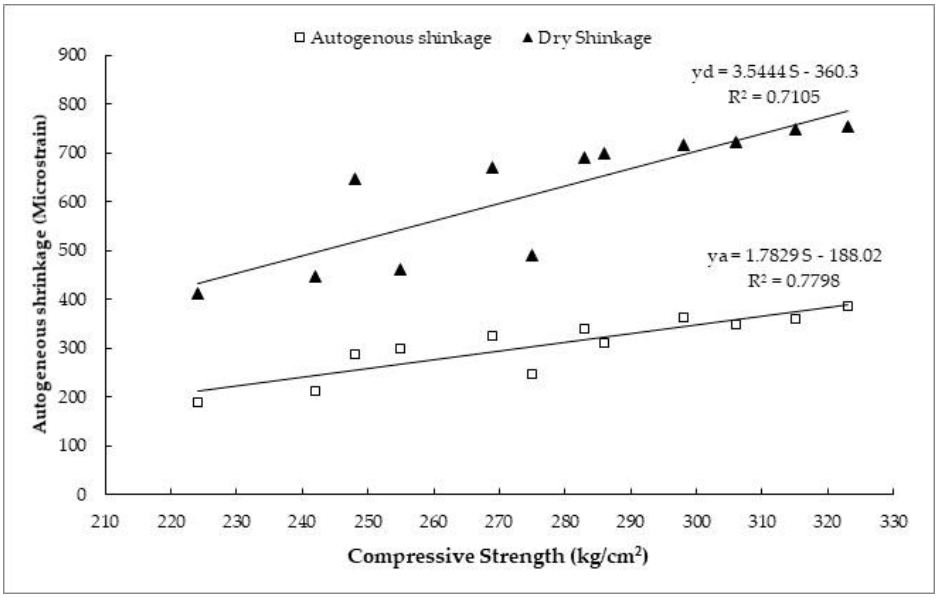

Figure 4. Relationship between Compressive Strength of concrete and Dry shrinkage, Autogenous shrinkage. (yd: dry shrinkage, ya: autogenous shrinkage, S: compressive strength, R^2: coefficient of correlation)

Figure 4 shows this linear relationship for various deformations of dry shrinkage and autogenous shrinkage with a relatively acceptable correlation coefficient. It is established that this relationship is sufficient for ordinary cement and natural pozzolan as reported by the researcher [22]. As the results show, it is clear that the relationship of autogenous shrinkage to compressive strength is well acceptable when the correlation coefficient is higher.

Figure 5-6 represents the dry shrinkage and autogenous shrinkage with compressive strength for each code of concrete. From these results, it will be shown that when the concrete has a compressive strength of more than 300 kg/cm^2, the cavitation decomposed stone dust mixture results in lower autogenous shrinkage of DSD than the OPC. And it can be seen that when the concrete still has a strength value of less than 280 kg/cm^2, the decomposed stone dust mixture increases the dry shrinkage. But when the strength is beyond this, the decomposed stone dust mixture will decrease the dry shrinkage value. Once this strength is exceeded the concrete contains decomposed stone dust, and when the compressive strength exceeds 300 kg/cm^2 the dry shrinkage of the decomposed stone dust concrete is also lower than that of the OPC with autogenous shrinkage. This result is in agreement with those reported by Armed et al. [22].

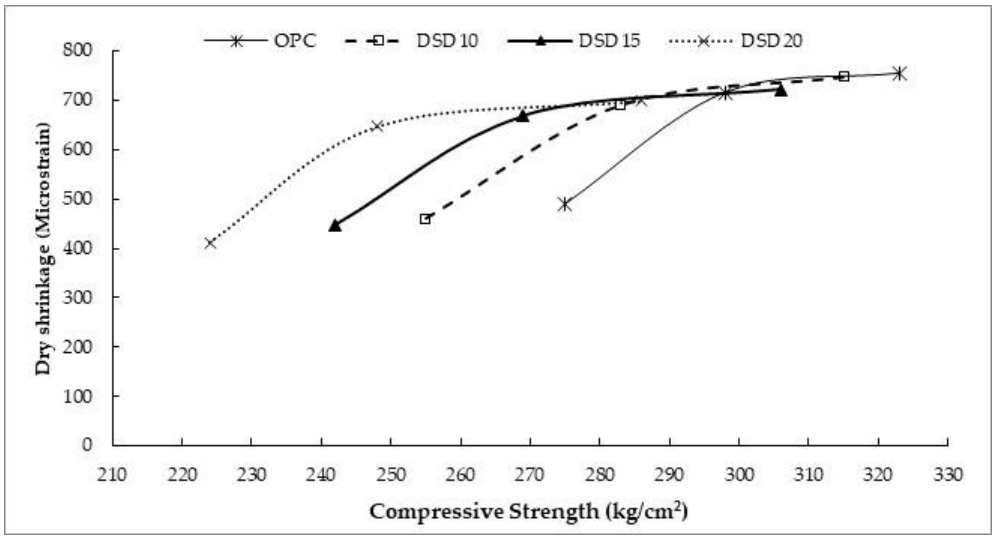

Figure 5. Variation of dry shrinkage according to compressive strength for several replacement rates of decomposed stone dust.

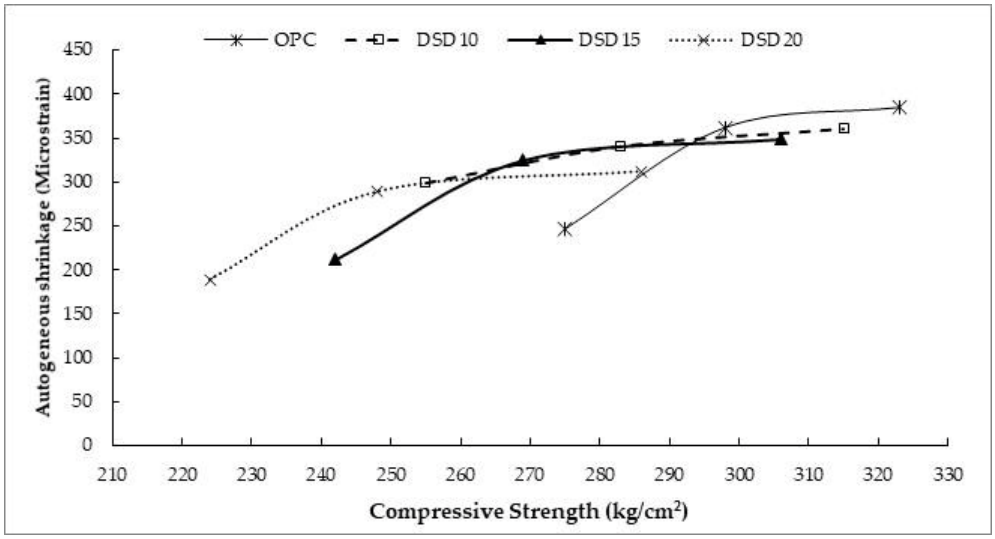

Figure 6. Variation of autogenous shrinkage according to compressive strength for several replacement rates of decomposed stone dust.

4. Conclusions

The test results are obtained from the research can be summarized as follows.

1. Concrete replacing cement with decomposed stone dust, helps to increase the formation time of concrete.

2. Concrete replacing cement with decomposed stone dust, reduces dry shrinkage of concrete.

3. Concrete replacing cement with decomposed stone dust, reduces the autogenous shrinkage of concrete.

4. The dry shrinkage has a greater shrinkage of the concrete sample than the autogenous shrinkage because the concrete sample exhibits rapid and constant loss of free water even at an extended curing life. Whereas the hydration reaction has a slower and lesser effect on the shrinkage of the concrete sample at the same time.

5. The partial replacement of cement with decomposed stone dust results in a decrease in compressive strength and the value decreased as the amount of decomposed stone dust increases.

6. The shrinkage of concrete varies with the compressive strength of concrete. When the concrete has a compressive strength of 300 kg/cm^2, the shrinkage behavior between the decomposed stone dust concrete and OPC will change.

7. Concrete replacing cement with 20% decomposed stone dust was the most suitable in this study. The initial formation time was 155 minutes, the final formation time was 305 minutes. The elapsed time was 150 minutes. From all the formation time mentioned before a curing time of 28 days, the result of autogenous shrinkage was 312 microns, the dry shrinkage value was 699 microns and the compressive strength was 286 kg/cm^2, respectively.

5. Acknowledgments

Thank you to Division of Engineering, College of Industrial Technology and Management, Rajamangala University of Technology Srivijaya that supported the equipment and testing room for this research.

Author Contributions:

Funding:

Conflicts of Interest:

References

[1] Sin Khaotham Pattanakij Co.,Ltd. (2009). Get to know the decomposed stone. Online: http://skpc.co.th/v2.2008/chemical_analysis.php. (12 January 2019)

[2] Choosakul, C. A Study of Decomposed-rock Dust as a Partial Replacement of Portland Cement for Bricking and Plastering Work. *In Proceeding of the sixth Annual Concrete Conference*. Phetchaburi, Thailand, October 20-22, 2010, pp. 213-217. (In Thai)

[3] Standard Specification for Coal Fly Ash and Raw or Calcined Natural Pozzolan for Use as a Mineral Admixture in Concrete. *Annual Book of ASTM Standards*, ASTM C618-01, 2001, Vol. 04.02.

[4] Choosakul, C. and Yongsata, K. High Strength Concrete Using Decomposed-Stone Dust. In *Proceeding of the twelfth Annual Concrete Conference*. Phetchaburi, Thailand, February 15-17, 2017 ,pp. MAT01-MAT06. (In Thai)

[5] Nemati, K. M. Strength of Concrete. In *Concrete Technology* University of Washington, USA, 2015, pp. 1-18.

[6] Mora-Ruacho, J.; Gettu, R.; Aguado, A. Influence of shrinkage-reducing admixtures on the reduction of plastic shrinkage cracking in concrete. *Cement and Concrete Research* 2009, *39*, 141-146.

[7] Claisse, P.A. Creep, shrinkage, and cracking of concrete. In *Civil Engineering Materials*; Butterworth-Heinemann: Oxford, UK, 2016, pp. 241-249.

[8] Portland Part 1 Specification. *Thai Industrial Standards Institute*, TIS. 15-2004, Ministry of Industry , Bangkok, 2004. (In Thai)

[9] Standard Specification Concrete Aggregates. *Annual Book of ASTM Standards*, ASTM C33-01, 1997, Vol. 04.02

[10] Standard Practice for Selecting Proportions for Normal, Heavyweight, and Mass Concrete. *ACI Manual of Concrete Practice*, ACI 211.1-91, 2000, Part 1.

[11] Alsadey, S.; Omran, A. Effect of the Type of Sand on the Properties of Concrete. *Journal of Engineering and Applied Sciences* 2021, *16*, 111-113.

[12] Standard Test Method for Fineness of Hydraulic Cement by the 45-m (No. 325) Sieve. Annual book of ASTM standard, ASTM C430-08, 2011, Vol. 04.02.

[13] Standard Test Method for Time of Setting of Concrete Mixtures by Penetration Resistance. *Annual Book of ASTM Standards*, ASTM C403-92, 1999, Vol. 04.02.

[14] Standard Testing Method for Slump of Hydraulic Cement Concrete. *Annual Book of ASTM Standards*, ASTM C143-90a, 2001, Vol. 04.02.

[15] Standard Test Method for Drying Shrinkage of Mortar Containing Hydraulic Cement. *Annual Book of ASTM Standards*, ASTM C596-09, 2017, Vol. 04.01.
[16] Standard Test Method for Length Change of Hardened Hydraulic-Cement Mortar and Concrete. *Annual Book of ASTM Standards*, ASTM C157/C157M-17, 2017, Vol. 04.02.
[17] Standard Test Method for Compressive Strength of Cylindrical Concrete Specimens. *Annual Book of ASTM Standards*, ASTM C39, 2001, Vol. 04.02.
[18] Cai, R.; He, Z.; Tang, S.; Wu, T.; Chen, E. The early hydration of metakaolin blended cements by non-contact impedance measurement. *Cement and Concrete Composites* 2018, *92*, 70-81.
[19] De Sensale, G.R.; Ribeiro, A.B.; Gonçalves, A. Effects of RHA on autogenous shrinkage of Portland cement pastes .*Cement and Concrete Composites* 2008, 30, pp. 892 –897.
[20] Neville, A. M. *Properties of Concrete*. 5th ed; Pearson Education Limited: Harlow, England, 2011.
[21] Mindess, S.; Young, J. F.; Darwin, D. *Concrete*. 2nd ed. Prentice-Hall, Upper Saddle River, NJ. 2003.
[22] Itim, A.; Ezziane, K.; Kadri, E. H. Compressive strength and shrinkage of mortar containing various amounts of mineral additions. *Construction and Building Materials* 2011, *25*, 3603-3609.

JSTR
ASEAN Journal of Scientific and Technological Reports

Research article

In silico screening of potential inhibitor from *Andrographis paniculata* constituents against three targets of SARS-CoV-2: Main protease, Spike protein, and Nsp15

Panita Kongsune[1*], Wansiri Innok[2] and Thanyada Rungrotmongkol[3]

[1] Department of Chemistry, Faculty of Science, Thaksin University, Phattalung, 93210, Thailand; dpanital@tsu.ac.th
[2] Department of Chemistry, Faculty of Science, Thaksin University, Phattalung, 93210, Thailand; paiipaiiwansiri@gmail.com
[3] Structural and Computational Biology Research Unit, Department of Biochemistry, Faculty of Science, Chulalongkorn University, Bangkok 10330, Thailand; t.rungrotmongkol@gmail.com
* Correspondence: dpanital@tsu.ac.th.

Citation:
Kongsune, P.; Innok, W.; Rungrotmongkol, T.. In Silico Screening of Potential Inhibitor from *Andrographis paniculata* Constituents Against Three Targets of SARS-CoV-2: Main Protease, Spike Protein and Nsp15. ASEAN J. Sci. Tech. Report. **2022**, *25(1)*, 69-77. https://doi.org/10.55164/ajstr.v25i1.245942.

Article history:
Received: January 22, 2022
Revised: March 21, 2022
Accepted: March 22, 2022
Available online: March 29, 2022

Publisher's Note:
This article is published and distributed under the terms of the Thaksin University.

Abstract: The current pandemic of COVID-19 is caused by Severe Acute Respiratory Syndrome Coronavirus 2 (SARS-CoV-2), which has increased the morbidity and mortality rate throughout the world. World Health Organization has declared this COVID-19 outbreak as a health emergency throughout the world. At this time, there are very few drugs against SARS-CoV-2. So, this study aimed to screen 91 *Andrographis paniculata* against three targets of SARS-CoV-2: main protease, spike protein, and Nsp15 by molecular docking. The calculation result revealed that mostly bioactive compounds from *Andrographis paniculata* are a good binding affinity with the main protease than that of Nsp15 and spike protein. The top six compounds and their interactions with the active site were visualized. Among them, 7,8-dimethoxy flavone-5-β-D-glucopyranosyloxy flavone and Stigmasterol compounds from *Andrographis paniculata* had a superior binding affinity of -11.65 and -11.33 kcal/mol toward the main protease. A detailed understanding of ligand-protein interaction could be helpful in further drug design and development for COVID-19 treatment.

Keywords: COVID-19; Molecular docking; Thai herbs; MPro; Nonstructural proteins

1. Introduction

Coronavirus disease 2019 (COVID-19), an infectious disease caused by SARS-CoV-2 (severe acute respiratory syndrome coronavirus-2) has become a pandemic. It has infected more than 285 million people all over the world since it was discovered and reported 5.5 million deaths by end of 2021 (https://www.worldometers.info/coronavirus/). COVID-19 is clinically characterized by fever, slight pain in the neck, headache, dry cough, breathing problem, vomit, and it might lead to death through multi-organ failure [1]. The SARS-CoV-2 re-emergence in Thailand especially in April 2021 has kept the government under high alert and has made a severe situation demanding fast treatment to prevent the infected patients. Currently, there are no efficient antiviral drugs for the prevention of COVID-19 infection. The current prevention

methods are directed on quarantine and containment of infected patients for preventing human-to-human transmission along with vaccinations. The need for rapid time-to-solution in drug discovery has become accentuated by the COVID-19 pandemic. Therefore, structure-based molecular docking for screening anti-SARS-CoV-2 potential drug candidates from natural sources is the main goal of this study.

The coronavirus is a single-strand RNA virus (+ssRNA) that can cause severe respiratory syndrome in humans [2]. SARS-CoV-2 (also called 2019-nCoV) is an enveloped, single-stranded, positive-sense RNA virus with genome sizes ranging from 26 to 32 kb and virion sizes from 50 to 200 nanometers in diameter. Four essential structural proteins, i.e., Spike protein (S), Envelope protein (E), Membrane protein (M), and Nucleocapsid protein (N) are found in SARS-CoV-2 and to generate the major components of the virus particle, polyprotein processing is an essential mechanism [3]. Each of the key viral proteins of the SARS-CoV-2 viral replication cycle steps such as spike protein, nonstructural proteins 15 (Nsp15), and main protease have been used as a target region for screening anti-SARS-CoV-2 potential drugs. The spike (S) glycoprotein homotrimer on the COVID-19 virus surface plays an essential role in receptor binding and virus entry in which it uses the angiotensin-converting enzyme 2 (AEC2) receptor for cell entry. The S protein is a multifunctional molecular machine that plays key role in the early steps of viral infection by interacting with host susceptibility factors, including receptors and proteases [4]. While the nonstructural proteins (Nsps) and the N protein are required for packaging of the viral genome into the newly assembled virion. SARS-CoV-2 Nsp15 is a uridine-specific endoribonuclease with a C-terminal catalytic domain belonging to the EndoU family that is highly conserved in coronaviruses [5]. The polyproteins are cleaved and transformed into mature nonstructural proteins by the main proteases and are responsible for playing a role in the replication/transcription process. Therefore, spike protien, Nsp15 and main protease could be an effective drug targets for anti-SARS-CoV-2.

The structural-based virtual screening of small molecules from natural sources with key viral proteins target will provide the potential drug candidates. Many natural products showed inhibitory activity on the COVID-19 virus. Andrographolide and its derivatives derived from *Andrographis paniculata* have been used for the treatment of COVID-19 virus with fever [6-7], sore throat, chronic cough, and other human diseases [8-9]. The herbs such as gallic acid, curcumin, and its derivatives and mushroom [1, 6, 10-11], have attracted increasing attention for COVID-19 virus agent targeting. Though several in vitro studies showed that natural compounds have anti-virus activity , their inhibition mechanism of action is not known and even more difficult to analyze at the molecular level using experimental methods. Therefore, comprehensive studies are required to determine their molecular interactions. Recently, several studies have used the molecular docking method to study the interactions and conformations of ligand against the SARS-CoV-2 virus [3, 10-12] which leads away to in vitro and in vivo studies. In this study, we aimed to explore the lead compound from *Andrographis paniculata* herb for their medicinal potentials as therapeutic agents against the spike protein, Nsp15, and the main protease of SARS-CoV2. So, the 91 bioactive molecules (Figure 1) were used to explore the lead compound for their medicinal potentials as therapeutic agents against influenza. A detailed understanding of ligand-protein interaction could be helpful in further drug design and development for COVID-19 treatment.

2. Materials and Methods

2.1. Compound data set

The 91 structures of *Andrographis paniculata* were structurally drawn using Gauss View [13]. Their three-dimensional (3D) structures were optimized at the Hartree-Fock level of theory with a 6-31G* basis set using the Gaussian 03 program [14]. The optimized structures (Figure 1) were viewed and converted to .pdb format using GaussView [13] for molecular docking study. The three-dimensional (3D) structures of the two targets of SARS-CoV-2*:* main protease and spike protein were retrieved from the Brookhaven Protein Data Bank (PDB) [15]. The PDB ID of main protease, spike protein and Nsp15 were 6XBG (Resolution*:* 1.45 Å, R-Value Free*:* 0.206, R-Value Work*:* 0.181*)* [16], 7BZ5 (Resolution*:* 1.84 Å, R-Value Free*:* 0.191, R-Value Work*:* 0.167) [17] and 6WXC *(*Resolution*:* 1.85 Å, R-Value Free*:* 0.194, R-Value Work*:* 0.171*)* [5], respectively. The water molecules were eliminated while the missing hydrogen atoms were added to this protein.

2.2. Molecular docking

The molecular docking technique was applied to study the binding orientation and affinity of the bioactive compounds from Thai herbs toward the binding site of the main protease of COVID-19 using Autodock 4.2 [18]. Partial atomic charges of protein and ligands were assigned using the Gasteiger–Marsili method [19] implemented in AutoDock Tools [20]. By semiflexible docking protocol, the protein molecule was kept rigid, while the ligand was flexible to attain a degree of freedom torsions bridged by the rotational parameter. The protein and ligands were converted to .pdbqt format after initial addition of hydrogen bonds and charges. These molecules were considered for docking analysis. The cubical grid box of 50 × 50 × 50 sizes with 0.375 Å was fixed around the key residues of the three proteins. UAW246 was re-docked into the main protease binding site for assessing binding affinity. Favipiravir, lopinavir, hydroxychloroquine, and ritonavir were used as control molecules for filtering bioactive compounds from *Andrographis paniculata* herbs. The autogrid4 parameter was used to attain a rigid grid box. Furthermore, autodock4 with Lamarckian genetic algorithms was conducted to obtain the best docking conformation. Note that the AutoDock estimates free energies of binding based on the typical molecular mechanics' energy terms for dispersion/repulsion, hydrogen bonding, and electrostatic interactions [21], torsional entropy upon binding, and the desolvation upon the ligand binding and corresponding hydrophobic effect [22].

The AutoDock estimates the free energy of binding *(*ΔG*)* based on empirical weighting factors*:*

$$\Delta G = \Delta G_{vdw} + \Delta G_{hbond} + \Delta G_{elec} + \Delta G_{tor} + \Delta G_{sol}$$

where ΔG_{vdw}, ΔG_{hbond}, and ΔG_{elec} are the typical molecular mechanics' energy terms for van der Waals, hydrogen bonding, and electrostatic interactions, respectively. While ΔG_{tor} characterizes the loss of torsional entropy upon binding and ΔG_{sol} displays the desolvation upon the ligand binding and corresponding hydrophobic effect.

3. Results and Discussion

The molecular docking was performed using the AutoDock program to screen the binding affinity of 482 bioactive compounds against the three targets of SARS-CoV-2*:* main protease, spike protein, and Nsp15. The 3D structure of these bioactive compounds from 91 *Andrographis paniculata* (A1-A91) compounds is shown in Figure 1. The key residues of main protease, spike protein, and Nsp15 are considered as active residues to bind with bioactive compounds. The binding energy (BE, kcal/mol) and the percentage of possible conformation or dock score (% DS) of 91 bioactive compounds were varying from -3.89 to -11.65 kcal/mol and 13 to 100%, respectively. The BE and %DS of bioactive compounds from *Andrographis paniculata* are summarized in Table 1.

The docking program was verified by re-docking of Tipiracil back into Nsp15 [5] binding site together with the re-docking of UAW246 [16] back into the main protease binding site. Tipiracil, an FDA-approved drug that is used in the treatment of colorectal cancer, as a potential anti-COVID-19 drug by interacting with the uridine binding pocket in the enzyme's active site of SARS-CoV-2 Nsp15. The docking model of Tipiracil and UAW246 were well-posed in the Nsp15 and main protease binding site, respectively *(*Figure not show*)*. The BE and % DS of Tipiracil and UAW246 re-docking were -5.09 and -6.58 kcal/mol and 45% and 7%, respectively, suggesting that the setting parameters were suitable for this study. Darunavir, favipiravir, hydroxychloroquine, lopinavir, remdesivir, and ritonavir were also docked into its binding site of the three targets of SARS-CoV-2*:* main protease, spike protein, and Nsp15 (Table 1). The result shows that all the well-known drugs are a good binding affinity in the cavity of the main protease than that of the spike protein. Lopinavir had the highest binding energy (-8.91 kcal/mol) but the %DS was quite low (4%) while favipiravir had the highest %DS (48%) but the binding energy is lower (-4.88 kcal/mol) than that of lopinavir in the binding pocket of the main protease. Most of the *Andrographis paniculata* compounds have lower BE than the known drugs. This finding result can be suggested that *Andrographis paniculata* is more effective in treating Covid-19 than the drug Fapiravir, which is commonly used in Thailand. However, to confirm this suggestion, the result from the experimental laboratory is necessary. The docking result revealed that mostly bioactive compounds are a good binding affinity with the main protease than that of the spike protein. On comparing the binding energy values of all compounds, the top twenty-four bioactive compounds and well-known drugs are shown

in Table 1. The 3,19-isopropylidene andrographolide, 7,8-dimethoxy flavone-5-ß-D-glucopyranosyloxy flavone, 14-acetyl-3,19-isopropylidene andrographolide, alpha1-Sitosterol, indosterol, oleanolic acid, and stigmasterol from *Andrographis paniculata* were possessed a higher binding affinity with the binding site of the COVID-19 main protease and Nsp15.

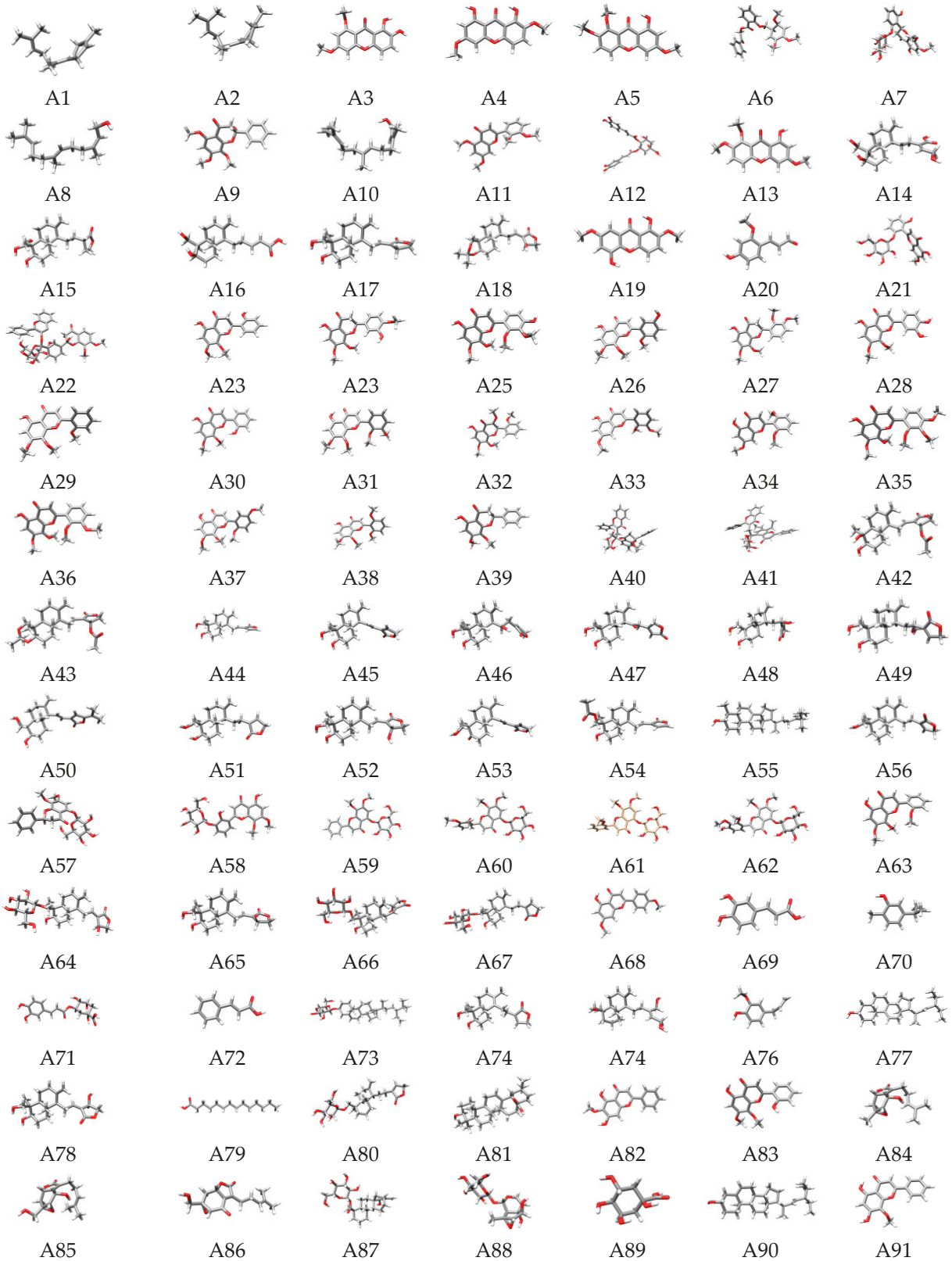

Figure 1. Structures of optimized geometry of 91 *Andrographis paniculata* compounds in HF/6-31 G* level of theory.

Table 1. The BE and %DS of commercial drugs and selected most favorable *Andrographis paniculata* compounds in the binding pocket of spike protein, Nsp15, and main protease.

Code	Name	Spike protein		Nsp15		Main protease	
		BE (kcal/mol)	%DS	**BE (kcal/mol)**	%DS	**BE (kcal/mol)**	%DS
	Redocking	-	-	-5.09	45	-6.58	7
a	Darunavir	-5.14	4	-7.17	4	-8.00	4
b	Favipiravir	-3.51	82	-3.44	29	-4.88	48
c	Hydroxychloroquine	-4.17	9	-5.35	21	-8.28	22
d	Lopinavir	-4.75	3	-5.85	3	-8.91	4
f	Remdesivir	-3.3	2	-5.51	3	-7.62	3
g	Ritonavir	-4.03	2	-3.71	2	-6.31	2
A3	*(Z)*-gamma-Bisabolene	-5.02	87	-6.03	89	-7.60	96
A10	2-hydroxy-5,7,8-trimethoxy flavone	-4.60	35	-6.17	42	-7.81	72
A12	3',2,5,7-tetramethoxy flavone	-4.96	54	-6.27	53	-8.29	61
A14	3,7,8-trimethoxy 1-hydroxyxanthone	-4.54	46	-6.10	89	-7.65	99
A19	**3,19-isopropylidene andrographolide**	**-6.41**	**44**	**-8.25**	**94**	**-10.08**	**91**
A23	5,2'-dihydroxy-7,8,-dimethoxy flavone-3'-ß-D-glucopyranosyloxy	-5.06	5	-7.43	13	-11.83	14
A33	5-hydroxy-3,7,8,2'-tetramethoxy flavanone	-4.43	23	-6.24	52	-8.49	66
A40	5-hydroxy-7,8-dimethoxy flavanone	-4.82	74	-5.93	60	-7.53	55
A41	7,8,2'-trimethoxy flavone-5-ß-D-glucopyranosyloxy flavone	-4.71	6	-6.77	16	-10.39	37
A42	**7,8-dimethoxy flavone-5-ß-D-glucopyranosyloxy flavone**	**-5.49**	**15**	**-8.23**	**14**	**-11.65**	**50**
A43	14-acetyl andrographolide	-5.48	23	-7.14	73	-9.03	30
A44	**14-acetyl-3,19-isopropylideneandrographolide**	**-6.54**	**94**	**-7.91**	**93**	**-10.36**	**54**
A51	14-deoxy-15-isopropylidene-11,12-didehydroandrographolide	-5.88	24	-7.61	45	-8.69	53
A55	19-o-acetyl anhydroandrographolide	-5.78	45	-7.20	31	-8.49	41
A56	alpha1-Sitosterol	-6.56	47	-9.11	97	-10.97	44
A57	Andrograpanin	-5.56	48	-7.05	51	-8.22	43
A66	Andrographolide	-5.71	48	-6.55	69	-8.62	53
A67	Andrographoside	-5.30	23	-6.79	11	-9.94	19
A68	Andropanoside	-5.54	32	-6.92	13	-9.32	12
A74	Daucosterol	-7.24	27	-8.75	44	-10.53	23
A78	**Indosterol**	**-7.18**	**87**	**-9.83**	**60**	**-10.56**	**48**
A82	**Oleanolic acid**	**-6.77**	**34**	**-10.07**	**56**	**-9.43**	**100**
A88	Paniculoside I	-5.62	23	-7.11	33	-11.35	44
A91	**Stigmasterol**	**-6.89**	**64**	**-9.10**	**90**	**-11.33**	**65**

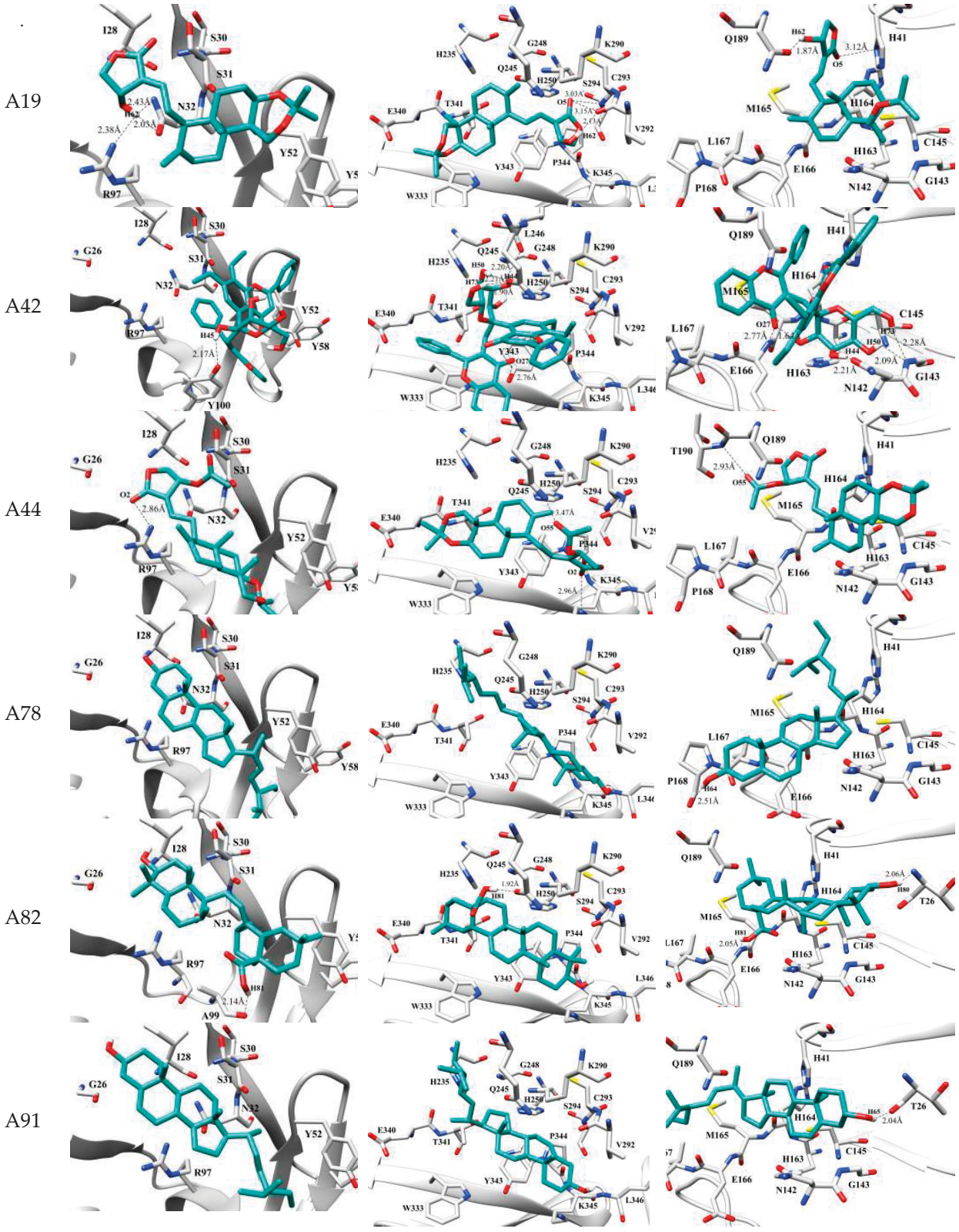

Figure 2. The hydrogen bond interaction and bond distances (Å) of six potential bioactive compounds from *Andrographis paniculata* (A19, A42, A44, A78, A82, and A91) with key amino acid in the binding pocket of the spike protein, Nsp15, and main protease of SARS-CoV-2.

However, the important criteria of strong interaction with key residues in the receptor-binding domain were also considered for finding potential inhibitors. The H-bond interaction of the top six bioactive compounds were shown in Figure 2. Considering all the hydrogen bond data given above, the hydrogen bonds of the 3,19-isopropylidene andrographolide, 7,8-dimethoxy flavone-5-ß-D-glucopyranosyloxy flavone, and stigmasterol ligand with key residues in the binding pocket of the main protease were found more than that of the other ligands. The important amino acid residues in the binding pocket of the main protease are H41, M49, F140, N142, G143, S144, C145, H164, M165, E166, P168, and Q189 [16]. While the important amino acid residues in the binding pocket of spike protein are G26, I28, S30, S31, N32, Y52, Y58, and R97, and the important amino acid residues in the binding pocket of Nsp15 are Q245, G248, H250, K290, C293, S294, E340, T341, Y343, P344, and K345. These hydrogen bond patterns seem to correspond with the binding affinities. From the computational findings, it can be suggested that the 3,19-isopropylidene andrographolide, 7,8-dimethoxy flavone-5-ß-D-glucopyranosyloxy flavone, and Stigmasterol compounds from *Andrographis paniculata* had a superior binding affinity of -11.08, -11.65, and -11.33 kcal/mol toward the main protease. However, the hydrogen bond of many compounds has counts in the active site of nsp15 > spike > the main protease, as opposed to BE that the main protease > nsp15 > spike. This is due to the molecular docking result could provide more interaction types besides hydrogen bonds such as van der Waals and electrostatic interaction.

4. Conclusions

In the present study, a set of commercial drugs and 91 structures of *Andrographis paniculata* (A1-A91) against three targets of SARS-CoV-2*:* spike protein, Nsp15, and main protease were screened by computational chemistry techniques. The docking results showed that mostly bioactive compounds are a good binding affinity with the main protease than that of spike protein and Nsp15 of SARS-CoV-2. Among them, 3,19-isopropylidene andrographolide, 7,8-dimethoxy flavone-5-ß-D-glucopyranosyloxy flavone, and Stigmasterol compounds from *Andrographis paniculata* had a superior binding affinity of -11.08, -11.65, and -11.33 kcal/mol toward the main protease. A detailed understanding of ligand-protein interaction could be helpful for further drug design and development for COVID-19 treatment.

5. Acknowledgements

This work was supported by National Higher Education, Science, Research and Innovation Policy Council, Thaksin University (Basic Research Fund; 64A105000028) Fiscal Year 2021. The authors would like to thank the Computational Chemistry Unit Cell, Faculty of Science, Chulalongkorn University, and the Department of Chemistry, Faculty of Science, Thaksin University, for providing research facilities, software packages, and computing times.

Author Contributions*:*

Funding*:* This research was funded by National Higher Education, Science, Research and Innovation Policy Council, Thaksin University *(*Basic Research Fund; 64A105000028*)* Fiscal Year 2021.

Conflicts of Interest*:* The authors declare no conflict of interest.

References

[1] Pulakuntla, S.; Lokhande, K.B.; Padmavathi, P.; Pal, M.; Swamy, K.V.; Sadasivam, J.; Singh, S.A.; Aramgam, S.L.; Reddy, V.D.. Mutational analysis in international isolates and drug repurposing against SARS-CoV-2 spike protein: molecular docking and simulation approach. *Virusdisease.* 2021, *32*, 1-13.

[2] Luo, L.; Qiu, Q.; Huang, F.; Liu, K.; Lan, Y.; Li, X.; Huang, Y.; Cui, L.; Luo, H.. Drug repurposing against coronavirus disease 2019 (COVID-19): A review. *Journal of Pharmaceutical Analysis.* 2021, *11*, 683-90.

[3] Hasan, M.; Parvez, M.S.A.; Azim, K.F.; Imran, M.A.S.; Raihan, T.; Gulshan, A.; Muhit, S.; Akhand, R.N.; Ahmed, S.S.U.; Uddin M.B.. Main protease inhibitors and drug surface hotspots for the treatment of

COVID-19: A drug repurposing and molecular docking approach. *Biomedicine & Pharmacotherap.* 2021, *140*, 111742.

[4] Wrapp, D.; Wang, N.; Corbett, K.S.; Goldsmith, J.A.; Hsieh, C.-L.; Abiona, O.; Graham, B.S.; Mclellan, J.S.. Cryo-EM structure of the 2019-nCoV spike in the prefusion conformation. *Science Advances.* 2020, *367*, 1260-3.

[5] Kim, Y.; Wower, J.; Maltseva, N.; Chang, C.; Jedrzejczak, R.; Wilamowski, M.; Kang, S.; Nicolaescu, V.; Randall, G.; Michalska, K.; Joachimiak, A.. Tipiracil binds to uridine site and inhibits Nsp15 endoribonuclease NendoU from SARS-CoV-2. *Communications Biology* 2021, *4:193*, 1-11.

[6] Murugesan, S.; Kottekad, S.; Crasta, I.; Sreevathsan, S.; Usharani, D.; Perumal, M.K.; Mudliar, S.N.. Targeting COVID-19 (SARS-CoV-2) main protease through active phytocompounds of ayurvedic medicinal plants – Emblica officinalis (Amla), Phyllanthus niruri Linn. (Bhumi Amla) and Tinospora cordifolia (Giloy) – A molecular docking and simulation study. *Computers in Biology and Medicine.* 2021, *136*, 104683.

[7] Murugan, N. A.; Pandian, C. J.; Jeyakanthan, J. Computational investigation on Andrographis paniculata phytochemicals to evaluate their potency against SARS-CoV-2 in comparison to known antiviral compounds in drug trials. *Journal of Biomolecular Structure and Dynamics.* 2021, *39*, 4415-26.

[8] Sukardiman, Ervina, M., Fadhil Pratama, M.R., Poerwono, H., Siswodihardjo, S. The coronavirus disease 2019 main protease inhibitor from *Andrographis paniculata* (Burm. f) Ness. *Journal of advanced pharmaceutical technology and research.* 2020, *11*, 157-62.

[9] Rajagopal, K.; Varakumar, P.; Baliwada, A.; Byran, G. Activity of phytochemical constituents of Curcuma longa (turmeric) and *Andrographis paniculata* against coronavirus (COVID-19): an in silico approach. *Future Journal of Pharmaceutical Sciences.* 2020, *6*, 104.

[10] Verma, D.; Mitra, D.; Paul, M.; Chaudhary, P.; Kamboj, A.; Thatoi, H.; Janmeda, P.; Jain, D.; Panneerselvam, P.; Shrivastav, R.; Pant, K.; Das Mohapatra, P. K. Potential inhibitors of SARS-CoV-2 (COVID-19) proteases PLpro and Mpro/ 3CLpro: molecular docking and simulation studies of three pertinent medicinal plant natural components. *Current Research in Pharmacology and Drug Discovery.* 2021, *2*, 100038.

[11] Xu, J.; Gao, L.; Liang, H.; Chen, S.-d. In silico screening of potential anti–COVID-19 bioactive natural constituents from food sources by molecular docking. *Nutrition.* 2021, *82*, 111049.

[12] Alghamdi, H. A.; Attique, S. A.; Yan, W.; Arooj, A.; Albulym, O.; Zhu, D.; Bilal, M.; Nawaz, M. Z. Repurposing the inhibitors of COVID-19 key proteins through molecular docking approach. *Process Biochemistry*. 2021, 110, 216-222.

[13] Dennington, R.; Keith, T.; Millam, J. *GaussView, Version 5. Semichem Inc.,* Shawnee Mission KS. 2009.

[14] Frisch, M. J.; Trucks, G. W.; Schlegel, H. B.; Scuseria, G. E.; Robb, M. A.; Cheeseman, J. R.; Scalmani, G.; Barone, V.; Petersson, G. A.; Nakatsuji, H.; Li, X.; Caricato, M.; Marenich, A. V.; Bloino, J.; Janesko, B. G.; Gomperts, R.; Mennucci, B.; Hratchian, H. P.; Ortiz, J. V.; Izmaylov, A. F.; Sonnenberg, J. L.; Williams; Ding, F.; Lipparini, F.; Egidi, F.; Goings, J.; Peng, B.; Petrone, A.; Henderson, T.; Ranasinghe, D.; Zakrzewski, V. G.; Gao, J.; Rega, N.; Zheng, G.; Liang, W.; Hada, M.; Ehara, M.; Toyota, K.; Fukuda, R.; Hasegawa, J.; Ishida, M.; Nakajima, T.; Honda, Y.; Kitao, O.; Nakai, H.; Vreven, T.; Throssell, K.; Montgomery Jr., J. A.; Peralta, J. E.; Ogliaro, F.; Bearpark, M. J.; Heyd, J. J.; Brothers, E. N.; Kudin, K. N.; Staroverov, V. N.; Keith, T. A.; Kobayashi, R.; Normand, J.; Raghavachari, K.; Rendell, A. P.; Burant, J. C.; Iyengar, S. S.; Tomasi, J.; Cossi, M.; Millam, J. M.; Klene, M.; Adamo, C.; Cammi, R.; Ochterski, J. W.; Martin, R. L.; Morokuma, K.; Farkas, O.; Foresman, J. B.; Fox, D. J. Gaussian 16 Revision a. 03. *Wallingford CT*, 2016, 2,

[15] Bernstein, F.C.; Koetzle, T.F.; Williams, G.J.; Meyer, E.F.; Brice, Jr.; M.D.; Rodgers, J.R.; Kennard, O.; Shimanouchi, T.; Tasumi, M. The Protein Data Bank: a computer-based archival file for macromolecular structures. *Journal of Molecular Bioogyl.* 1977, *112*, 535-42.

[16] Sacco, M.D.; Ma, C.; Lagarias, P.; Gao, A.; Townsend, J.A.; Meng, X.; Dube, P.; Zhang, X.; Hu, Y.; Kitamura, N.; Hurst, B.; Tarbet, B.; Marty, T.M.; Kolocouris, A., Xiang, Y.; Chen, Y.; Wang, J.. Structure and inhibition of the SARS-CoV-2 main protease reveal strategy for developing dual inhibitors against M(pro) and cathepsin L. *Science Advances.* 2020, *6*, eabe0751.

[17] Wu, Y.; Wang, F.; Shen, C.; Peng, W.; Li, D.; Zhao, C.; Li, Z.; Li, S.; Bi, Y.; Yang, Y.; Gong, Y.; Xiao, H.; Fan, Z.; Tan, S.; Wu, G.; Tan, W.; Lu, X.; Fan, C.; Wang, Q.; Liu, Y.; Zhang, C.; Qi, J.; Gao, G.F.; Gao, F.; Liu, L. *Science.* **2020,** *368* (6496), 1274-1278.

[18] Morris, G.M.; Goodsell, D.S.; Halliday, R.S.; Huey, R.; Hart, W.E.; Belew, R.K.; Arthur, O. Automated docking using a Lamarckian genetic algorithm and empirical binding free energy function. *Journal of Computational Chemistry.* 1998, *19*, 1639-62.

[19] Gasteiger, J.; Marsili, M. Iterative partial equalization of orbital electronegativity-a rapid access to atomic charges. *Tetrahedron.* 1980, 36, 3219-28.

[20] Morris, G.M.; Huey, R.; Lindstrom, W.; Sanner, M.F.; Belew, R.K.; Goodsell, D.S.; Arthur, O. AutoDock4 and AutoDockTools4: automated docking with selective receptor flexibility. *Journal of Computational Chemistry.* 2009, *30*, 2785-91.

[21] Huey, R.; Morris, G.M.; Olson, A.J.; Goodsel, D.S. A semiempirical free energy force field with charge-based desolvation. *Journal of Computational Chemistry.* 2007, *28*, 1145-52.

[22] Ermakova, E. Structural insight into the glucokinase-ligands interactions. Molecular docking study. *Computational Biology Chemistry.* 2016, *64*, 281-96.

Lists of Reviewers

Manuscripts of research articles and academic articles of ASEAN Journal of Scientific and Technological Reports (AJSTR). ISSN 2773-8752 (Online), Volume 25, No. 1 (January - March 2022) were reviewed by the reviewers as follows:

1.	Prof. Dr. Saksit Chanthai	Faculty of Science, Khon Kaen University
2.	Assoc. Prof. Dr. Burachat Chatveera	Faculty of Engineering, Thammasat University
3.	Assoc. Prof. Dr. Charlie Navanugraha	Faculty of Environment and Resource Studies, Mahasarakham University
4.	Assoc. Prof. Dr. Dheerawan Boonyawan	Faculty of Science, Chiang Mai University
5.	Assoc. Prof. Dr. Kittiwet Kuntiyawichai	Faculty of Engineering, Khon Kaen Unversity
6.	Assoc. Prof. Dr. Sompong O-Thong	Faculty of Science, Thaksin University
7.	Asst. Prof. Dr. Apichart Sonthisombat	Faculty of Engineering, Rajamangala University of Technology Thanyaburi
8.	Asst. Prof. Dr. Artit Chingsungnoen	Faculty of Science, Mahasakham University
9.	Asst. Prof. Dr. Kitiyaporn Wittayanarakul	Faculty of Sciences, Khon Kaen University
10.	Asst. Prof. Dr. Noppamas Pukkhem	Faculty of Science, Thaksin University
11.	Asst. Prof. Dr. Pathumwadee Yotmanee	Faculty of Science, Ramkhamhaeng University
12	Asst. Prof. Dr. Pattamarat Rattanachuay	Faculty of Science, Prince of Songkla University
13.	Asst. Prof. Dr. Prawit Kongjan	Faculty of Science and Technology, Prince of Songkla University
14.	Asst. Prof. Dr. Rattana Jariyaboon	Faculty of Science and Technology, Prince of Songkla University
15.	Asst. Prof. Dr. Saowapa Chotisuwan	Faculty of Science and Technology, Prince of Songkla University
16.	Asst. Prof. Dr. Sornchai Intachai	Faculty of Science, Thaksin University
17.	Asst. Prof. Dr. Thawatchai Tepnual	Faculty of Science, Thaksin University
18.	Asst. Prof. Sittichoke Janyong	Faculty of Science and Fisheries Technology, Rajamangala University of Technology Srivijiaya
19.	Dr. Adisak Intana	College of Computing, Prince of Songkla University
20.	Dr. Korawit Prutsachainimmit	Faculty of Technology and Environment, Prince of Songkla University
21.	Dr. Wanida Petlamul	College of Innovation and Management, Songkhla Rajabhat University
22.	Dr. Win Win Myo	Faculty of Computing, University of Information Technology
23.	Dr. Wirawut Lephon	Faculty of Industrial Technology, Phibunsongkhram Rajabhat
24.	Prof. Dr. Saksit Chanthai	Faculty of Science, Khon Kaen University

JSTR
ASEAN Journal of Scientific and Technological Reports

Article type

Type of the Paper (Article, Review, Communication, etc.) *about 8,000 words maximum*

Title (Palatino Linotype 18 pt, bold)

Firstname Lastname[1], Firstname Lastname[2] and Firstname Lastname[2*]

[1] Affiliation 1; e-mail@e-mail.com
[2] Affiliation 2; e-mail@e-mail.com
* Correspondence: e-mail@e-mail.com; (one corresponding authors, add author initials)

Abstract: A single paragraph of about 400 words maximum. Self-contained and concisely describe the reason for the work, methodology, results, and conclusions. Uncommon abbreviations should be spelled out at first use. We strongly encourage authors to use the following style of structured abstracts, but without headings: (1) Background: Place the question addressed in a broad context and highlight the purpose of the study; (2) Methods: briefly describe the main methods or treatments applied; (3) Results: summarize the article's main findings; (4) Conclusions: indicate the main conclusions or interpretations.

Keywords: keyword 1; keyword 2; keyword 3 (List three to ten pertinent keywords specific to the article yet reasonably common within the subject discipline.)

Citation:
Lastname, F.; Lastname, F.; Lastname, F. Title. *ASEAN J. Sci. Tech. Report.* **2022**, *25*(X), xx-xx. https://doi.org/10.55164/ajstr.vxxix.xxxxxx

Article history:
Received: date
Accepted: date
Available online: date

Publisher's Note:
This article is published and distributed under the terms of the Thaksin University.

1. Introduction

The introduction should briefly place the study in a broad context and highlight why it is crucial. It should define the purpose of the work and its significance. The current state of the research field should be carefully reviewed and critical publications cited. Please highlight controversial and diverging hypotheses when necessary. Finally, briefly mention the main aim of the work. References should be numbered in order of appearance and indicated by a numeral or numerals in square brackets—e.g., [1] or [2,3], or [4–6]. See the end of the document for further details on references.

2. Materials and Methods

The materials and methods should be described with sufficient details to allow others to replicate and build on the published results. Please note that your manuscript's publication implicates that you must make all materials, data, computer code, and protocols associated with the publication available to readers. Please disclose at the submission stage any restrictions on the availability of materials or information. New methods and protocols should be described in detail, while well-established methods can be briefly described and appropriately cited.

Interventional studies involving animals or humans, and other studies that require ethical approval, must list the authority that provided approval and the corresponding ethical approval code.

2.1 Subsection

2.1.1. Subsubsection

3. Results and Discussion

This section may be divided by subheadings. It should provide a concise and precise description of the experimental results, their interpretation, as well as the experimental conclusions that can be drawn.Authors should discuss the results and how they can be interpreted from previous studies and the working hypotheses. The findings and their implications should be discussed in the broadest context possible. Future research directions may also be highlighted.

3.1. Subsection

3.1.1. Subsubsection

3.2. Figures, Tables, and Schemes

All figures and tables should be cited in the main text as Figure 1, Table 1, etc.

Figure 1. This is a figure. Schemes follow the same formatting.

Table 1. This is a table. Tables should be placed in the main text near the first time they are cited.

Title 1	Title 2	Title 3
entry 1	data	data
entry 2	data	data [1]

[1] Table may have a footer.

3.3. Formatting of Mathematical Components

This is example 1 of an equation:

$$a = 1, \tag{1}$$

The text following an equation need not be a new paragraph. Please punctuate equations as regular text. This is example 2 of an equation:

$$a = b + c + d + e + f + g + h + i + j + k + l + m + n + o + p + q + r + s + t + u \tag{2}$$

The text following an equation need not be a new paragraph. Please punctuate equations as regular text. The text continues here.

4. Conclusions

Concisely restate the hypothesis and most important findings. Summarize the significant findings, contributions to existing knowledge, and limitations. What are the future directions? Conclusions MUST be well stated, linked to original research question & limited to supporting results.

5. Acknowledgements

Should not be used to acknowledge funders – funding will be entered as a separate. As a matter of courtesy, we suggest you inform anyone whom you acknowledge.

Author Contributions: For research articles with several authors, a short paragraph specifying their individual contributions must be provided. The following statements should be used "Conceptualization, X.X. and Y.Y.; methodology, X.X.; software, X.X.; validation, X.X., Y.Y. and Z.Z.; formal analysis, X.X.; investigation, X.X.; resources, X.X.; data curation, X.X.; writing—original draft preparation, X.X.; writing—review and editing, X.X.; visualization, X.X.; supervision, X.X.; project administration, X.X.; funding acquisition, Y.Y. All authors have read and agreed to the published version of the manuscript." Please turn to the CRediT taxonomy for the term explanation. Authorship must be limited to those who have contributed substantially to the work reported.

Funding: Please add: "This research received no external funding" or "This research was funded by NAME OF FUNDER, grant number XXX" and "The APC was funded by XXX". Check carefully that the details given are accurate and use the standard spelling of funding agency names at https://search.crossref.org/funding. Any errors may affect your future funding.

Conflicts of Interest: Declare conflicts of interest or state "The authors declare no conflict of interest." Authors must identify and declare any personal circumstances or interest that may be perceived as inappropriately influencing the representation or interpretation of reported research results. Any role of the funders in the design of the study; in the collection, analyses or interpretation of data; in the writing of the manuscript, or in the decision to publish the results must be declared in this section. If there is no role, please state "The funders had no role in the design of the study; in the collection, analyses, or interpretation of data; in the writing of the manuscript, or in the decision to publish the results".

References

References must be numbered in order of appearance in the text (including citations in tables and legends) and listed individually at the end of the manuscript. We recommend preparing the references with a bibliography software package, such as EndNote, ReferenceManager to avoid typing mistakes and duplicated references. Include the digital object identifier (DOI) for all references where available.

Citations and references in the Supplementary Materials are permitted provided that they also appear in the reference list here.

In the text, reference numbers should be placed in square brackets [ ] and placed before the punctuation; for example [1], [1–3] or [1,3]. For embedded citations in the text with pagination, use both parentheses and brackets to indicate the reference number and page numbers; for example [5] (p. 100), or [6] (pp. 101–105).

1. Author 1, A.B.; Author 2, C.D. Title of the article. *Abbreviated Journal Name* Year, *Volume*, page range.
2. Author 1, A.; Author 2, B. Title of the chapter. In *Book Title*, 2nd ed.; Editor 1, A., Editor 2, B., Eds.; Publisher: Publisher Location, Country, 2007; Volume 3, pp. 154–196.
3. Author 1, A.; Author 2, B. *Book Title*, 3rd ed.; Publisher: Publisher Location, Country, 2008; pp. 154–196.

4. Author 1, A.B.; Author 2, C. Title of Unpublished Work. *Abbreviated Journal Name* stage of publication (under review; accepted; in press).
5. Author 1, A.B. (University, City, State, Country); Author 2, C. (Institute, City, State, Country). Personal communication, 2012.
6. Author 1, A.B.; Author 2, C.D.; Author 3, E.F. Title of Presentation. In Title of the Collected Work (if available), Proceedings of the Name of the Conference, Location of Conference, Country, Date of Conference; Editor 1, Editor 2, Eds. (if available); Publisher: City, Country, Year (if available); Abstract Number (optional), Pagination (optional).
7. Author 1, A.B. Title of Thesis. Level of Thesis, Degree-Granting University, Location of University, Date of Completion.
8. Title of Site. Available online: URL (accessed on Day Month Year).

Reviewers sugestion

1. Name, Address, e-mail
2. Name, Address, e-mail
3. Name, Address, e-mail
4. Name, Address, e-mail

URL link:

Notes for Authors >> https://drive.google.com/file/d/1r0zegnIVeQqe4iLQyT1xDEIinNggINPD/view?usp=sharing
https://drive.google.com/file/d/1r0zegnIVeQqe4iLQyT1xDEIinNggINPD/view?usp=sharing

Online Submissions >> https://ph02.tci-thaijo.org/index.php/tsujournal/user/register

Current Issue >> https://ph02.tci-thaijo.org/index.php/tsujournal/issue/view/16516

AJSTR Publication Ethics and Malpractice >> https://ph02.tci-thaijo.org/index.php/tsujournal/ethics

Journal Title Abbreviations >> http://library.caltech.edu/reference/abbreviations


มหาวิทยาลัยทักษิณ THAKSIN UNIVERSITY
ปัญญาและจริยธรรมนำการพัฒนา Intelligence and Ethics guide Development

สถาบันวิจัยและพัฒนา มหาวิทยาลัยทักษิณ
222 หมู่ 2 ต.บ้านพร้าว อ.ป่าพะยอม จ.พัทลุง 93210
โทรศัพท์ 074-609-600 ต่อ 7242 โทรศัพท์ 074-609-655
E-mail Address: tsujournal@tsu.ac.th, aseanjstr@tsu.ac.th